REACTOR MATERIALS

A Quarterly Technical Progress Review

Prepared for DIVISION OF TECHNICAL INFORMATION, USAEC, by
E. M. SIMONS and ASSOCIATES, BATTELLE MEMORIAL INSTITUTE

Fall 1966

● VOLUME 9

● NUMBER 3

TECHNICAL PROGRESS REVIEWS

To meet the needs of industry for concise summaries of current atomic developments, the Atomic Energy Commission is publishing this series, Technical Progress Reviews. Issued quarterly, each of the reviews digests and evaluates the latest findings in a specific area of nuclear technology and science.

The journals published in this series are:

Isotopes and Radiation Technology P. S. Baker, A. F. Rupp, and associates
Oak Ridge National Laboratory

Nuclear Safety Wm. B. Cottrell, W. H. Jordan, J. P. Blakely, and associates
Nuclear Safety Information Center, Oak Ridge National Laboratory

Power Reactor Technology
Argonne National Laboratory

Reactor Materials E. M. Simons and associates
Battelle Memorial Institute

See the back cover for availability information.

The views expressed in this publication do not necessarily represent those of the United States Atomic Energy Commission, its divisions or offices, or of any Commission advisory committee or contractor.

Availability of Reports Cited in This Review

Unclassified AEC reports are available for inspection at AEC depository libraries and are sold by the Clearinghouse for Federal Scientific and Technical Information, National Bureau of Standards, U. S. Department of Commerce, 5285 Port Royal Road, Springfield, Va., 22151. Some of the reports cited are not available owing to their preliminary nature; however, the information contained in them will eventually be made available in formal progress or topical reports.

Unclassified reports issued by other Government agencies or private organizations should be requested from the originator.

Unclassified British and Canadian reports may be inspected at AEC depository libraries. British reports are sold by the British Information Service, 45 Rockefeller Plaza, New York, N. Y.; Canadian reports (AECL series) are sold by the Scientific Document Distribution Office, Atomic Energy of Canada, Ltd., Chalk River, Ontario, Canada.

Classified U. S. and foreign reports identified in this journal as Classified may be purchased by properly cleared Access Permit Holders from the Division of Technical Information Extension, U. S. Atomic Energy Commission, P. O. Box 1001, Oak Ridge, Tenn., 37830. Such reports may be inspected at classified AEC depository libraries.

Contents

Reactor Materials

Vol. 9, No. 3

I Fuel and Fertile Materials

Uranium Metal and Alloys 151
Plutonium 153
Thorium 155
Metal–Ceramic Fuels 155
Coated-Particle Fuel Materials 156
Uranium and Thorium Oxides 157
Uranium Carbides, Nitrides, Phosphides, Sulfides, and Arsenides 159
Fuel–Water Reactions 161
Mechanism of Corrosion of Fuel Alloys . . . 161
Basic Studies of Irradiation Effects in Fuel Materials 162
References 163

II Moderator Materials

Graphite 166
Beryllium Metal and Alloys 167
Beryllium Oxide 169
Solid Hydrides 169
References 170

III Nuclear Poisons

Hafnium 171
Dispersion and Nonmetallic Poison Materials 171
References 173

IV Cladding and Structural Materials

Corrosion 174
Metal–Water Reactions 179
Selected Mechanical Properties of Cladding and Structural Materials 180
Selected Metallurgical Aspects of Cladding and Structural Materials 183
Diffusion Studies 188
Radiation Effects in Nonfuel Materials 189
Ceramic Technology 193
References 194

V Special Fabrication Techniques

Melting, Casting, and Fabrication 197
Rolling, Swaging, and Coextrusion 198
Plating 198
Pressure Bonding 200
Nondestructive Testing 200
References 201

Issued quarterly by the U. S. Atomic Energy Commission. Use of funds for printing this publication approved by the Director of the Bureau of the Budget on July 8, 1966.

Reactor Materials is one of a series of quarterly technical progress reviews broadly covering the field of nuclear science and technology. Under the auspices of the USAEC Division of Technical Information, *Reactor Materials* is prepared by Battelle personnel from worldwide literature. It covers properties, behavior, and fabrication processes of materials applicable to nuclear reactor components and associated equipment.

The reader will recognize that the scope of this Review is too broad to permit detailed coverage of every topic. Rather, the authors and editors attempt to combine the highlights of significant new developments into an information summary of current research for both management and the technical specialist. As a rule, enough of the results are presented to define the research and summarize the findings. For readers desiring more information on any particular topic, a complete set of references is provided at the end of each section.

Each quarter a number of bibliographies, monographs, and books appear on subjects within the scope of *Reactor Materials*. Although the main purpose of this Review is to call attention to findings that are new and significant, such publications are noted in the text because they often represent excellent compilations of available information on important materials topics.

E. M. SIMONS
D. L. KELLER
R. W. ENDEBROCK
Battelle Memorial Institute

Section

I

Reactor Materials

Fuel and Fertile Materials

Uranium Metal and Alloys

Unalloyed Uranium

The British[1] performed thermal-conductivity measurements on uranium specimens cut from rods irradiated in the Calder Hall Reactor. The rods had been irradiated up to 4500 Mwd/metric ton at temperatures between 250 and 450°C (482 and 842°F). Measurements were made on specimens 3 in. long and 1.15 in. in diameter in a divided-bar apparatus at a mean temperature of 60°C (140°F). The thermal conductivity decreased with irradiation dose, the rate of change being much more rapid during the first few hours of irradiation. At fuel temperatures above 320°C (680°F), the initial decrease was of the order of 5%, after which the rate of decrease became small at about 0.35% per 1000 Mwd/metric ton. At fuel temperatures of 250°C (482°F), the initial decrease was greater, amounting to about 12%.

The high initial rate of decrease is ascribed to irradiation growth effects, and the smaller subsequent rate of decrease is ascribed to the combined effect of porosity resulting from inert-gas fission-product atoms and the accumulation in solid solution of solid fission-product atoms. The extent of the decrease is reduced by an enhancement of thermal conductivity due to thermal annealing processes.

To study the grain-size dependence of fracture in alpha uranium, the Canadians[2] measured fracture stresses over a range of grain sizes at temperatures from −196 to 270°C (−320 to 518°F). The Hall–Petch relation was valid at the extremes of temperature but inapplicable in the brittle-to-ductile transition region near 100°C (212°F). The results were interpreted in terms of the deformation and fracture modes, and their variation over the temperature range was studied.

Investigators at Savannah River Laboratory[3] report that network substructures were produced in uranium by the eutectoid decompositions of the gamma and beta phases. One network, corresponding to the beta grain and subgrain boundaries, was composed of either incipient precipitates (zones of segregated impurity or alloying elements) when the cooling rate through the transformation was rapid, or of real particles when the cooling rate was slow or the alloy content high. A second network, corresponding to the gamma grain boundaries, was apparent because the beta phase nucleated at the gamma grain boundaries, and, during rapid cooling, either incipient or real precipitates outlined each of the beta regions as they grew into the original gamma grains. The incipient precipitates could be revealed only by certain etchants, such as HNO_3, whereas the real precipitates could be delineated either by the HNO_3 etch or by electropolishing. The incipient precipitates were readily visible by transmission electron microscopy as tiny zones of high lattice strain. The presence of these network structures increased the work-hardening exponent and embrittled the uranium.

Investigators[4] at Sandia Corp. studied the feasibility of using the ion-plating process to coat depleted uranium with a protective layer of aluminum. Coatings less than 0.5 mil in thickness provide good corrosion protection for the uranium in condensing water vapor at 95°C (203°F) for up to 96 hr. The relative influences of various techniques of surface preparation and various deposition parameters were determined. Vacuum-evaporated coatings were totally inadequate for corrosion protection.

Several articles of interest dealing with the physical metallurgy of unalloyed uranium have appeared in the *Journal of Nuclear Materials*. These include "The M_s Temperature for Pure Uranium,"[5] "Surface Structure in Beta-Quenched Uranium,"[6] and "The Crystallography of Deformation Twinning in Alpha Uranium."[7]

Alpha-Phase Uranium Alloys

The growth of UAl_2 precipitates in uranium–250 ppm iron–700 ppm aluminum was studied by the British.[8] On heating specimens in the alpha and beta ranges, the number of precipitates diminished, and the average size of those remaining increased. The variation of the average particle radius with time was of the form $r^n = At$. In the alpha range, n varied from about 5 at 590°C (1094°F) to about 4 at 655°C (1211°F). The exponent n was essentially constant at a value of 3 in the beta range, and as a consequence the number of particles decreased as the reciprocal of the annealing time. The activation energies for the growth process, interpreted in terms of a diffusion-controlled solubility mechanism, were 3.2 ± 0.2

ev in the alpha phase and 3.5 ± 0.1 ev in the beta phase.

The effects of thermal history on the kinetics of the $\beta \rightarrow \alpha$ phase change in pure uranium and in two uranium–chromium alloys were examined by Townsend and Burke.[9] The heat-treatments were arranged to enable the effects associated with beta grain size to be separated from those due to submicroscopic changes governed by the quenching temperature. Transformation at temperatures near the equilibrium transition temperature is retarded by the increasing of the beta quenching temperature. In the alloys this retardation is shown to be due to an increase in beta grain size; in the pure metal the results suggest that, although beta grain size is the most important factor governing transformation rate, it is not the only one. Transformation at temperatures in the martensitic and bainitic ranges is accelerated by increasing the quenching temperature, because of the removal of grain boundaries that tend to arrest the growth of alpha crystals.

Investigators at National Lead Co. of Ohio[10] have reported on their studies of uranium with small additions of carbon. Uranium containing from 50 to 900 ppm carbon showed dispersions of coarse and fine particles arranged in networks. These fine networks, visible in both as-cast and heat-treated uranium, were of two different forms. First and most predominant was the "colony" form of precipitate. The particles in the colonies were of submicron (0.1 to 0.25 μ) size and precipitated on dislocation structures. The second was the Widmanstätten form of precipitate. These particles were also submicron (0.1 to 0.25 μ) in size. The Widmanstätten network appeared to have a definite orientation. Diffraction patterns showed that in all cases the alpha orientation in relation to the particles was (1 0 0) alpha, and the direction of alignment was close to the [1 1 1] alpha. This caused a speculation that the (1 0 0) alpha–[1 1 1] alpha plane and direction have a closely paralleling habit plane and direction in either the beta or gamma phases, upon which the particles precipitated.

The size of these particles prevents their identification by selected-area diffraction. Identification was therefore based on similar diffraction contrasts between primary particles and submicron particles, the primary particles being those particles which were optically resolvable. Both the primary particles and submicron particles showed a change of contrast from very dark to very light when the foil was tilted slightly. Electron-diffraction patterns of the primary particles showed them to be uranium carbide. Thus it was reasoned that submicron particles showing the same contrast effects were also composed of uranium carbide.

The formation of the primary carbides followed the kinetics of dendritic growth by a "point diffusion effect." These dendrites were formed within the liquid + UC phase field and grew in a manner prescribed by time and saturation.

Uranium samples with carbon contents of 40, 140, and 270 ppm showed progressive increases in network particle density. Approximately 80% of the sample surface was composed of network phase at 270 ppm carbon content. The formation of primary carbide particles began when the carbon content was between 140 and 270 ppm. However, a few primary carbides were visible in samples containing less than 140 ppm carbon, and these were attributed to melt–crucible interactions. As the carbon content was increased to 860 ppm, the network phase decreased progressively whereas the primary carbides increased in number. Melting studies on the uranium samples containing 270 ppm and 700 ppm carbon showed the solidus isotherm occurring at $1137 \pm 2°C$ ($2079 \pm 4°F$). By comparison, high-purity uranium samples (< 120 ppm total impurities, including 4 ppm carbon) melted at $1130 \pm 2°C$ ($2066 \pm 4°F$).

A tentative peritectic-phase diagram is proposed which more fully agrees with the experimental data than does a eutectic diagram. The ratio of network phase to primary carbide-particle phase fixed the peritectic at approximately 200 ppm carbon, and the melting studies placed the peritectic isotherm at 1137°C (2079°F).

Gamma solutionizing and subsequent aging treatments showed that dilute carbon alloys of uranium were not suitable for dispersion-hardening processes. The increase and subsequent decrease in hardness and, hence, strength during aging is caused more by stress relief of the quenched structure than by matrix precipitation. The as-quenched structure showed many loops (prismatic) and a considerable number of "superjogs," which increased the hardness over that of the as-cast structures. Aging for 3 min at 600°C (1112°F) produced an increase in hardness, indicated by the interactions of glide dislocations and loops. Aging for 7 min produced maximum hardness, indicated by partial entanglement of dislocations during interaction with the loop structure. Thereafter aging caused a decrease in hardness indicated by the climb of dislocations into subboundaries. Precipitation occurred on these subboundaries within 15 min. Complete stress removal occurred in samples aged for 11 min at 600°C (1112°F). Matrix precipitation occurred after approximately 2 hr and increased the hardness slightly.

Workers at Atomics International[11] are investigating the swelling resistance of specifically designed fine-dispersion uranium-alloy fuels that contain trace amounts of additives at temperatures from 550 to 645°C (1022 to 1193°F) and burnups from 0.8 to 1.9 at.%. Table I-1 gives the data obtained thus far. These data indicate that solution-treated alloys (or solution-treated and quenched alloys) are superior to any of the thermally produced dispersion alloys.

Constitution studies[12] indicate the existence of the compounds U_2Tc and UTc_2. The uranium–UCo_2–UMn_2 system[13] at 600 and 700°C (1112 and 1292°F) has been determined. Two nonvariant four-phase

Table I-1 VOLUME CHANGES IN IRRADIATED URANIUM-ALLOY SPECIMENS[11]

Capsule 1, 0.8 at.% burnup, 645°C (1193°F)		Capsule 2, 1.4 at.% burnup, 550°C (1022°F)		Capsule 3, 0.8 at.% burnup, 550°C (1022°F)		Capsule 4, 1.4 at.% burnup, 645°C (1193°F)	
Alloy composition (balance U),* wt.%	V/V_0	Alloy composition (balance U),* wt.%	V/V_0	Alloy composition (balance U),* wt.%	V/V_0	Alloy composition (balance U),* wt.%	V/V_0
4 Mo control	91.1	4 Mo control		4 Mo control	51.1	4 Mo control	
4 Mo–0.2 Si f.d.	36	Mo–0.1 Si c.d.	27.5	4 Mo–0.1 Si	8.7	4 Mo–0.1 Si s.t.	34.8
4 Mo–0.1 Si s.t.	17.6	Mo–0.1 Si s.t.	10.7	4 Mo–0.1 Si s.t.	5.8	10 Mo control	46.3
10 Mo control	38.9	10 Mo control	50	10 Mo control	29.4	10 Mo–0.1 Sn f.d.	62
10 Mo–0.1 Sn f.d.	39	10 Mo–0.1 Sn f.d.	25.1	10 Mo–0.1 Sn f.d.	27.9	10 Mo–0.1 Sn f.d.	59.7
10 Mo–0.1 Sn	13.9	10 Mo–0.1 Sn	4.9	10 Mo–0.1 Sn	17.9	10 Mo–0.1 Sn	15.2

*The abbreviations f.d. = fine dispersion; c.d. = coarse dispersion; s.t. = solution treated.

equilibria were found at 750 and 690°C (1382 and 1274°F). The compounds U_6Co and U_6Mn exhibit complete solid solubility, and the solubility of ternary additions in UCo_2 and alpha uranium is practically nil and in beta and gamma uranium is small.

The Swedish[14] have published their latest supplement to a continuing bibliography on "Radiation Effects on Solid, Uranium-Based Nuclear Fuel Materials."

Dilute Uranium Alloys

Zirconium–9.3 wt.% uranium-alloy driver tubes were irradiated by Savannah River.[15] These tubes have a 2.3-in. outside diameter by 1.96-in. inside diameter and are clad inside and out with Zircaloy-2. Burnups of up to 1.83 at.% at time-averaged central metal temperatures up to 540°C (1002°F) and under 1200-psi coolant pressure resulted in volume increases of up to 5.1%, which was less swelling than anticipated. This swelling occurred as an increase in wall thickness and was caused principally by the formation of solid fission products, with a lesser contribution due to precipitation of fission gases in small bubbles. The reactor pressurization, as well as impurities in the cores, may have limited the fission-gas swelling. Much larger volume increases occurred during postirradiation annealing for 74 hr at 600°C (1112°F) under low external restraint.

(M. S. Farkas)

Plutonium

Plutonium Metal and Alloys

Workers at Los Alamos Scientific Laboratory[16] are continuing their measurements of solubility of selected elements in liquid plutonium. Results obtained with niobium are shown below:

Temperature °C	Temperature °F	Solubility, atoms Nb/10^3 atoms Pu
700	1292	11.0
750	1382	14.4
800	1472	16.9
850	1562	20.5
900	1652	26.8
950	1742	31.4

Attempts at growing single crystals of high-purity alpha plutonium by annealing at temperatures up to 475°C (887°F) and at pressures between 31 and 78 kbars have resulted in some increase in grain size, but none of the material approached very large-grained or single-crystal alpha plutonium. The grain size was relatively uniform over a wide range of conditions, indicating that grain size is not particularly a function of the varied parameters.[17]

Some of the results of Battelle–Northwest[18] studies to determine the physical properties of arc-cast plutonium-base intermetallic compounds are reported in Table I-2.

Argonne National Laboratory[19] is continuing the development of uranium–plutonium–titanium and uranium–plutonium–zirconium alloys. Between the solidus temperature, 1150°C (2102°F), and 654°C (1208°F), a uranium–12.9 at.% plutonium–22.5 at.% zirconium alloy is single-phase gamma-uranium solid solution. Between 654 and 596°C (1206 and 1104°F), the alloy consists of alpha uranium and gamma solid solution. Below 596°C the phases in the alloy are alpha uranium and delta uranium–zirconium. A uranium–11.9 at.% plutonium–25.7 at.% titanium alloy consists of gamma solid solution between the 1140°C (2084°F) solidus and 856°C (1573°F). Between 856 and 644°C (1573 and 1190°F), the alloy consists of gamma and a ternary compound that is based on U_2Ti. At lower temperatures down to 558°C (1036°F), solid solution based on the beta and eta phases in the uranium–plutonium system appears to exist in equilibrium with the $(U,Pu)_2Ti$ phase and zeta uranium–plutonium. Both alloys were repeatedly thermally cycled through their phase transformations with essentially no effect.[20] Thermal conductivities of several uranium–plutonium–titanium and uranium–plutonium–zirconium alloys were measured. The results are shown in Table I-3.

The French[21] have reported the results of a rather extensive investigation of uranium–plutonium–iron alloys. Compositions investigated were uranium–25 wt.% plutonium–0.5 wt.% iron, uranium–25 wt.% plutonium–1.0 wt.% iron, and uranium–25 wt.% plutonium–1.5 wt.% iron. Some of the significant findings of the study are presented below:

1. The 0.5 wt.% iron alloy powdered after a 15-day exposure to room-temperature air.

2. No evidence of self-supporting inflammability was observed at temperatures up to 660°C (1220°F) in air.

3. At temperatures below the transformation, the alloys are composed of zeta uranium–plutonium and $(U,Pu)_6Fe$.

4. In compatibility tests with stainless steel, a $(U,Pu)_6Fe$ phase formed at the alloy–stainless-steel interface. The reaction zone was smallest with the 1.0 wt.% iron alloy.

5. Cycling between 50 and 400°C (122 and 752°F) had no effect on the alloys. Anomalous behavior was noted when alloys were cycled through the transformation.

6. Physical-property data generated in the study are summarized in Table I-4. (V. W. Storhok)

Plutonium Compounds

Chalk River found that PuO_2 prepared from the oxalate at 750°C (1382°F) results in high-density UO_2-PuO_2 pellets on sintering.[22] Densities ranging from 10.60 to 10.67 g/cm³ are reported for pellets with up to 1 wt.% PuO_2 sintered for $2\frac{1}{2}$ hr at 1200 to 1300°C (2192 to 2372°F) in 10 vol.% hydrogen in argon. The effect of stoichiometry on the melting point of mixed oxides is reported by Lyon and Baily of General Electric Company.[23] The melting point of a 20 wt.% PuO_2 mixed oxide increased from 2645 to 2790°C (4800 to 5055°F) as the O/M ratio decreased from 2.06 to 1.97. Batch preparation of UO_2-2 wt.% PuO_2 spherical particles is under study at Battelle–Northwest as feed material for vibrationally compacted fuel elements. Densities greater than 90% of theoretical have been reported[24] for 2200-g batches. Improved nitrate-removal methods are required for the sol-gel preparation of PuO_2 spherical particles. Good reproducibility has been demonstrated between 20-g batches at Oak Ridge National Laboratory (ORNL) in the preparation of 110- to 150-μ-diameter spherical particles.[25]

As part of their $UO_2-PuO_2-ZrO_2$ fuel program, workers at Nuclear Materials & Equipment Corp. measured lattice parameters for sintered mixed powders and sintered pellets.[26] The CaO additives have a stabilizing effect on the unit cell size. Pellets from several compositions performed well when thermally cycled from room temperature to 1250°C (2782°F). Good structural and dimensional stability was exhibited by the low ZrO_2 compositions.

Argonne has produced 350-g and 1-kg melts of PuC by direct reaction of elemental plutonium in a graphite crucible.[27] Carbon content is controlled by reaction temperature and holding time. Ten to 15% Pu_2C_3 as dendrites and an unidentified phase within the Pu_2C_3 are observed in the PuC matrix. Mixed (U,Pu)C powders have been prepared in a fluidized bed by reacting uranium–20 wt.% plutonium alloy with hydrogen to produce uranium–plutonium hydride, then reacting the hydride with propane.[28] Initial investigations indicate that (U,Pu)C powder with acceptable oxygen, nitrogen, and hydrogen contents can be prepared by this method. Studies at Atomics

Table I-2 PHYSICAL PROPERTIES OF SEVERAL PLUTONIUM-BASE INTERMETALLIC COMPOUNDS[18]

Compound	Density, g/cm³	Melting temperature	Thermal expansion coefficient, 10^{-6}/°C	Thermal expansion coefficient, 10^{-6}/°F	Young's modulus, 10^6 psi	Hardness, DPHN
Pu_3Rh_2		1040 ± 35°C (1904°F)	9	5	6	
Pu_3Ir_2		1400 ± 50°C (2552°F)	14	9	18	
PuPd		1150 ± 40°C (2102°F)	12	7	11	
Pu_3Pt_2		1240 ± 50°C (2264°F)	11	6	12	
Pu_6Os_2	16.89	1500 ± 50°C (2732°F)	13	7	10	321
Pu_6Ru_2	14.75	1160 ± 45°C (2120°F)	11	6	10	320
Pu_2Co	14.28	<950°C (<1742°F)	18	10	16	255
Pu_6Si_2	11.89	1380 ± 40°C (2516°F)	17	10	12	398

Table I-3 THERMAL CONDUCTIVITIES OF SEVERAL URANIUM–PLUTONIUM–ZIRCONIUM AND URANIUM–PLUTONIUM–TITANIUM ALLOYS (AT.%)[20]

Temp., °C	Thermal conductivity,* watt/(cm)(°C) U–11 Pu–30 Ti	U–10 Pu–13 Ti	U–15 Pu–15 Zr	U–15 Pu–25 Zr
100	0.087†	0.10†	0.11†	0.092†
200	0.117	0.139	0.142	0.117
300	0.142	0.171	0.177	0.144
400	0.163	0.201	0.210	0.171
500	0.184	0.228	0.241	0.197
600	0.201	0.254	0.264	0.219
700	0.216	0.278	0.280	0.234
800	0.23†	0.302	0.293	0.248
900		0.33†	0.30†	0.260†

*Probable accuracy, ±10%.
†Extrapolated.

Table I-4 PHYSICAL PROPERTIES OF URANIUM–25 WT.% PLUTONIUM–1 AND 1.5 WT.% IRON ALLOYS[21]

	1 wt.% Fe	1.5 wt.% Fe
Density, g/cm³	18.5	18.3
Solidus temperature	705 ± 5°C (1300°F)	680 ± 5°C (1256°F)
Transformation temperature	595 ± 3°C (1103°F)	590 ± 3°C (1094°F)
Coefficient of linear thermal expansion between 20 and 590°C (68 and 1094°F), 10^{-6}/°C	17.6 ± 0.4	20 ± 0.5
Thermal conductivity, watt/(cm)(°C)	0.093 ± 0.006	0.093 ± 0.006
Electrical resistivity, μohm-cm	77 ± 5	77 ± 5
Heat of fusion, cal/g	6.61	
Heat of fusion, cal/gram mole	1560 ± 110	
Young's modulus, dynes/cm²	9.5×10^{11}	10.2×10^{11}

International,[11] using cerium as a substitute for plutonium, indicate good agreement for melting vaporization losses in the investigation of carbide fuel processes.

Investigations continue[29] on carbon-stabilized and carbon/nitrogen-stabilized uranium–plutonium monoxide produced by the carbon reduction of mixed UO_2 and PuO_2 in helium or vacuum. A sample containing 91 wt.% (U,Pu)(OCN) was intact after a 137-hr exposure to boiling water but disintegrated in 550°F (288°C) water.

Gas–metal reaction has been used[19] to prepare (U,Pu)S solid solutions, but extended heat-treatment below 1700°C was required for homogenization. Reaction sintering of US–PuS mixed powders has produced the most promising material to date. The melting points of PuS and US are reported as 2350 ± 30°C and 2470 ± 15°C (4262 and 4478°F), respectively.

Solid solutions of UN–PuN have been prepared at Battelle–Northwest by compacting and sintering (1800°C, 4 hr, 1 atm N_2) mixed –200-mesh UN and PuN powders.[30] Irregular departure from Vegard's law was then observed for lattice parameters in the middle to high PuN compositions; also, there was an unexplained volume increase. Carbothermic oxide-reduction synthesis has not proved successful, yielding a two-phase mixture of unhomogeneous (U,Pu)N and UO_2, plus some residual carbon.

(W. M. Pardue)

Thorium

Studies in France[31] have shown that the thermal conductivity of thorium rises steadily between 60 and 95°K (108 and 171°R). It was also postulated that the rise continues between 300 and 923°K (540 and 1660°R). The results of the measurements are shown in Fig. I-1.

Measurements were also made of the thermoelectric power of high-purity van Arkel thorium between 5 and 115°K (9 and 207°R). The results are plotted in Fig. I-2, along with values obtained previously using lower purity metal. (R. L. Martin)

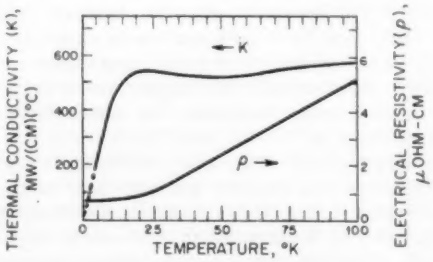

Fig. I-1 The thermal conductivity and electrical resistivity of thorium as a function of temperature between 5 and 100°K (9 and 180°R).[31]

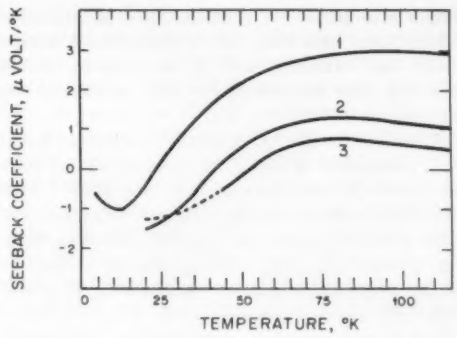

Fig. I-2 The thermoelectric power of thorium as a function of temperature between 5 and 115°K (9 and 207°R).[31] *Curve 1: present results; curves 2 and 3: results of earlier studies.*

Metal-Ceramic Fuels

Cermet Fuels (Over 50 Vol.% Ceramic Phase)

Several relations between mechanical properties and structure were formulated by Cope in a review of mechanical-property data for nuclear cermets.[32] Low- and medium-volume nuclear cermets, which possess a continuous metallic matrix and which have no real bond with the ceramic phase, are shown to resemble the matrix metal in their manner of plastic deformation and to resemble voided metal in their tensile properties. Their macroscopic ultimate tensile strength is proportional to the minimum matrix load-bearing section. The achievable strength of a well-consolidated cermet can be calculated from the minimum matrix cross-sectional area presented at an equatorial section through a plane of spheres, equivalent in volume to that of the ceramic investment, packed in a simple cube lattice. The concept of a "minimum matrix interstitial volume" is introduced, which appears to account quantitatively for the observed decrease in cermet tensile-elongation values at fracture as the ceramic volume is increased. Cermet elastic constants, and the reduction of area in the fractured zone, appear to be influenced by the comparative incompressibility of the ceramic-phase particles. (R. A. Smith)

Dispersion Fuels (Less Than 50 Vol.% Ceramic Phase)

Martin-Marietta Co. reports the development of a new fabrication process for the PM Core 3 fuel elements.[33] The method involves extruding the tubular dispersion core containing 23.6 to 42 vol.% UO_2 loadings with a suitable binder, cold hydrostatically pressing to densify the core, and final hot-gas isostatic pressing to complete the densification and the bonding of the tubular cladding to the core. This

technique eliminated (1) contamination of core-cladding interfaces with UO_2, (2) nonbond areas between the core and cladding, and (3) occurrence of UO_2-filled crack type defects in the UO_2–stainless-steel dispersion cores.

Workers at Battelle–Columbus[34] completed metallurgical evaluation of duplicate compartmented packs rolled to a 6:1 reduction at 1175 and 1200°C (2057 and 2192°F), prepared with niobium-coated ZrB_2 and uncoated ZrB_2 and atomized type 347 stainless-steel-matrix powder of −325 +500 mesh and −270 +325 mesh and irregularly shaped stainless-steel powder of −270 +325 mesh. Each specimen contained 37 wt.% UO_2 and 1 wt.% ZrB_2 in a stainless-steel matrix. The specimens rolled at 1175°C showed no adverse effects in general structure from the slightly lower rolling temperature and very little reaction between the poison particles and the stainless-steel matrix. The atomized stainless-steel-matrix powder of both mesh sizes produced superior dispersion structures compared with those obtained with irregularly shaped stainless steel. In addition, fabrication of 37 wt.% depleted UO_2 in stainless steel containing 1.2 mg boron/cm^2 of active plate surface in the form of niobium-coated ZrB_2 was initiated. Cores prepared with the atomized stainless steel showed a higher green density than those prepared from irregularly shaped stainless steel; however, they did not have adequate handling strength. Increased green-pressing pressures did not improve the green strength for the full-size cores. Consequently a study was made with various blends of irregularly shaped and atomized stainless-steel powder to find a ratio between the two powders which would provide the most satisfactory compromise between superior blending and resulting dispersion structure of atomized powder and the interlocking strength of the irregular particles. Results indicated that a blend of 12% irregular and 88% atomized powders produced a good dispersion with 37 wt.% UO_2 and satisfactory green strength to permit handling when green pressed at 42 kg/mm^2 (30 tsi).

Coated-Particle Fuel Materials

Particle Coating

Oak Ridge has issued a report[35] based on computer-produced selection of reviews of recent reports, articles, and patents on coated nuclear-fuel particles. As judged by the number of available reports, pyrolytic carbon (PyC) coatings are currently of most interest.

In related work, problems concerned with the carbon coating of large-diameter (530 μ) uranium carbide particles in a 1-in.-diameter fluidized-bed unit are being investigated.[36] Complications associated with nonisothermal coating conditions resulting from high fluidizing-gas throughputs are discussed. For reproducible results, isothermal systems are recommended. With CH_4 as the coating reactant, the upper temperature limit of the isothermal system is 1600°C (2912°F). In the isothermal system it is reported to be possible to deposit PyC coatings of the same type on both the 520- and 200-μ-diameter particles. During deposition of porous PyC coatings from acetylene on 460-μ-diameter ThO_2 particles, it was found that a significant temperature rise within a 1-in.-diameter bed occurred on initiation of the coating reaction. The temperature rise, caused by the exothermic pyrolysis of the acetylene, measured in one case was 70°C (126°F) on the reactor wall and 190 to 225°C (342 to 405°F) within the bed. It is suggested that, with a number of thermocouples located in the bed, the areas of high deposition rates can be identified.

Evaluation of low-density, porous PyC coatings (about 0.6 g/cm^3) has revealed[37] that the coating can be deformed as much as 35% before crushing, whereas coatings with intermediate or high densities could be deformed only 15%. (N. D. Veigel)

Irradiation and Evaluation of Coated-Particle Fuels

A large number of PyC-coated dense $(Th,U)C_2$ and porous $(Th,U)O_2$ particles have been examined by General Atomic[38] to study the effects of coating structure and thickness on the integrity of the coating. These fuels were irradiated at 1350 to 1700°C (2460 to 3090°F) to burnups of 10 to 13% of the fissionable atoms. Each of the coatings evaluated had an inner buffer (or sacrificial) layer, and the total coating thicknesses varied from 85 to 190 μ. Type BISO used a porous buffer layer with an isotropic outer coating; type ISO–ISO used an isotropic buffer layer with a similar outer coating.

The integrity of the coating increased with increasing coating thickness (with constant fuel-particle diameter). Extrapolation of the data indicated that a minimum coating-thickness to fuel-particle-diameter ratio (T/D) of 0.5 may be required for stable coatings under these high-temperature irradiation conditions. It appeared that the isotropic buffer layer was roughly equivalent in stability to the porous buffer layer. Thick buffer layers appeared to be more effective than thin buffer layers (with the same total coating thickness) for enhancement of radiation stability.

The effectiveness of an inner buffer layer toward improving coating integrity has also been observed by workers at Oak Ridge.[36] From postirradiation examinations of 10 samples of PyC-coated UO_2 and $(Th,U)C_2$ particles irradiated in sweep-gas experiments, they concluded that the primary radiation damage to PyC is from fission recoils, and an inner porous layer is very beneficial. This layer acts as a

sacrificial material which protects the outer coating and shrinks during irradiation to form an internal void space.

From these and other experimental results at Oak Ridge with coated oxide fuels,[39] it was concluded that UO_2 particles are superior to UC_2 particles for the following reasons: (1) UO_2 does not flow into cracks and voids as does UC_2, so that the gap between the core and coating is maintained; (2) UO_2 does not diffuse into PyC as does UC_2, even at 1800 to 2000°C (3272 to 3632°F); (3) uranium contamination in the coating is kept to a lower level during fabrication with UO_2 cores; and (4) UO_2 is less reactive and therefore easier to handle during fabrication.

In another series of experiments at Oak Ridge,[40] nine types of PyC-coated fuel particles were studied as part of the Gas-Cooled Reactor program. About 500-μ-diameter particles of UC_2, $(U,Th)C_2$, or $(U,Th)O_2$ fuel were coated with either two-layer (duplex) or three-layer (triplex) PyC. The particles were supplied by three vendors and Oak Ridge. Dimensions, densities, coating contamination, and coating structure were determined before irradiation. The exposures were made in the Oak Ridge Research Reactor in continuously monitored sweep-gas experiments at temperatures from 1000 to 1370°C (1832 to 2500°F), with burnups to 20 at.% of the uranium. Fractional fission-gas release rates from 10^{-3} to 10^{-6} were measured. In two tests 1% of the coatings failed. The duplex coatings had spearhead cracks and reactions at the fuel core–coating interface. The triplex coatings did not show this effect. The fission gas released from intact particles appeared to be a result of uranium contamination in the coating.

Results from over 70 fuel compacts examined metallographically at Harwell[41] have shown that PyC–SiC–PyC coatings on $(Th,U)C_2$ fuel particles withstand a wide range of irradiation conditions, including temperatures of 800 to 1600°C (1472 to 2912°F) and burnups of 0.2 to 10% of the fissionable atoms, without signs of failure. The few results on solid-fission-product release show a reduction in the release of strontium by a factor 10 to 100 below that through plain PyC coatings. Long-lived fission-gas release from these particles is on the order of 10^{-5} (R/B) at 1000°C and 10^{-4} at 1500°C (2732°F). Evidence suggests, however, that the actual release from intact particles is as low as 10^{-6} at 1300°C (2372°F) and that the observed release comes from the 1% of the particles that were broken during either fabrication or handling.

In a unique irradiation experiment at Los Alamos,[42] capsules containing extruded-graphite-matrix fuel samples were exposed to the neutron pulse generated by the Kiwi Transient Nuclear Test (Kiwi-TNT). The fuel compacts were loaded with 19 different types of PyC-coated UC_2 and UO_2 particles. The effects of neutron flux, fuel composition, core diameter, coating thickness, and sample temperature on the graphite-matrix damage and the coated-particle damage were investigated. From visual, metallographic, and radiographic examinations of the recovered samples, it was concluded that: (1) the total energy deposition was by far the most significant variable, giving complete destruction of the samples at the highest fission-rate levels and little or no change at the lowest; (2) particles with large core sizes showed more damage than those with small cores; (3) neither coating thickness nor sample temperature significantly affected damage; and (4) particles with UO_2 cores were more easily damaged than those with UC_2 cores, because of the high CO_2 pressures produced at the very high temperatures reached in the carbon-coated UO_2 particles. (N. E. Miller)

Uranium and Thorium Oxides

Fabrication

Canadian investigators[43] are conducting low-temperature hydrogen sintering studies on large UO_2 pellets that have been prepared from powders containing oxygen/uranium ratios of 2.3. It is much easier to obtain high-density pellets during low-temperature sintering when a dilute hydrogen atmosphere is utilized. It is postulated that, when a dilute reducing atmosphere is utilized, the sintering rate is enhanced as a result of the longer dwell time in the hyperstoichiometric state. Because the pellet is fully sintered while still hyperstoichiometric and reduction to $UO_{2.00}$ is relatively slow, acceptable pellets can be easily fabricated by this technique.

The same investigators have produced pellets having densities of 95% of theoretical by grinding ThO_2 powder for 20 min in a tungsten carbide vibratory mill, green pressing, and sintering for 4 hr at 1650°C (3000°F). (T. R. Wright)

Properties and Behavior of Uranium Oxide Fuels

Measurements by General Electric[44] on the vapor pressure of urania are summarized in Fig. I-3, along with earlier results by Ackermann et al., for near-stoichiometric UO_2. The Ackermann equation, used to plot the broken line, came from data for temperatures below 2000°K (rather than from data for the 2500-to-2900°K range shown). The melting points[45] of hypostoichiometric UO_2 were measured, with the results shown in Fig. I-4. The data points are averages of several determinations, with a mean deviation of less than 10°C.

Kubit, McClintock, and Ferrari[46] have studied the behavior of water vapor in UO_2 fuel elements clad with type 304 stainless steel. Their results are summarized in Fig. I-5. The hydrogen formed from decomposition of water vapor initially absorbed in

the fuel decreases with continuing irradiation. This observation can be attributed to reaction of the hydrogen with fission-product zirconium to form a solid phase. As burnup increases, the amount of fission-product zirconium formed is more than enough to account for the observed hydrogen decrease. The calculated partial pressure of hydrogen near the beginning of the hydriding process is 6.25 atm at 500°C.

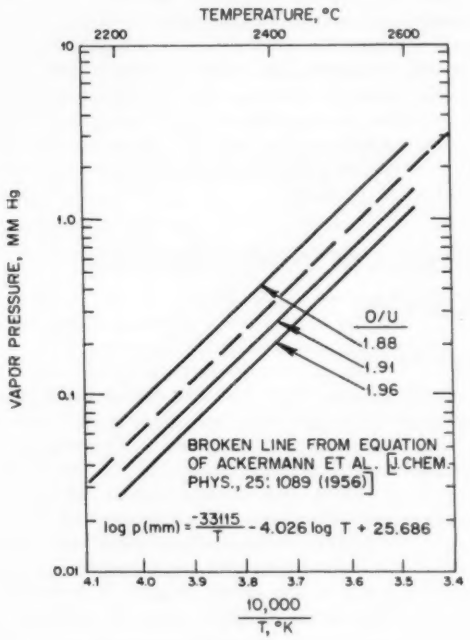

Fig. I-3 Vapor pressure of urania.[44]

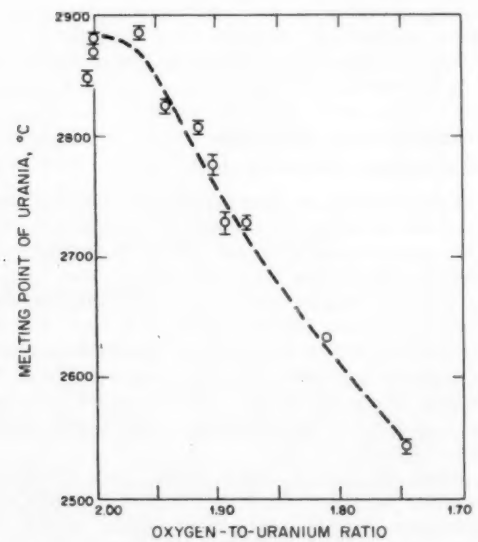

Fig. I-4 Melting point of UO_{2-x}.[45]

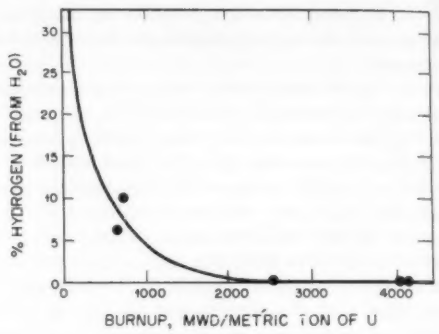

Fig. I-5 Reaction of water vapor in UO_2 fuel during irradiation.[46]

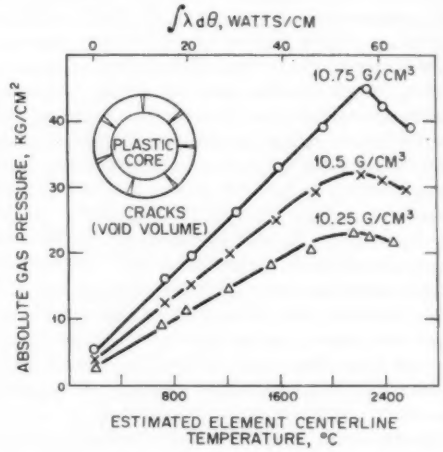

Fig. I-6 Variation of gas pressure with heat rating (or UO_2 temperature).[47] *Element void volume on assembly, 1.7 cm^3 (2.5%). Elements prefilled with 10 cm^3 xenon. Burnup 600 Mwd per metric ton of uranium.*

The Canadians[47] have measured fission-gas pressures in UO_2 fuel elements during irradiation. These elements consisted of sintered UO_2 pellets with densities ranging from 10.25 to 10.72 g/cm^3 and clad with thin, collapsible, stainless-steel sheaths. Void volume in the elements was estimated to be less than 2.5% of the total fuel volume. Details of the results are shown in Figs. I-6 and I-7. The decrease in pressure at high temperatures shown in Fig. I-6 is thought to be a consequence of fuel expansion, with a resulting increase in the volume of the cracks in the outer regions of the fuel.

Measurements of uranium self-diffusion in urania were performed in France,[48] using alpha-particle

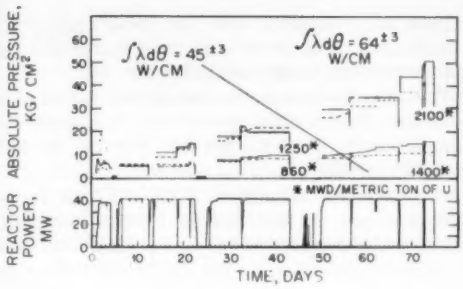

Fig. I-7 Variation in fission-product gas pressure during continued operation.[47] UO_2 density: —10.25 g/cm³; ···10.5 g/cm³; ---10.75 g/cm³.

spectrometric techniques. For stoichiometric UO_2, the self-diffusion coefficient for uranium was 5×10^{-16} cm²/sec at 1700°C (3092°F). Higher diffusion coefficients were observed for hyperstoichiometric oxides.

(R. H. Barnes)

Uranium Carbides, Nitrides, Phosphides, Sulfides, and Arsenides

Properties and Behavior

Los Alamos[49] found that a eutectic exists between the UC_2–YC_2 solid solution containing 15 mole % YC_2 and graphite at a temperature of 2420°C (4388°F). The YC_2–graphite eutectic is placed at 2275°C (4127°F), suggesting a quasi-binary eutectic trough between the dicarbide solid solution and graphite most of the way across this ternary system.

Davidson, Riley, and Taub[50] have studied the compatibility of ZrC–18 mole % UC with molybdenum, niobium, and tungsten. Allinson and Rivière[51] have studied the compatibility of molybdenum, niobium, tungsten, tantalum, and rhenium with ZrC–50 mole % UC. With molybdenum, the former investigators report liquid-phase sintering at 1800°C (3272°F); the latter investigators report considerable reaction at 1860°C (3380°F). With niobium, both investigations showed severe reaction at 1800 and 1750°C (3272 and 3182°F), respectively. With tungsten, the former investigators suggest a solution of tungsten into the carbide; the latter investigators observed no reaction at 2080 or 2170°C (3776 or 3938°F). The latter investigators observed a reaction of the carbide with tantalum at 2190°C (3974°F) but no reaction of carbide with rhenium at 2100°C (3812°F).

Using the technique of constitutional control of the activity of carbon in the three-phase region, UC–UFe_2–Fe, Herbst and Jordan noted[49] that a UC–Fe mixture containing less than 50 at.% carbon did not react with type 316 stainless steel after 1500 hr at 750°C (1382°F), whereas unalloyed UC containing less than 50 at.% carbon reacted with stainless steel in 24 hr at 750°C.

The reaction of UC–20 mole % PuC with various potential fast-reactor structural materials has been studied by Argonne workers.[52] They found no reaction with chromium and tungsten in seven days at 1100°C (2012°F). A 4- to 8-μ thick continuous reaction layer formed on molybdenum, niobium, and tantalum in seven days at 1100°C. Severe reaction or melting was observed with type 304 stainless steel, Hastelloy X, and vanadium at 1100°C. Stainless steel showed no reaction, and Hastelloy X showed 8 μ of reaction with the fuel in 42 days at 800°C (1472°F). The discrepancy between the results of Herbst and Jordan and those of Argonne workers with regard to the compatibility of carbides with stainless steel is as common as the number of investigations of this system. A patent that claims to offer an explanation for some of these discrepancies has been issued to Webb.[53]

The effect of reducing the carbon content of UC (thus permitting free uranium to exist) in lowering the hot hardness (and hence the high-temperature strength) of the UC and the effect of tungsten additions in improving its high-temperature strength were confirmed by workers at Atomics International,[54] as indicated in Figs. I-8 and I-9. Similarly, the effect of stoichiometry on the high-temperature

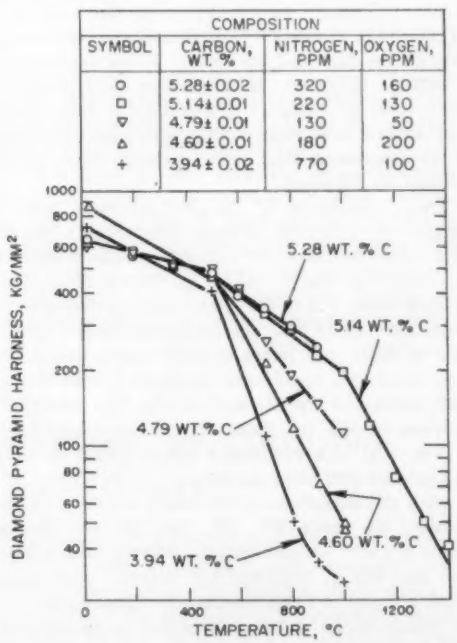
COMPOSITION
SYMBOL | CARBON, WT. % | NITROGEN, PPM | OXYGEN, PPM
○ | 5.28±0.02 | 320 | 160
□ | 5.14±0.01 | 220 | 130
▽ | 4.79± 0.01 | 130 | 50
△ | 4.60± 0.01 | 180 | 200
+ | 3.94 ± 0.02 | 770 | 100
DIAMOND PYRAMID HARDNESS, KG/MM²
5.28 WT. % C
5.14 WT. % C
4.79 WT. % C
4.60 WT. % C
3.94 WT. % C
TEMPERATURE, °C

Fig. I-8 Hot hardness of UC, as affected by change in carbon content.[54]

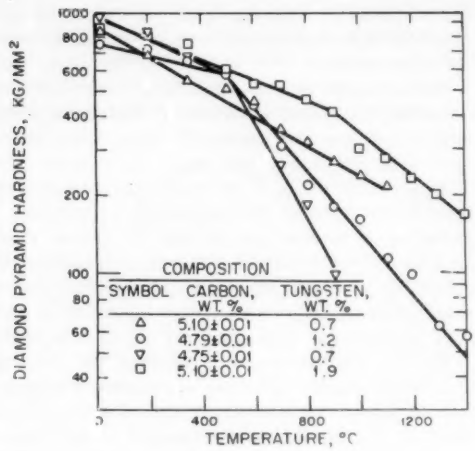

Fig. I-9 Hot hardness[54] of tungsten-doped UC.

short-term, compressive yield strength of UC was demonstrated by Nelson and Foster.[55] The results, shown in Figs. I-10 and I-11 also illustrate the relatively superior strength of U_2C_3 as compared with UC, UC_2, and mixtures of UC and UC_2. Free uranium is believed to be responsible for the poor strength of the 4.6 wt.% carbon alloy.

Stachura, Cordy, and Silberberg have continued their experiments with UC in the Transient Reactor Test, TREAT.[56] An excursion to the melting point of UC, 2450°C (4442°F), produced no gross deformation of the fuel and no change in the stainless-steel cladding. However, an excursion to a temperature over 3100°C (5612°F) dispersed the fuel, cladding, and sodium bond rather uniformly within the capsule. It is suggested that local sodium-vapor pressure caused the dispersal.

Four specimens of $(U_{0.8}Pu_{0.2})C$ have been irradiated[57] to a burnup of over 11% of the metal atoms (3.8×10^{21} fissions/cm³) at an average surface temperature of 600°C (1112°F). Diameter changes ranged from 1.9 to 6.0%, and density changes ranged from 13.6 to 18.3%. The stainless-steel cladding on two of these specimens became brittle and ruptured. The other two specimens were clad in niobium, and this remained ductile and intact. The reported gas release of 30% for these specimens seems high for a fuel that was recovered either intact or in large pieces and with little swelling.

With the exception of UP, which oxidizes relatively slowly, the fuels UC, UN, UP, US, and UAs ignite when heated[58] as powders in flowing oxygen between 300 and 400°C. The fuel UN reacts[59] with oxygen to form a layer of U_2N_3, sandwiched between the UN and an outer layer of UO_2. At higher temperatures UC has been observed to form a two-phase layer of UC_2 and UO_2, sandwiched between the UC and an outer layer of UO_2. In these two cases it appears that the oxygen is combining with the metal and that the metalloid is being freed or at least driven to a higher activity without being oxidized.

The UP–US system is a complete series of solid solutions. The melting points vary in a nearly linear fashion from 2575°C (4667°F) for UP to 2465°C (4470°F) for US.[60]

The thermal diffusivity of US was approximately 0.05 cm²/sec at 200°C (392°F), 0.07 cm²/sec at 800°C (1472°F), and 0.08 cm²/sec at 1200°C (2192°F).[61]

(W. Chubb)

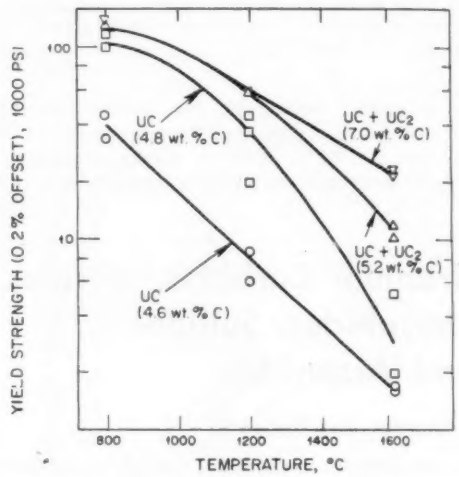

Fig. I-10 The 0.2% offset yield strength of uranium–carbon alloys as a function of temperature.[55] ▽, UC + UC_2 (7.0 wt. % carbon); △, UC + UC_2 (5.2 wt. % carbon); □, UC (4.8 wt. % carbon); ○, UC (4.6 wt. % carbon).

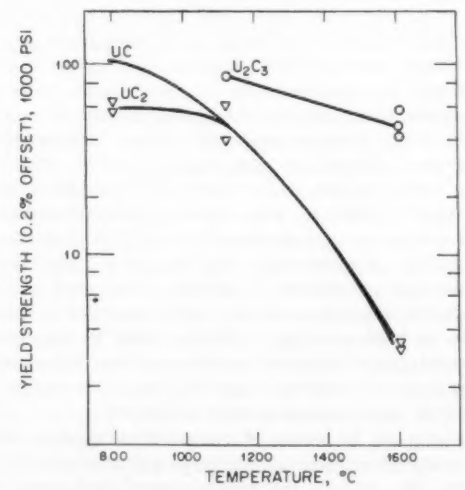

Fig. I-11 The 0.2% offset yield strength of UC, U_2C_3, and UC_2 as a function of temperature.[55] ○, U_2C_3; ▽, UC_2.

Fabrication

McLaren and Atkinson[62] at Harwell studied the effects of particle size, compacting pressure, sintering temperature, and sintering time on the final sintered density of UN. Conclusions drawn were: (1) UN can be sintered to approximately 95% of theoretical density in argon at 1700°C (3092°F), (2) sintered density varies considerably with sintering temperature up to 1700°C, and (3) increasing the compacting pressure has a beneficial effect over the pressure range of 20 to 80 tsi.

In other work at Harwell, Harder, Read, and Sowder[63] investigated the reduction and sintering of hyperstoichiometric carbides in hydrogen. The authors studied the sintering and removal of excess carbon from hyperstoichiometric UC, (U,Pu)C, Pu_2C_3, and $UC-Pu_2C_3$ mixtures in hydrogen.

Workers at Argonne[28] have continued to conduct experiments on the synthesis of UC and UN powders. Experiments indicate that the production of acceptable UC product by the fluidized-bed technique will require (1) the reduction of the oxygen content, which has been running from 0.5 to 1.2 wt.%, and (2) increasing the fluidized-bed temperature to 750°C (1382°F) or higher to complete the reaction $U(solid) + CH_4(gas) \rightarrow UC(solid) + 2H_2(gas)$ in reasonable time. Thermodynamic calculations indicated that carburization can be limited to the formation of the monocarbide by the selection of suitable hydrogen-to-carbon atom ratios in the fluidizing gas (e.g., >49.0 at 750°C).

The synthesis of UN, by reacting uranium shot or turnings with nitrogen, in which the bulk of the nitridation takes place above 1150°C (2100°F), produces UN that can be ground to powder having a bulk density of 7 to 8 g/cm³. In comparison, the bulk density of UN synthesized by reacting uranium turnings at 800 to 900°C (1472 to 1702°F) and denitriding at 1100 to 1400°C (2282 to 2552°F) under vacuum is 4 to 5 g/cm³. If oxygen contamination occurs during the grinding operation, the bulk density of the powder is drastically reduced. The objective of the program is to produce a high-bulk-density UN powder, which is a prerequisite for satisfactory sodium–UN paste preparation. (D. S. Acuncius)

Fuel–Water Reactions

Results of the fuel–water reaction experiments conducted during the Kiwi-TNT destructive test in January 1965 in Nevada have now been reported by Argonne.[20] This test afforded an opportunity to obtain metal–water reaction data during a short-period (0.6 msec) transient. The Kiwi-TNT transient gave nearly adiabatic heating, thus simulating a very "fast" reactor excursion.

Prior to the Kiwi-TNT power excursion, capsules containing typical reactor fuel materials were placed at various distances from the reactor. The data on the extent of uranium–water reaction for the unclad-uranium-alloy (5 wt.% zirconium, 1.5 wt.% niobium) pins are given in Table I-5. The extent of reaction of uranium with water was determined by analyses of the meltdown residues, rather than by direct hydrogen measurement. This was necessary because the hydrogen-sampling valves had been damaged during the Kiwi-TNT destructive test.

Table I-5 METAL–WATER REACTION DATA FOR URANIUM ALLOY* FUEL SUBJECTED TO KIWI-TNT SHORT-PERIOD TRANSIENT[20]

Test	Distance,† ft	Estimated fission-energy input, cal/g	Estimated peak adiabatic core temperature‡ °F	°C	Condition of fuel after transient	Metal–water reaction, %	$d_{s/v}$,§ mils
1	2/3	420	6872	3800 (L + V)	Fragments and fine particles	77	6
2	2	200	6872	3800 (L + V)	Completely melted into fine particles	76	3
3	3	125	4532	2500 (L)	Fragments and fine particles	52	6
4	3.5	100	3992	2200 (L)	Melted into globules and fines	65	21
5	5	63	2071	1133 (L)	Melted into globules and fines	21	19
6	6	50	2071	1133 (S + L)	Partially melted	3.4	98

*Uranium–5 wt.% zirconium–1.5 wt.% niobium, 20% enriched, 0.2 in. in diameter by 0.5 in. long.
†Distance between autoclave and reactor vessel.
‡Physical state of sample at that temperature indicated by V (vapor), L (liquid), and S (solid).
§Mean volume-to-surface particle size of fragmented sample.

The data show a clear increase in the amount of chemical reaction with increasing peak uranium temperatures. In addition, the Kiwi-TNT results are generally consistent with two other, quite independent, sets of data on high-temperature uranium–water reactions. These are TREAT meltdown experiments and condenser-discharge tests previously reviewed. (A. W. Lemmon, Jr.)

Mechanism of Corrosion of Fuel Alloys

An electrochemical corrosion mechanism was proposed by Harwell to account for the improved resistance to water and steam resulting from additions of iron to UC.[64] On the basis of the results of anodic polarization studies and galvanic couple tests, it was concluded that the UC was anodically polarized by the cathodic iron additions. Hydrogen, which was thought to be responsible for the rapid corrosion of unalloyed

UC, was believed to collect on the cathodic iron phase, thus lowering the attack on the carbide matrix.
(W. E. Berry)

Basic Studies of Irradiation Effects in Fuel Materials

Metals

In an Argonne report[65] the surface-diffusion migration of an isolated pore in a solid is analyzed in detail. The results, which are similar to earlier results, are applied in analyses of bubble coalescence during postirradiation annealing. Coalescence is considered as resulting from: (1) random migration of bubbles, in which case the results confirm earlier results that the mean bubble radius should be proportional to $t^{1/5}$ (time); and (2) biased migration (migration with a driving force) of bubbles. In the latter case the predicted mean radius increases linearly with time. In both cases the bubble-size distribution is calculated and used to predict the swelling of the solid, which is about 15% greater in the first case, and up to 65% greater in the second case, than predicted by approximate treatments based on change in the mean bubble radius with time.

At Harwell[66] replicas taken from cathodically vacuum etched and fractured surfaces have been compared with the results from thin-film electron microscopy to determine the limitations of each technique. Cathodic etching enlarges bubbles approximately 150 A in diameter by a factor of approximately 2; only cleavage surfaces from the fracture produces results comparable with the bubble-size distributions obtained by using other techniques. With bubbles less than 500 A, the thin-film technique is no longer reliable. The results give an experimental value for the surface energy of alpha uranium of 1000 ergs/cm^2.

A study made in Russia[67] considers a new cause of macrostresses in fuel elements, namely, uneven swelling of the fissioning material brought about by the fact that the fission products are not produced at equal rates over the cross section of the fuel element. The resulting stresses are calculated under certain simplifying assumptions, using a fuel element in the form of a long, solid, cylindrical rod as an example. The joint action of the stresses due to uneven swelling and the thermal stresses is considered for brittle material, for plastic material with negligible creep (metal at relatively low temperature), and plastic material with appreciable creep (relatively high temperature level). It is shown that the uneven swelling must be taken into account in the strength calculations in the cases of brittle material and material with negligible creep

The plastic deformation of alpha-uranium monocrystals was studied by the Soviets,[68] using various crystallographic orientations and various temperatures. An explanation is given for the shape of the stress–strain curves as a function of the action of the basic systems of plastic deformation. The monocrystals were irradiated by neutrons in a reactor at temperatures up to 100°C (212°F) with integrated fluxes up to 4×10^{20} neutrons/cm^2. It was shown that irradiation increases the critical shearing stress in the (0 1 0) plane by factors of 3 to 5 and decreases the relative linear expansion and the region of light slip. Annealing of monocrystals irradiated with up to 5.5×10^{17} neutrons/cm^2 leads to recovery of the mechanical properties.

Indices for predicting anisotropic irradiation growth in uranium based on the preirradiation measurements of thermal expansion, electrical resistivity, and X-ray diffraction were correlated by the British[69] with the dimensional changes encountered in uranium irradiated in the burnup range of 0.04 to 0.12% of the heavy atoms at a temperature of 260 ± 5°C (500 ± 9°F). The specimens were taken from the rim and core of uranium rods and comprised core electropolished, rim electropolished, and rim machined groups. The correlation coefficients between actual irradiation growth and that predicted from the indices of expansivity and resistivity were highly significant, but that from the X-ray index was rather less so. Regression equations for predicting radioinduced length change were derived from analysis of the experimental data, and these were found to be superior for prediction purposes to the growth indices in this range of burnup. In view of the different textures and irradiation behaviors of the three group classifications, it was recommended that prediction equations, derived separately for each group of specimens, be used.

Ceramics

Studies in Israel[70] show that, when the fraction of gas released from a powder is so large that the smallest particles are largely depleted, the commonly used equivalent sphere model for calculating diffusion coefficients from the experimentally measured release is not valid. An approximate model was formulated which takes into account the continuous depletion of small grains. On the basis of this model, a multiplying function M was derived for correcting diffusion coefficients obtained by the equivalent sphere model.

The emission of ^{133}Xe from UO_2/Y_2O_3 and ThO_2/Y_2O_3 solutions containing up to 30 mole % yttrium oxide has been investigated by the British[71] by heating in the range 800 to 1600°C (1472 to 2912°F) after a short irradiation. It was concluded that the migration of ^{133}Xe in these systems does not rely on the presence of vacancies on the oxygen sublattice. The results of a series of experiments on the emission of ^{133}Xe from a stressed sample of uranium dioxide suggest that dislocations in the lattice play no part in the migration of ^{133}Xe.

In West Germany,[72] study of diffusion of rare gases in KF, KCl, and KI indicate that an interstitial mechanism governs migration in KF at all temperatures and in KCl and KI at high temperatures. Another German study[73] employed two methods of measuring diffusion of ^{133}Xe in UC in the temperature range between 950 and 1830°C (1742 and 3326°F). Continuous measurements were made in high vacuum, and discontinuous measurements were made with a gas stream. Results from both methods were in agreement. The activation energy of xenon diffusion was 54 to 82 kcal/mole.

Pratt & Whitney Aircraft[74] developed a technique for studying the migration of inert gases in nuclear fuels, using ion bombardment and replication electron microscopy. Helium atoms were agglomerated into 100 to 5000 A bubbles that moved up a temperature gradient. The velocity, which was found to be inversely proportional to the bubble size, indicated a surface-diffusion-controlled mechanism.

In Japan[75] the release behavior of fission gases in uranium metal, UO_2, and uranium carbides, irradiated at a relatively low temperature (below 100°C) to low dosage, was studied in out-of-pile experiments. Fission gas (^{133}Xe) released from a specimen by fission-fragment recoil is mostly captured in the wall of the irradiation capsule or in the specimen support structure. The amount of fission gas released into the void space of the capsule is proportional to the surface area and to the fuel burnup and is controlled by a knockout release mechanism. The number of uranium atoms considered to take part in the knockout mechanism by evaporation or displacement due to the intrusion of a recoil fission fragment is estimated to be about 1.4×10^5 to 2.5×10^5 atoms for uranium metal and about 5×10^4 to 10×10^4 atoms for UO_2 and uranium carbides.

Rogers[76] studied mass transport and grain growth by fission fragments in thin films of UO_2. An average fission fragment leaving the surface ejects about 5×10^4 uranium atoms from vacuum-deposited UO_2 of 50 A grain size. Atoms are ejected as vapor from uranium-deposited thin films of UO_2 owing to ionization and heating in the path of the fission fragment and not as discrete particles due to displacement spikes, as was found in the case of solid uranium metal. Fission fragments cause grains to grow in vacuum-deposited UO_2, owing to ionization and heating, in a region containing about 1.5×10^7 uranium atoms. The initial high rate of ejection falls to a low value owing to irradiation grain growth.

Irradiation of ZrO_2-UO_2 fuels by Bettis workers[77] resulted in homogenization of the cubic and tetragonal phases present in ZrO_2 + 46 wt.% UO_2 by 5×10^{20} fissions/cm^3. The homogenization can be satisfactorily defined by a diffusion equation, if a value for the diffusion constant $D = 3.32 \times 10^{-14}$ cm^2/sec is used. This D value indicates that a single fission homogenizes a volume containing 1.66×10^7 atoms. This number is two orders of magnitude too large to be explained by Brinkman's displacement-spike hypothesis. Calculations based on Konobeevsky's hypothesis of a thermal pulse show that the liberation of 23 Mev of thermal energy at the center of such a volume is sufficient to cause homogenization. This seems well within the capabilities of a fission event.

(F. A. Rough)

References

1. A. Garlick and D. Shaw, The Thermal Conductivity of Irradiated Uranium, *J. Nucl. Mater.*, 16: 333-340 (1965).
2. C. F. St. John and E. Teghtsoonian, Grain Size Dependence of Fracture in α-Uranium, *J. Nucl. Mater.*, 17: 111-115 (1965).
3. C. L. Angerman and R. T. Huntoon, Network Structures in Uranium and Its Alloys, USAEC Report TID-21760, Savannah River Laboratory, Mar. 19, 1965.
4. R. D. Bland, J. E. McDonald, and D. M. Mattox, Ion-Plated Coatings for the Corrosion Protection of Uranium, USAEC Report SC-DR-65-519, Sandia Corp., October 1965.
5. R. D. Townsend and J. Burke, The M_s Temperature for Pure Uranium, *J. Nucl. Mater.*, 17: 279-281 (1965).
6. D. J. Drobnjak, Surface Structure in Beta-Quenched Uranium, *J. Nucl. Mater.*, 17: 37-42 (1965).
7. A. G. Crocker, The Crystallography of Deformation Twinning in Alpha Uranium, *J. Nucl. Mater.*, 16: 306-326 (1965).
8. A. F. Smith, The Isothermal Growth of UAl_2 Precipitates in Uranium Containing 250 ppm Iron and 700 ppm Aluminum, *J. Less-Common Metals*, 9: 233-243 (1965).
9. R. D. Townsend and J. Burke, The Effects of Thermal History on the Kinetics of the Phase Change in Uranium and Uranium-Chromium Alloys, *J. Nucl. Mater.*, 17: 215-266 (1965).
10. W. A. Althaus, M. M. Cook, and R. J. Bieker, A Study of As-Cast and Heat-Treated Uranium–Uranium Carbide Alloys by Optical and Electron Microscopy, USAEC Report NLCO-968, National Lead Co. of Ohio, February 1966.
11. Atomics International, Quarterly Technical Progress Report, AEC Unclassified Programs, July–September 1965, USAEC Report NAA-SR-11650, Dec. 22, 1965.
12. J. B. Darby, Jr., A. F. Berndt, and J. W. Downey, Some Intermediate Phases in the Thorium-Technetium and Uranium-Technetium Systems, *J. Less-Common Metals*, 9: 466-468 (December 1965).
13. G. Petzow and O. A. Sampaio, A Contribution to the Constitution of Uranium-Rich Uranium–Cobalt–Manganese Alloys (in German), *Z. Metallk.*, 56: 503-508 (August 1965).
14. W. Uhlmann, Radiation Effects on Solid, Uranium-Based Nuclear Fuel Materials, Vol. 5, No. 3, A Bibliography, Swedish Report VDDIT-16 (5.3), November 1965.
15. C. L. Angerman and G. R. Caskey, Jr., Irradiation Behavior of Zr–U Driver Tubes for HWCTR, USAEC Report DP-994, Savannah River Laboratory, October 1965.
16. Los Alamos Scientific Laboratory, Quarterly Status Report on Advanced Reactor Technology (ART) for Period Ending January 31, 1966, USAEC Report LA-3482, February 1966.
17. Nuclear Materials and Equipment Corp., Growth of Single Crystals of Plutonium, Progress Report October 1–December 31, 1965, USAEC Report NUMEC-3428-17, Feb. 1, 1966.
18. J. M. Taylor, Physical Properties of Several Plutonium-Base Intermetallic Compounds, USAEC Report BNWL-SA-385, Battelle–Northwest, Nov. 1, 1965.
19. Argonne National Laboratory, Reactor Development Program Progress Report, January 1966, USAEC Report ANL-7152, Feb. 24, 1966.

20. Argonne National Laboratory, Reactor Development Program Progress Report, December 1965, USAEC Report ANL-7132, Jan. 25, 1966.
21. P. Barthelemy and R. Boucher, Study of U-Pu-Fe Alloys (Masurca Critical Experiment), USAEC Report ANL-Trans-224 from French Report CEA-R-2792, 1965.
22. H. R. Longfield, unpublished, October 1965.
23. W. L. Lyon and W. E. Baily, The Melting Point of Plutonia–Urania Mixed-Oxide Fuels, *Trans. Am. Nucl. Soc.*, 8(2): 376 (November 1965).
24. R. E. Bardsley and R. E. Lyon, Preparation of UO_2–PuO_2 Spheres. USAEC Report BNWL-SA-413, Battelle–Northwest. Nov. 15, 1965.
25. W. D. Burch (Comp.), Transuranium Quarterly Progress Report for Period Ending February 28, 1965, USAEC Report ORNL-3880, Oak Ridge National Laboratory. January 1966.
26. Nuclear Materials and Equipment Corp., UO_2–PuO_2–ZrO_2 Fuel Development Program Progress Report, October 1–December 31, 1965, USAEC Report NUMEC-3505-11. Jan. 25, 1966.
27. W. G. Tope, Production of Plutonium Monocarbide by Reaction of Elemental Plutonium and Carbon, USAEC Report ANL-6969, Argonne National Laboratory, July 1965.
28. Argonne National Laboratory, Chemical Engineering Division Semiannual Report, January–June 1965, USAEC Report ANL-7055, October 1965.
29. R. L. Forbes, N. Fuhrman, J. Andersen, and K. Taylor, Study of Uranium–Plutonium Monoxides. Quarterly Progress Report, July 1–September 30, 1965, USAEC Report UNC-5138, United Nuclear Corp. and The Carborundum Co., Oct. 30, 1965.
30. E. T. Weber, UN–PuN Solid Solution Studies, USAEC Report BNWL-SA-414, Battelle–Northwest, Oct. 14, 1965.
31. P. Haen and G. T. Meaden, The Thermal Conductivity, Thermoelectric Power, and Electrical Resistivity of Thorium Between 5 and 100°K, *Cryogenics*, 5: 194-198 (August 1965).
32. L. H. Cope, The Mechanical Properties of Nuclear Cermets, *Metallurgia*, 72: 165-177 (October 1965).
33. W. Brittain et al., Tubular Core Development Program–PM Core 3 Materials and Processes Status Report MND-2706-13, Martin-Marietta Co., Nuclear Division, December 1964.
34. D. L. Keller, Progress Relating to Civilian Applications During February 1966, USAEC Report BMI-1765, Battelle Memorial Institute, Mar. 1, 1966.
35. R. L. Pilloton, Machine-Assembled Reviews on Coated Nuclear Fuel Particles, USAEC Report ORNL-TM-1335, Oak Ridge National Laboratory, December 1965.
36. Oak Ridge National Laboratory, Gas-Cooled Reactor Program Semiannual Progress Report for Period Ending September 30, 1965, USAEC Report ORNL-3885, February 1966.
37. Oak Ridge National Laboratory Status and Progress Report, December 1965, USAEC Report ORNL-3911, Jan. 6, 1966.
38. C. S. Luby, Description and Results of the P9 Coated Particle Irradiation Experiment, USAEC Report GA-6485, General Atomic Division, General Dynamics Corp., Sept. 15, 1965.
39. R. G. Wymer and J. H. Coobs, Preparation, Coating, Evaluation, and Irradiation Testing of Sol-Gel Oxide Microspheres. USAEC Report ORNL-P-1725, Oak Ridge National Laboratory, Sept. 27, 1965.
40. J. G. Morgan, P. E. Reagan, and E. L. Long, Jr., Evaluation and Irradiation Effects Studies on Pyrolytic-Carbon-Coated Fuel Particles, USAEC Report ORNL-3923, Oak Ridge National Laboratory, March 1966.
41. Report on Work at AERE for the DRAGON Project, April–October 1965, British Report DP-Report-397, December 1965.
42. W. U. Geer, C. G. Hoffman, and J. F. Kerrisk, The Behavior of Coated Particles in a Large Nuclear Transient (Kiwi TNT), USAEC Report LA-3367, Los Alamos Scientific Laboratory, Sept. 1, 1965.
43. Atomic Energy of Canada Ltd., unpublished, Dec. 31, 1965.
44. General Electric Company, Nuclear Materials and Propulsion Operation, High-Temperature Materials Program Progress Report No. 54, Part B, USAEC Report GEMP-54B, Dec. 20, 1965. (Classified)
45. R. E. Latta and R. E. Fryxell, Determination of the Melting Point of UO_{2+x}, *Trans. Am. Nucl. Soc.*, 8(2): 375 (November 1965).
46. C. J. Kubit, D. R. McClintock, and H. M. Ferrari, The Behavior of Water Vapor in UO_2 During Irradiation, *Trans. Am. Nucl. Soc.*, 8(2): 429 (November 1965).
47. M. J. F. Notley, R. DesHaies, and J. R. MacEwan, The Fission-Product Gas Pressures in UO_2 Fuel During Irradiation, *Trans. Am. Nucl. Soc.*, 8(2): 424 (November 1965).
48. J.-F. Marin and H. Michaud, Application of a Spectrometry to the Measurement of Low Diffusion Coefficients: Case of Uranium Dioxide, *Compt. Rend.*, 261: 693 (July 19, 1965).
49. W. E. Roake and H. J. Anderson, personal communication.
50. K. V. Davidson, R. E. Riley, and J. M. Taub, Compatibility of Refractory Metals with Solid Solution UC-ZrC at Elevated Temperatures, USAEC Report LA-3307, Los Alamos Scientific Laboratory, February 1965.
51. J. D. Allinson and J. C. Rivière, High Temperature, Short-Term Compatibility of Some Refractory Metals with the Thermionic Converter Fuel UC-ZrC, *J. Nucl. Mater.*, 17(2): 97-110 (1965).
52. Argonne National Laboratory, Reactor Development Program Progress Report, September 1965, USAEC Report ANL-7105, Oct. 20, 1965.
53. B. A. Webb, Method of Preventing Carburization of Fuel Element Cladding Metals by Uranium Carbide Fuels, U. S. Patent No. 3,219,541, to USAEC, Nov. 23, 1965.
54. Atomics International, Report to the 21st High Temperature Fuels Committee Meeting, USAEC Report NAA-SR-Memo-11724, Nov. 15, 1965.
55. S. G. Nelson and E. L. Foster, High Temperature Compression Strengths of Uranium-Carbon Alloys, *Trans. Am. Nucl. Soc.*, 8(1): 38-39 (June 1965).
56. S. J. Stachura, R. N. Cordy, and M. Silberberg, Uranium Carbide Transient Heating Studies, Phase II, *Trans. Am. Nucl. Soc.*, 8(1): 305 (June 1965).
57. A. Strasser, J. Cihi, and R. Martin, Irradiation Behavior of Solid Solution Uranium-Plutonium Carbides, USAEC Report UNC-MTL-5117, United Nuclear Corp., December 1965.
58. Y. Baskin, Oxidation Behavior of Uranium Monophosphide, *J. Am. Ceram. Soc.*, 48(3): 153-156 (March 1965).
59. E. J. McIver, V. J. Wheeler, R. M. Dell, and E. Wait, The Oxidation and Ignition of UN and UC, Part II. Single Crystal Oxidation Studies, British Report AERE-R-4985, September 1965.
60. Argonne National Laboratory, Fuels and Materials Development Program Quarterly Progress Report for Period Ending June 30, 1965.
61. Battelle–Northwest, Ceramics Research and Development Quarterly Report, April–June 1965, USAEC Report BNWL-150, Dec. 7, 1965.
62. J. R. McLaren and P. W. M. Atkinson, The Sintering of Uranium Mononitride, *J. Nucl. Mater.*, 17: 142-148 (1965).
63. B. R. Harder, J. Read, and R. G. Sowder, The Reduction and Sintering of Hyperstoichiometric Carbides in Hydrogen, *J. Nucl. Mater.*, 17: 203-214 (1965).
64. J. E. Antell and K. A. Peakall, Electrochemical Aspects of the Hydrolysis of UC-10% Fe, *Corrosion Sci.*, 5(11): 739-744 (November 1965).
65. E. E. Gruber, On the Theory of Migration and Co-

alescence of Bubbles in Solids, USAEC Report ANL-7079, Argonne National Laboratory, November 1965.
66. J. E. Bainbridge and B. Hudson, On the Techniques for Observing Fission Gas Bubbles in Uranium, *J. Nucl. Mater.*, 17(3): 237-244 (June 25, 1965).
67. Yu. I. Likhachev, V. P. Zvonnarev, and V. Ya. Pupko, Internal Stresses Due to Uneven Swelling of Fissioning Materials, *At. Energ. (USSR)*, 18(5): 483-487 (1965).
68. F. P. Butra, Z. F. Evkina, O. L. Fufaeva, I. A. Korobeinikov, and L. M. Lebedev, Temperature and Neutron Irradiation Effects on Plastic Deformation of Alpha Uranium Single Crystals, *At. Energ. (USSR)*, 19: 372-380 (October 1965).
69. G. F. Slattery, and J. A. McLeish, Relative Efficacy of Various Types of Texture Measurements as Means of Predicting Irradiation Growth in Uranium, *J. Nucl. Mater.*, 17: 192-199 (October 1965).
70. H. Shaked, Single Theory for the Release of Fission Gas From Powders, *J. Nucl. Mater.*, 17: 136-141 (October 1965).
71. G. Long, W. P. Stanaway, and D. Davies, Experiments Relating to the Mechanism of the Diffusion of Xenon-133 in Uranium Dioxide, British Report AERE-M-1251, January 1964.
72. Hahn-Meitner-Institut fuer Kernforschung, Diffusion of Rare Gases in Solids, Quarterly Report No. 21, July–September 1965, USAEC–Euratom Report EURAEC-1489, October 1965.
73. K. Papathanassopulos, Diffusion of ^{133}Xe in UC Nuclear Fuel as a Function of Composition and Radiation Dose, (Thesis), 67 pp., AED-Diss. 64-573, Technical University, Brunswick, Germany, 1964.
74. M. A. DeCrescente and E. G. Selleck, Fission Gas Migration Studies in Uranium Carbide, USAEC Report PWAC-476, Pratt & Whitney Aircraft, CANEL, October 1965.
75. Y. Osawa, Fission Gas Release From Nuclear Fuels II. Release During Low Temperature, Low Dose Irradiation, *J. Nucl. Sci. Techn., (Tokyo)*, 2: 296-303 (August 1965).
76. M. D. Rogers, Mass Transport and Grain Growth Induced by Fission Fragments in Thin Films of Uranium Dioxide, *J. Nucl. Mater.*, 16: 298-305 (1965).
77. R. M. Berman, The Homogenization and Densification of $ZrO_2 + UO_2$ Fuels Under Irradiation, USAEC Report WAPD-301, Westinghouse Electric Corp., Bettis Atomic Power Laboratory, January 1966.

Section

II

Reactor Materials

Moderator Materials

Graphite

An analysis is reported[1] of the observed radiation damage caused by fast and thermal neutrons in the boronated graphite used for the shield in the Enrico Fermi Fast Breeder Reactor (EFFBR). The analytical method was applied to experimental irradiation test data for exposures calculated to equal or exceed those which will be received in the EFFBR shield. The boronated graphite tested included black and gray material, each containing 4 or 7 wt.% B_4C. Transverse and parallel orientations of each type were tested in thermal reactors at temperatures of 600 to 750°F (316 to 400°C) and 750 to 900°F (400 to 482°C). Exposures ranged up to 5.5×10^{23} displacements/cm^3 for both materials. Dimensional changes as great as 3% were observed.

G values* for radiolytic oxidation of grade A graphite in various coolant atmospheres were determined by British investigators.[2] With direct measurement of weight loss and total radiation dose, results indicate *G* values of 1.2 ± 0.08 atoms/100 ev in 0.35 vol.% CO/CO_2, 0.95 ± 0.06 in 0.4 vol.% CO/CO_2, and 0.37 ± 0.02 in 0.5 vol.% CO/CO_2 + 400 ppm (by volume) CH_4. With certain exceptions, similar values were obtained on graphites with both higher and lower open porosity than that of grade A.

Thermally induced plastic strain of grade AGOT graphite has been investigated at Oak Ridge.[3] A constant tensile stress of 600 psi was applied to 0.5-in.-diameter specimens that were cycled at temperatures up to 1800°C (3272°F). A 10-in. section of the specimen was heated to temperature, held for 15 min, and cooled to room temperature. The specimen was returned to its initial state by a high-temperature anneal after each cycle. Without this anneal, no plastic strain was noted beyond the first cycle. Figure II-1 summarizes the data.

The theoretical curve derived from the microscopic stress–strain behavior of thermally cycled graphite as given by Jenkins and Williamson† can be described by the equation:

$$\epsilon_{\text{plastic}} = 2\beta\sigma_m \Delta\sigma - \beta\sigma_m^2 \quad \text{for } \Delta\sigma > 2\sigma_m$$

where σ_m is the applied stress and $\Delta\sigma$ is the change in local stress due to thermal effects and is approximated as

$$\Delta\sigma = (\alpha_c - \alpha_a)\, E\, \frac{\Delta T}{2}$$

where α_c and α_a = the expansion coefficients of the individual crystallites in the c and a directions
E = Young's modulus
ΔT = the temperature cycle
β = a parameter measuring the extent of the plastic behavior

The values used for these parameters were

$$(\alpha_c - \alpha_a) = (3.0 \times 10^{-6}) + (4.45 \times 10^{-10})T$$
$$E = (1.5 \times 10^{-6}) + (2.0 \times 10^{-4})T$$
$$\beta = 0.7 \times 10^{-10} \text{ psi}^{-2}$$

Creep data were obtained[3] for grades CGB and AGOT graphites tested under irradiation from 130 to 370°C (266 to 698°F). Parabolic beam creep specimens were used, and the deflection data obtained were the sum of both creep deformation and dif-

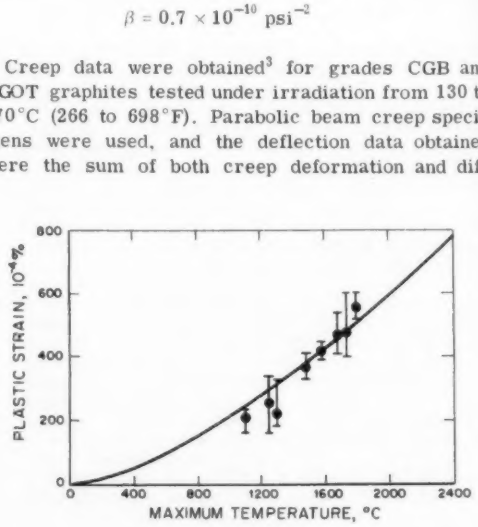

Fig. II-1 Plastic strain in AGOT graphite due to thermal cycling from room temperature with 600-psi applied stress.[3] Vertical lines indicate data spread, and filled circles represent average values; solid line represents theoretical relation.

*G value is defined as the number of carbon atoms gasified per 100 electron volts absorbed by the gas in the open pores of the graphite.

†G. M. Jenkins and G. K. Williamson, *J. Appl. Phys.*, 34: 2837-2841 (1963).

ferential growth due to a flux gradient. The differential growth was separated from the total deformation by two methods. First, the total deformation was plotted against stress at 100 Mwd/adjacent ton exposure intervals. The deformation extrapolated to zero stress was the deflection caused by differential growth. Figure II-2 gives the results obtained using this method.

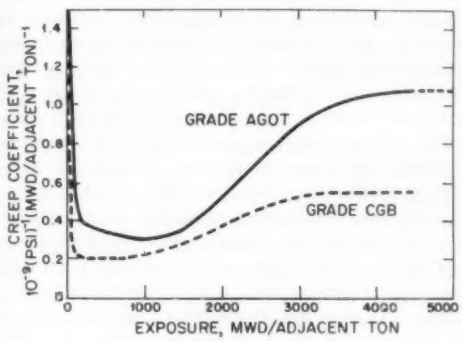

Fig. II-2 Creep coefficient of graphite under irradiation[3] at 130 to 180°C.

The second method was essentially the same, except that tangent deformation rates were used in place of total deformation. When these rates are plotted against stress at 100 Mwd/adjacent ton exposure intervals, the slope is the creep coefficient and the zero intercept is the deflection rate due to the differential growth. Figure II-3 presents the results obtained using this method.

The significant characteristic of these data is the variation of creep coefficient with exposure. A proposed explanation of increased creep rate due to closing of Mrozowski cracks in graphite is not in agreement with all the data. For example, creep results at 400°C (752°F) to exposure levels of 10^5 Mwd/adjacent ton have indicated a continuous creep-rate coefficient.[4] Furthermore, thermal-cycling tests have shown plastic yielding from 1000 to 2000°C (1832 to 3632°F) without an abrupt change due to crack closure.

Data from Oak Ridge and other sources have shown an inverse proportionality of creep coefficient to the elastic modulus, as illustrated in Fig. II-4.

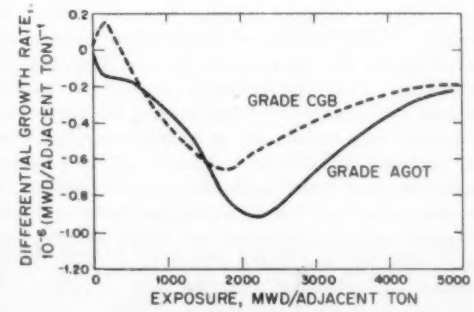

Fig. II-3 Differential growth rate of graphite creep specimens[3] at 130 to 180°C.

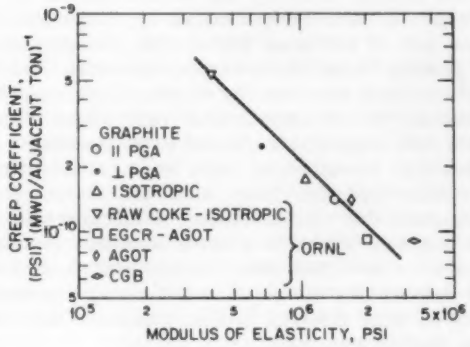

Fig. II-4 Relation of the creep coefficients of various grades of graphite to Young's modulus[3] at 400°C.

Beryllium Metal and Alloys

Books and Meeting Proceedings

The proceedings of a short course in beryllium, given at UCLA in March 1963, are now available in book form.[5] The book, edited by H. H. Hausner, is a compilation of lectures given by invited speakers from the industry. A rather broad coverage of beryllium processing is provided, extending from the reduction of the ore through the fabrication of hardware components. The broadest coverage area is in subjects dealing with fabrication of beryllium. Most of the information presented is still current. The discussions of forging are somewhat outdated, in the light of rapid advances and broader understanding of forging processes made in recent years. For example, powder forging is generally not now considered a likely fabrication process for beryllium since improved properties can be achieved by forging solid block. This publication is recommended as a good source of information on beryllium for the general reader.

Proceedings of the 1963 Gatlinburg Conference on the physical metallurgy of beryllium have also been published.[6] This conference was sponsored by the USAEC through Oak Ridge National Laboratory, and participants from the United States and the United Kingdom attended. Several reports in the general area of purification and its effect on properties of beryllium were presented. Also, some information is given on the properties of polycrystalline materials, especially ingot sheet. A review of structural

applications in the United Kingdom is included. Much of the work in this publication has been supplemented by later conferences and publications, but it is of value to the interested reader.

Alloying of beryllium was the subject of a meeting held by the Materials Advisory Board (MAB) Committee on Beryllium Metallurgy.[7] Summaries of various alloy programs now in existence were presented in the report. Currently, the studies fall into three groups: (1) solid-solution alloys, (2) dispersion alloys, and (3) two-phase alloys of the Lockalloy type. In general, it was recommended that more work in solid-solution strengthening be done. This would be applicable to strengthening of ingot sheet. There were also suggestions related to the possibility of dispersion strengthening ingot sheet. Alloys of the Lockalloy type with lower aluminum content were suggested. Also, the possibility of strengthening by alloying both phases in a duplex structure was suggested by the Committee. Further investigation of the reversibility of certain metallurgical reactions, such as those involving silicon, aluminum, and iron, was also recommended.

Kendall of Aerospace Corporation discussed intermetallic materials, including borides, in a chapter of a recent book.[8] Data on chemical, mechanical, and physical properties of these materials are reviewed. Synthesis and fabrication methods that may lead to materials of improved quality are discussed.

Purification

The MAB issued a report on its recent meeting covering purification of beryllium.[9] An investigation of the effect of purity is under consideration as one approach to the problem of improving beryllium ductility and toughness. The Franklin Institute discussed vacuum distillation, a purification method by which the impurity content of beryllium has been reduced to as low as 8 at. ppm. Deformation in single crystals prepared by various means of purification was discussed by Nuclear Metals. Single crystals of intermediate purity were prepared by zone leveling, as discussed by Brush Beryllium Co.; however, the impurities were very evenly distributed throughout the single crystal. Also discussed was a high-purity sponge beryllium that is being produced by the Bureau of Mines at Albany. Final purity of the sponge is controlled by producing a high-purity beryllium chloride that is reduced by lithium. Alloyd General Corp. reported that significant increases in purity had been realized through vacuum distillation, both by crucible-free and by electron-beam melting. Summaries of more recent research programs, including the joint U.S.–U.K. program, were given.

A report[10] was completed by the MAP Panel on the purification of beryllium, which covered the state of the art as well as recommendations for future studies along these lines. This report, which is a broad review of the subject, describes current purification methods, including both the commercial and the laboratory techniques now utilized. A review of the effects of specific impurity elements on the mechanical properties of both single-crystal and polycrystalline beryllium is included. The difficulties of evaluating the effect of purification on the mechanical properties of beryllium are outlined, including the need for careful control of microstructure and the difficulty in obtaining this control.

The Committee noted that further reduction in metallic impurities would not likely result in improvement of mechanical properties. However, they recommended that studies to effect further reductions in carbon, nitrogen, and oxygen, coupled with studies to analyze for these elements, be implemented. They also recommended that quenching-and-aging and internal-friction studies be undertaken to determine whether the effects of these elements are manifested in highly purified beryllium. The mechanical behavior of alloyed high-purity beryllium in both single-crystal and polycrystalline form was another area recommended for future studies. Finally, the Committee recommended that studies be undertaken to determine mechanical properties of high-purity polycrystalline beryllium of various grain sizes and preferred orientations.

Fabrication

A report[11] has recently been made available through the Redstone Scientific Information Center covering fabrication of beryllium. Primary fabrication procedures such as rolling, extrusion, forging, drawing, and powder metallurgy are discussed. Forming, machining, and joining are also discussed in some detail. A section that describes some of the current structural applications is included.

Joining

Some of the factors affecting brazing of beryllium were studied at the Massachusetts Institute of Technology.[12] The major objectives of the program were to improve wetting of beryllium by braze alloys, to accomplish joining by a true capillary brazing procedure, and to develop an improved heat source for brazing. A low-voltage electron-beam heating unit was designed for use as a heat source. Titanium was chosen as a surface activator to promote wetting. Vacuum evaporation of titanium onto the surfaces to be brazed was chosen as the most desirable method for applying the activator. Silver alloys produced relatively good joints with this method because the titanium layer and the short heating cycle prevented extensive reaction between the braze and the base metal. Gold–nickel braze alloys were unsuccessful because of extensive reaction and diffusion-void formation with the beryllium base metal. However, exceedingly good joints were achieved using 1100 aluminum as the braze alloy.

Irradiation Effects

Phillips Petroleum Company studied the displacement and helium-atom production rate for fast neutrons reacting with a beryllium lattice piece in the Materials Testing Reactor.[13] Results of compression tests on samples of the piece are given. Electron microscopy shows helium-bubble growth only at high exposures. X-ray diffraction shows no change in the beryllium peaks. The lattice parameter changed less than 0.2% for exposures of 1.45×10^{22} neutrons/cm^2. Bowing of the lattice pieces was analyzed in terms of the gaseous atoms present. The measured strain corresponded to a growth of approximately $0.2\%/10^{22}$ neutrons/cm^2 (>1 Mev).

Phillips Petroleum[14] also studied changes in mechanical properties, gas release, and growth in extruded beryllium after irradiation at 750°C (1382°F) to an integrated fast flux of 7.5×10^{20} neutrons/cm^2. When the samples were compressed, fracture occurred by cleavage in planes parallel to the extrusion direction. Significant losses in ultimate strength and ductility were noted in the irradiated material. On the other hand, the yield strength increased.

Electron-microscopic examinations of fracture surfaces indicated that helium bubbles were forming on grain boundaries and inclusions in the metal. There was no apparent preference for type of inclusions. In general, there were few voids within the grains. (H. D. Hanes)

Beryllium Oxide

The crystalline transformations of two BeO materials, Minox AAA and a sulfate-derived BeO, were studied by the British.[15] The impurity contents of these materials are given in Table II-1. The $\alpha \rightarrow \beta$ transformation occurred between 2050 and 2100°C (3722 and 3812°F) for the Minox BeO, but at the significantly higher temperatures of 2100 to 2250°C (3812 to 4082°F) for the sulfate-derived BeO. The $\beta \rightarrow \alpha$ reversion took place at about 50°C lower than the $\alpha \rightarrow \beta$ transformation range. After cooling to room temperature, both samples of BeO gave diffraction patterns similar to those obtained before heating. (M. C. Brockway)

Table II-1 IMPURITIES (PPM) IN BeO POWDERS[15]

Element	Minox AAA	Sulfate BeO
Ca	20	130
Fe	30	15
Mg	10	20
Al	60	35
K	15	Not detected
Na	60	<50
Li	0.7	8
B	8.4	0.3
F	50	Not detected
Si	100	80
P	70	Not detected
Cl'	320	Not detected
SO_4	300	1340

Solid Hydrides

Zirconium Hydride

Dilatometric studies with crystal-bar zirconium containing 100 ppm hydrogen, conducted at Chalk River,[16] showed that, after heat-treatment put hydrogen into solution, cooling to room temperature followed by reheating resulted in an increase in length at a given temperature. It was deduced that this lengthening resulted from a sequence of events: hydrogen supersaturation, followed by precipitation of a metastable hydride on cooling. On reheating, this hydride converts to a more stable form which persists to a temperature higher than that at which it formed originally. There is a temperature span from 295 to 331°C (558 to 628°F) in which the hydride is present on reheating from lower temperatures but absent on cooling from solution temperatures. Further investigation showed that this phenomenon had no marked effect on the creep rate of the material.

Coleman and Hardie[17] have examined the mechanism of hydrogen embrittlement of zirconium by studying the initiation sites and the path of propagation for cracks over the range 293 to 443°K (68 to 338°F). The specimens contained 100 ppm hydrogen as a grain-boundary precipitate. The polished surfaces of deformed Charpy specimens and the fracture surfaces of slow-bend specimens were studied by means of electron microscopy. It was concluded that (1) fracture originates at broken hydrides resulting largely from dislocation pileups, (2) propagation occurs in a similar manner in ductile and brittle samples, and (3) microcracks link up at hydrides by ductile failure of the zirconium metal, causing separation of the fracture surfaces.

Self-diffusion of zirconium in zirconium hydride prepared from crystal-bar zirconium has been measured at Atomics International.[18] Hydrides in the composition range $ZrH_{1.63}$ to $ZrH_{1.69}$ were prepared, and ^{95}Zr was deposited as oxalate on the surface. The tagged atoms were then allowed to diffuse through the hydride lattice. Both volume diffusion near the surface and grain-boundary diffusion at greater depth were observed. The activation energy for volume diffusion was estimated to be 28 kcal/mole as compared to 35 kcal/mole for reactor-grade zirconium sponge, which was measured previously. The volume-diffusion constant was found to range from 3.1×10^{-12} cm^2/sec at 770°C (1418°F) to 3.3×10^{-11} cm^2/sec at 988°C (1810°F).

Hydrided Zirconium Alloys

Because of the increased demand for hydriding of cold-worked and heat-treated zirconium alloys, a

method has been developed at Chalk River[19] for fast and reproducible hydriding at low temperatures. It was found that hydrogen could be introduced at temperatures as low as 280°C (536°F) by vapor blasting the specimens to remove the oxide film on the surface, followed by homogenizing at 400°C (752°F). During the hydriding a higher pressure of hydrogen was employed than is normally used to reach the same N_H level.

A detailed procedure for mounting, polishing, and etching of hydrided zirconium–uranium alloys for metallographic studies has been published by Atomics International.[20] The essential operations are (1) rough grinding with silicon carbide papers, (2) rough polishing with 30-μ diamond paste and kerosene, (3) fine polishing with levigated alumina (Linde B) in a 10 wt.% oxalic acid solution on Microcloth, using moderate pressure on a "wet" cloth at high revolutions per minute, and (4) anodizing the specimen surface, using a 10 wt.% oxalic acid electrolyte and a cell potential of 10 to 20 volts at about 0.5 amp/in.^{2} for 2 to 5 sec. The result is a surface in which the various phases are distinguished by bright and highly contrasting colors.

The hexagonal lattice constants for $ZrC \cdot ZrH_2$ have been determined by X-ray diffraction at Atomics International.[18] The values are: $a_0 = 3.3467 \pm 0.0001$ A, $c_0 = 5.4898 \pm 0.0001$ A, $c/a = 1.640$.

Lithium Hydride

The standard free energy of formation of solid lithium hydride has been determined from electromotive-force measurements in experiments at Argonne.[21] The measurements were made over the temperature range 675 to 885°K (756 to 1134°F) by use of a cell having as cathode an Armco iron surface over which hydrogen is passed, and as anode, molten lithium metal. The following values for the heat and free energy of formation and entropy were calculated:

	800°K (981°F)	298°K (77°F)
$\Delta H°$, cal/mole	−20,940	−21,790
$\Delta F°$, cal/mole	−6,740	−16,160
$\Delta s°$, cal/(deg)(mole)	−17.7	−18.9

These values are in good agreement with those of previous investigators. (H. H. Krause)

References

1. R. E. Dahl, Correlation of Radiation Damage in Boronated Graphite, USAEC Report BNWL-199, Battelle–Northwest, February 1966.
2. B. W. Ashton, J. Standring, and M. T. Jaquiss, Determination of G(-C) Values for P.G.A. and Other Graphites in the Windscale A.G.R., British Report TRG-Report-1120, Nov. 4, 1965.
3. Oak Ridge National Laboratory, Gas-Cooled Reactor Program Semiannual Progress Report for Period Ending September 30, 1965, USAEC Report ORNL-3885, February 1966.
4. Papers presented at the Seventh Biennial Conference on Carbon, Case Institute of Technology, Cleveland, Ohio, June 21–25, 1965:
   a. B. S. Gray, J. E. Brocklehurst, and A. A. McFarlane, Irradiation Induced Plasticity in Graphite, Paper 182.
   b. A. H. Perks and J. H. W. Simmons, Dimensional Changes and Radiation Creep of Graphite at Very High Neutron Doses, Paper 188.
5. H. H. Hausner (Ed.), *Beryllium, Its Metallurgy and Properties*, University of California Press, Berkeley, Calif., 1965.
6. Conference on the Physical Metallurgy of Beryllium Held at Gatlinburg, Tennessee, April 30–May 1, 1963, USAEC Report CONF-170, Oak Ridge National Laboratory.
7. National Academy of Sciences–National Research Council, Materials Advisory Board, Fourth Progress Report by the Committee on Beryllium Metallurgy of the Materials Advisory Board, Report MAB-199-M(4), Aug. 20, 1965.
8. E. G. Kendall, Intermetallic Materials, Carbides, Borides, Beryllides, Nitrides, and Silicides, *Ceramics for Advanced Technologies*, pp. 143-183, John Wiley & Sons, Inc., New York, 1965.
9. National Academy of Sciences–National Research Council, Materials Advisory Board, Third Progress Report by the Committee on Beryllium Metallurgy of the Materials Advisory Board, Report MAB-199-M(3), June 1, 1965.
10. National Academy of Sciences–National Research Council, Materials Advisory Board, Status of the Purification of Beryllium, Report of the Committee on Beryllium Metallurgy Panel on Purification, Report MAB-211-M, October 1965.
11. A. F. Gerds and F. W. Boulger, The Fabrication of Beryllium, Report RSIC-227, Battelle Memorial Institute, May 1964.
12. C. M. Adams, Jr., and S. Weiss, Brazing of Beryllium, Report E-1734, Massachusetts Institute of Technology, February 1965.
13. J. M. Beeston, *Gas Formation and Compression Fractures in Irradiated Beryllium*, American Society for Testing and Materials, Special Technical Publication, No. 380, pp. 395-417, 1965.
14. W. C. Francis (Ed.), Annual Progress Report on Reactor Fuels and Materials Development for FY 1965, USAEC Report IDO-17154, Phillips Petroleum Company, February 1966.
15. T. W. Baker and P. J. Baldock, The X-Ray Diffraction Intensities of the High Temperature (β) Phase of Beryllium Oxides, *J. Nucl. Mater.*, 19: 210-211 (1966).
16. Atomic Energy of Canada Limited, unpublished, 1965.
17. C. E. Coleman and D. Hardie, Some Observations on the Fracture Characteristics of Hydrided Alpha Zirconium, *J. Less-Common Metals*, 10(1): 12-21 (January 1966).
18. Atomics International, Quarterly Technical Progress Report, AEC Unclassified Programs, July–September 1965, USAEC Report NAA-SR-11650, Dec. 22, 1965.
19. E. E. Sexton, A Technique for Low-Temperature Hydriding of Zirconium Alloys, Canadian Report AECL-2511, November 1965.
20. J. W. Raymond and D. T. Shoop, The Metallography of Zirconium-Base Alloy Hydrides, USAEC Report NAA-SR-Memo-10927, Atomics International, Feb. 5, 1965.
21. C. E. Johnson, R. R. Heinrich, and C. E. Crouthamel, Thermodynamic Properties of Lithium Hydride by an Electromotive Force Method, *J. Phys. Chem.*, 70(1): 242-246 (January 1966).

Section

III

Reactor Materials

Nuclear Poisons

Hafnium

In a study at the University of Pittsburgh,[1] oxygen was found to increase the hardness of hafnium as shown in Table III-1.

Table III-1 EFFECT OF OXYGEN ON ROOM-TEMPERATURE HARDNESS OF HAFNIUM[1]

Oxygen content	Hardness, R_A
50	48
280	55.8
680	59.5
820	60.7
1250	64.3

Table III-2 shows the effect of oxygen on the tensile properties of hafnium. Increased oxygen content decreases the ductility and increases the strength at room temperature. At elevated temperatures these effects are less pronounced. In fact, in some cases the elongations increased with increasing oxygen content.

Mechanical properties of welded hafnium, with various oxygen contents, are given in Table III-3. The yield and ultimate strengths of unnotched weld metal are generally higher than those for wrought annealed strip (Table III-2). Ductility, on the other hand, is substantially lower in the weld metal.

Impact test results for hafnium with various oxygen contents are shown in Fig. III-1. At 600°F increasing oxygen produces gradually increasing impact strength. At lower temperatures the impact strength increases with oxygen content up to about 400 to 600 ppm and then falls off sharply. (M. Kangilaski)

Dispersion and Nonmetallic Poison Materials

Workers at Oak Ridge National Laboratory conducted a postirradiation nondestructive examination

Table III-2 SUMMARY OF TENSILE-TEST RESULTS FOR HAFNIUM–OXYGEN ALLOYS[1]

Oxygen content, ppm	75°F (24°C)		300°F (149°C)		600°F (316°C)		900°F (482°C)		1200°F (649°C)	
	Long.	Trans.	Long.	Trans.	Long.	Trans.	Long.	Trans.	Long.	Trans.
0.2% offset yield strength, 1000 psi										
50	24.3	34.4	13.1	24.1	16.1	19.5	10.2	11.1	8.4	8.1
280	28.0	29.4	36.5	40.1	15.0	19.6	10.2	12.5	7.5	8.2
680	28.9	38.3	23.7	35.9	21.8	23.7	12.0	13.8	8.8	10.0
820	33.6	38.2	28.0	37.6	23.3	23.7	11.0	14.2	8.1	9.4
1250	49.4	60.2	40.9	49.6	23.8	32.2	14.4	19.0*	11.7*	12.9*
								18.2†	11.1†	11.9†
Ultimate tensile strength, 1000 psi										
50	60.5	49.4	48.6	44.3	42.3	35.1	28.0	23.0	18.7	15.3
280	66.8	62.2	69.4	61.7	39.0	32.2	29.2	24.2	18.5	15.3
680	78.5	75.6	59.9	54.2	54.4	39.0	28.9	25.3	17.0	16.4
820	77.9	74.1	61.3	54.9	55.3	34.4	28.7	25.0	16.7	15.5
1250	92.0	89.0	68.2	63.9	49.5	47.4	30.8	27.6	20.1	18.3
Total elongation, %										
50	43	46	48	55	50	63	51	51	60	46
280	36	43	45	47	49	63	51	53	66	52
680	33	30	46	43	50	61	57	57	67	57
820	33	31	45	46	54	61	61	55	74	63
1250	29	18	40	43	55	54	62	50	76	64
Reduction of area, %										
50	46	46	47	54	46	66	79	85	84	90
280	47	46	44	50	54	66	73	80	83	87
680	44	39	45	46	54	65	75	78	80	85
820	32	42	47	49	53	64	75	80	82	84
1250	34	24	45	48	54	62	71	75	82	86

*Upper yield. †Lower yield.

Table III-3 AVERAGE TENSILE-TEST RESULTS OF WELDMENTS MADE IN HAFNIUM STRIP WITH VARIOUS LEVELS OF OXYGEN

Oxygen content, ppm	Notched specimens: Yield strength, 1000 psi	Notched specimens: Ultimate tensile strength, 1000 psi	Notched specimens: Elongation, %	Notched specimens: Reduction of area, %	Estimate of values for unnotched specimens: Yield strength, 1000 psi	Estimate of values for unnotched specimens: Ultimate tensile strength, 1000 psi	Estimate of values for unnotched specimens: Elongation, %	Estimate of values for unnotched specimens: Reduction of area, %
Room temperature results								
50	54.0	67.1	5.5	17.5	39.4	60.8	20.3	19.6
680	75.2	80.5	2	1.5	55.0	72.7	7.4	1.6
820	85.7	86.4	2	3	62.5	78.5	7.4	3.3
1250		37.1				33.7		
300°F (149°C) results								
50	46.6	59.1	6	16	32.6	53.3	21.4	16
680	61.9	80.4	5.5	22	43.3	72.3	19.6	22
820	55.1	74.4	7	19	38.6	67.0	25.0	19
1250	74.2	82.7	3	4	51.9	74.5	10.7	4
600°F (316°C) results								
50	41.3	49.8	7	29	28.9	44.8	30.0	29
680	46.3	58.4	7.5	28	32.4	52.2	26.3	28
820	37.8	56.1	7.5	31.5	26.4	50.4	26.8	32.5
1250	46.6	52.8	4.5	12.5	32.6	47.6	16.1	12.5

of a control element after 10.1 Mw-years of service in the Stationary Medium Power Reactor.[2] This element consists of four composite absorber plates welded to form a square hollow tube and contains a dispersion of 37 wt.% Eu_2O_3 in a stainless-steel matrix that is clad with stainless steel. The examination showed the element to be in excellent condition, with no evidence of damage, swelling, or nonuniform burnup. It is planned to irradiate this element further.

Tensile data for hafnium carbide containing free carbon, as reported by the U. S. Bureau of Mines,[3] are shown in Table III-4. There was no evidence of plastic yielding at temperatures up to 1450°C (2640°F). However, nonlinear stress–strain curves were obtained for specimens containing 10.0 to 11.5 wt.% carbon at temperatures of 2150 and 2400°C (3900 and 4350°F).

In studies to evaluate the use of three refractory metals as binders for zirconium diboride,[4] mixtures of zirconium diboride with chromium, molybdenum, and tungsten powders were cold pressed and resistance sintered to a high density. The sintered compacts were examined metallographically and then tested for crushing strength, hardness, oxidation rate, and mechanical shock. Compacts containing chromium exhibited the greatest compressive strength, thermal-shock resistance, and oxidation resistance. Those containing molybdenum and tungsten exhibited less desirable properties.

Stansfield[5] has presented thermal-expansion data for polycrystalline HfO_2-ZrO_2 bodies between 900 and 2500°C (1650 and 4530°F). Dilatometric techniques were used to obtain the data on heating and cooling. Below the phase transformation, thermal expansion was only slightly composition dependent. Above the transformation, however, the expansion coefficients increased significantly with ZrO_2 content. The change in length at transformation ranged from 0.37 to 0.75%, but no composition dependence was noted.

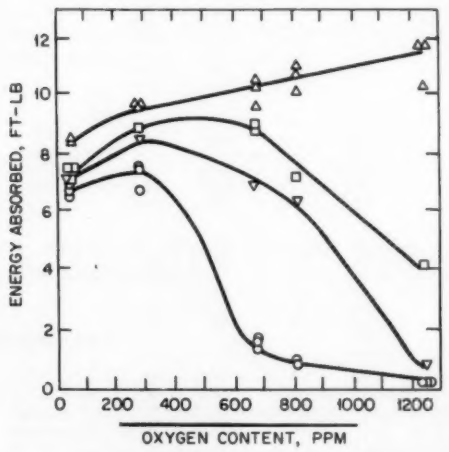

Fig. III-1 Effect of oxygen content on impact strength of hafnium at various temperatures.[1] ○, room-temperature tests; ▽, 200°F tests; □, 300°F tests; △, 600°F tests.

Table III-4 TENSILE DATA[3] FOR HYPERSTOICHIOMETRIC HfC

Test temperature °C	Test temperature °F	Ultimate strength, psi	Young's modulus, 10^6 psi
20	68	*	33.7
1050	1920	*	18.73
1450	2640	*	17.2
2150	3900	17,130	16.2†
2400	4350	12,660	6.93†

*Stress–strain curves were linear up to fracture, but values were not given.

†Stress–strain curves exhibited no linear portion; slope of curve at 10,000 psi was used to calculate an elastic modulus.

Phase-equilibrium studies for the system WO_3–B_2O_3 were carried out by Levin,[6] using both metallographic and X-ray diffraction techniques. The system was a simple eutectic type with no compounds, solid solutions, or immiscibility gap. The melting point of WO_3 was 1435°C (2615°F) and that of B_2O_3, 450°C (842°F). (E. G. Smith, Jr.)

References

1. J. G. Goodwin, The Effects of Oxygen on Some Properties of Hafnium (Thesis), USAEC Report WAPD-T-1683, University of Pittsburgh, 1965.
2. A. E. Richt, Interim Postirradiation Examination of a Europium-Bearing Control Rod from the Stationary Medium Power Reactor, USAEC Report ORNL-TM-1407, Oak Ridge National Laboratory, March 1966.
3. Bureau of Mines, Albany Metallurgy Research Center, Quarterly Metallurgy Progress Report Number 29, October 1–December 31, 1965, USAEC Report USBM-RC-1220.
4. M. E. Tyrrell and C. W. Houck, Metallic Binders for Zirconium Diboride: Chromium, Molybdenum, and Tungsten, Report BM-RI-6549, Norris Metallurgy Research Laboratory, 1964.
5. O. M. Stansfield, Thermal Expansion of Polycrystalline HfO_2–ZrO_2 Solid Solutions, *J. Am. Ceram. Soc.*, 48: 436-437 (Aug. 21, 1965).
6. E. M. Levin, The System WO_3-B_2O_3, *J. Am. Ceram. Soc.*, 48: 491-492 (Sept. 21, 1965).

Section IV

Reactor Materials

Cladding and Structural Materials

Corrosion

Corrosion of Zirconium Alloys

The structure of thin oxide films formed on zirconium under various conditions was studied by electron microscopy and electron diffraction by Japanese scientists.[1] Monoclinic ZrO_2 was produced by heating in air at 300 to 500°C (572 to 932°F), dipping in fused salt (50 g of $NaNO_3$, 50 g of KNO_3, 1 g of MnO_2) at 400°C (752°F), or heating above 1100°C (2012°F) the tetragonal oxide films that had been produced by wet oxidation. Tetragonal and monoclinic ZrO_2 were detected in films produced by wet oxidation in concentrated HNO_3, cathodic treatment in 5% H_2SO_4, immersion in 35% HCl, or water quenching after heating to 400°C (752°F) in air. It was believed that production of the metastable tetragonal ZrO_2 crystals was partly due to the existence of water or hydrogen in the oxidizing atmosphere.

Tritium was used to study hydrogen uptake by zirconium alloys at Chalk River.[2] It was found that hydrogen was incorporated in the oxide film when samples were corroded in aqueous media. Hydrogen was not incorporated in the oxide films on zirconium alloys by heating in hydrogen or by cathodically charging in aqueous solutions. Hydrogen ingress into the metal during pretransition corrosion was believed to be controlled by a thin barrier layer of oxygen-saturated metal at the oxide–metal interface. During pretransition oxidation in tritium/H_2O, tritium was not absorbed until exchange between the tritium and water occurred, thus indicating that the hydrogen that enters zirconium during oxidation in steam or water comes from the aqueous component rather than from any gaseous hydrogen.

The corrosion and hydriding characteristics of Zircaloy-2 in 8*M* HCl were investigated by Oak Ridge National Laboratory in considering materials for the Transuranium Processing Plant.[3] Hydrogen uptake and corrosion rates increased with increasing exposure temperature. Hydrogen content ranged from 200 ppm after a 3000-hr exposure at 35°C (95°F) to 4200 ppm after 3000 hr at 105°C (221°F). Corrosion rates ranged from 0.7 mil/year at 35°C to 3.1 mils/year at 105°C. Specimens exposed at 75°C (167°F) and higher temperatures cracked when subjected to the 2T bend test (the specimens contained >1600 ppm hydrogen).

(W. E. Berry)

Aluminum-Alloy Corrosion

Electrochemical measurements of in-pile corrosion were conducted at Mol, Belgium.[4] It was found that the passivating properties of the oxide film on aluminum are improved by pile irradiation, and are even more pronounced when the aluminum is in galvanic contact with stainless steel. Austenitic stainless steels also exhibited improved passivity under irradiation. Passivated stainless steel was more resistant to chloride pitting during irradiation, but the reverse was true for nonpassive stainless-steel surfaces. Irradiation increased the corrosion of carbon steel. Thicker films were found on zirconium, niobium, and tantalum that had been irradiated. It was concluded that the effects of irradiation on the corrosion process were mainly effects in the solution rather than in the metal.

(W. E. Berry)

Stainless-Steel Corrosion

The corrosion behavior of austenitic stainless steels in superheated steam was studied by British workers.[5] After 12,000-hr exposures, 20/25/niobium stainless steel was superior to 18/8 or 18/8/niobium alloys. Total weight gain of 850°C (1562°F)-annealed and ground specimens of 20/25/niobium alloy in 650°C (1202°F) steam was about 25 mg/dm^2. This same material exhibited a weight gain of 150 mg/dm^2 in 750°C (1382°F) steam.

The oxidation in steam of stainless-steel and nickel-base alloys is also being studied in Sweden.[6] After 5000-hr exposures to 550°C (1022°F) steam containing 20 ppm oxygen, the following weight gains were obtained: 18/11 stainless steel, 105 mg/dm^2; 20/35 stainless steel, 75 mg/dm^2; Incoloy 800, 45 mg/dm^2; and 16/75 chromium–nickel alloy, 7 mg/dm^2. Metallographic examination revealed a tendency toward intergranular attack in the low-nickel alloys, particularly in the 18/11 alloy.

Reaction rates of type 304 stainless steel with steam at 1400°C (2552°F) were studied by Argonne National Laboratory.[7] About one-third of a sample, 0.75 in. in diameter by 0.25 in. long, was reacted in about 10 min. The reaction was accompanied by considerable swelling and foaming. A comparison of reaction-rate curves based on hydrogen evolution per gram of sample revealed no effect of steam pressure in the range of 1 to

12 atm. This study is discussed in more detail under the heading Metal–Water Reactions.

Chemical and radiochemical analyses of fuel-cladding material, fuel-cladding corrosion-product films, fuel-cladding corrosion deposits, and circulating corrosion products for the Yankee and Saxton nuclear power reactors were summarized by Taylor and Cohen.[8] In the neutral water coolant of the Yankee Reactor, the circulating corrosion products and the deposits had similar chemistry. They were depleted in chromium with respect to the base-metal composition. The corrosion film was highly enriched in chromium and depleted in iron with respect to the base metal. In the boric acid–potassium hydroxide-treated Saxton water, the circulating corrosion products were similar to the base metal in composition, and the chromium content of the film was significantly lower than that in the Yankee Reactor. A marked decrease in radioactivity from the cladding to the film indicated that the corrosion oxide film was largely deposited rather than originating from the base metal.

Electron-microscope studies of alloys susceptible to transgranular stress-corrosion cracking were made at U. S. Steel Corporation.[9] On the basis of the results, it was postulated that the stress-corrosion-environment characteristics which are necessary for the nucleation of transgranular cracking are: (1) a surface film must form over most of the alloy surface; (2) the environment must be able to support tunnel corrosion in the film; (3) the mechanical properties of the film must be such that it can be ruptured by slip; and (4) the repair rate of the surface film must be slow enough and the creep rate of the specimen fast enough for the environmental conditions necessary for tunnel corrosion to be established at the exposed slip step. (W. E. Berry)

Base-Metal Corrosion

The possibility of nitriding and embrittling certain structural alloys in the Argon Cell were investigated by Argonne.[10] After 2000 hr of exposure to argon–5 vol. % nitrogen at 900°C (1652°F), Incoloy 800, Hastelloy C, and Hastelloy X did not pass the 2T bend test, whereas Inconel 600, type 304 stainless steel, and type 316 stainless steel passed the bend test. The penetration of a nitride phase was 1 mil in Incoloy 800, 3 mils in type 316 stainless steel, and 2 mils in the other alloys. (W. E. Berry)

Protective Coatings for Refractory Metals

"Coated Refractory Metal Technology — 1965" is the title of a report[11] issued by the Materials Advisory Board Subpanel on protective coatings. This report describes the coating materials receiving current emphasis and the processes by which these materials are applied to the metal substrates. On the basis of a review of the data available and discussions with representatives of coating vendors, users, and research organizations, the Subpanel expressed the following conclusions in regard to the properties of coated refractory metals:

1. Coated refractory metals will almost always exhibit mechanical properties that are inferior to those of uncoated material.
2. A given coating composition and associated coating process can be modified to minimize such detrimental effects.
3. A given coating system can have different effects on different refractory metals.
4. The oxidation protective life of coatings is significantly affected by alloy composition, temperature, pressure, time–temperature profile, strain, and coating thickness. The effects of these parameters are interdependent.
5. As a result of "defect failures," the minimum coating life can be considerably less than the average coating life.
6. No single coating chemistry or application process can be selected as the best available coating for all, or even for the majority, of the applications.
7. The use of the current coatings on refractory-metal foils of less than 10-mils thickness appears to be impractical because of the adverse effects of the coatings on mechanical properties.

The Subpanel stated that the most significant shortcomings of the state of the art of coatings are:

1. Insufficient life at pressures below about 100 torrs and at temperatures above 2500°F (1371°C) in oxidizing atmospheres
2. The increase in the ductile-to-brittle transition due to coating
3. Lack of reliable oxidation protection on hardware, particularly at edges

The French Advisory Group for Aeronautical Research and Development (AGARD) has prepared a handbook containing data on the physical, mechanical, chemical, welding, fabrication, and other miscellaneous properties of the refractory metals niobium, tantalum, molybdenum, tungsten, and their alloys.[12] The handbook also contains data on the properties of the coated refractory metals. (J. J. English)

Corrosion by Liquid Metals and Fused Salts

CORROSION BY SODIUM

A U. S. Atomic Energy Commission book,[13] *Reactor Technology, Selected Reviews — 1965*, contains a 105-page chapter entitled "Sodium Technology." This covers materials for sodium-cooled reactors, presenting thoroughly documented discussions of materials selection, corrosion by sodium, control of sodium purity, and experience gained with operating nuclear plants. This book is available for $4.50 as TID-8541 from Clearinghouse for Federal Scientific and Technical Information, Springfield, Va. 22151.

Along these same lines, a talk, "Technology of Liquid Metals," presented in Italy by Savage of Oak Ridge, has been published.[14] It comments on the sodium technology research and development programs of the National Committee of Nuclear Energy (CNEN) and gives a detailed, practical set of ground rules for sodium handling and for the design and operation of sodium-loop components.

The process tubes in a Sodium Graphite Reactor (SGR) concept are required to be joined in the reactor and separated for replacement in the event of a tube failure. To evaluate brazing as the joining method, workers at Atomics International[15] tested nickel-base brazing alloys for 10,000 hr in a sodium thermal-convection loop at 1200 and 700°F (the anticipated upper and lower joint temperatures, respectively). They noted that nickel–chromium–silicon–boron (CM 53) and nickel–silicon–boron (CM 52) alloys were the most resistant to sodium attack. The nickel–chromium–boron (CM 60) would be good for only short-term use (<1500 hr) or lower temperature (< 700°F) applications. Problems were encountered with progressively increasing remelt temperatures, cracking, and porosity. The investigators believe that the latter two can be overcome by an improved joint design.

Analyses of specimens that had been exposed to a 1200°F (650°C) high-carbon sodium environment at MSA Research Corp.[16] revealed extensive surface carburization of types 304 and 316 stainless steel but a uniform carbon increase throughout 2¼ chromium–1 molybdenum steel tabs. The type 304 stainless showed a greater carbon pickup and deeper penetration than type 316 stainless for the same exposures. Comparison of carbide case thicknesses of stressed and unstressed stainless tabs suggests that stress may enhance carburization. The rupture, yield, and tensile strengths of type 316 stainless steel are actually increased by exposure to high-carbon sodium. However, the material suffers a drastic loss in ductility (and consequently in impact resistance) and becomes notch sensitive.

In evaluating vanadium alloys as cladding materials for sodium-cooled fast reactor fuels, Argonne workers found that short-time exposure of recrystallized vanadium–20 wt.% titanium sheet to 650°C (1202°F) sodium apparently decreases its creep resistance.[17] This is illustrated by Fig. IV-1.

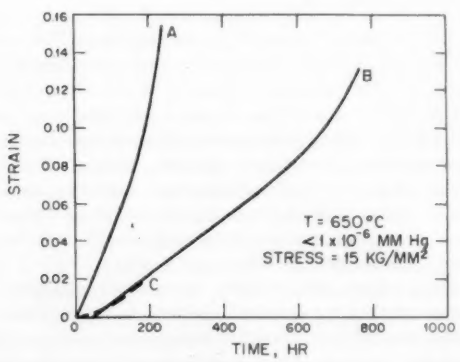

Fig. IV-1 Effect of sodium on creep of vanadium–20 wt.% titanium.[17] Curve A, seven-day preexposure to 650°C sodium; Curves B and C, seven-day preexposure to vacuum at 650°C.

The Babcock & Wilcox Co., in the process of developing an improved sodium-heated steam generator, investigated the effects of a water-to-sodium leak on the Croloy 2¼ components.[18] Static immersion tests of Croloy 2¼ specimens were conducted in (1) aqueous NaOH solutions at 140 to 700°F (60 to 371°C), (2) anhydrous (98.6 wt.%) NaOH at 900°F (482°C), (3) sodium–NaOH mixtures from 900 to 1400°F (482 to 760°C), and (4) sodium–NaOH–NaH mixtures at 900°F (482°C). The following observations were made:

1. *Aqueous NaOH* corrodes Croloy 2¼ by simple solution at a rate that depends more on temperature than on concentration, and is linear with time; the maximum is 2.67 in./year at 900°F.
2. *Sodium–NaOH mixtures* attack Croloy 2¼ very slowly at low NaOH concentrations and temperatures below 900°F; however, the rate increases rapidly with increases in either temperature or NaOH content.
3. *Adding NaH to sodium–NaOH mixtures* actually decreases the rate of attack of Croloy 2¼, the mechanism of corrosion being simple solution. However, without the NaH, corrosion is characterized by the formation of intergranular oxide and subsequent removal of whole grains from the metal surface.
4. *Decarburization* of Croloy 2¼ steel did not occur in aqueous NaOH; nor did it occur at 1400°F (760°C) in sodium with 90 ppm Na_2O, in a 5 wt.% NaOH–sodium mixture at 1375°F (746°C), or in the sodium–NaOH–NaH system at 900°F (482°C).

Argonne studies[10] of the wetting of UN powders by sodium, to test the concept of a slurry or paste blanket, are yielding results that may be relevant to the case of a cladding leak in a UN-fueled sodium-cooled reactor. The workers noted that, at 300°C (572°F), about ½ hr of intimate contact and stirring of –200 +325-mesh UN powder in sodium (5 vol.% solids) was required for complete wetting of the solids; at 250°C (482°F), 1 hr was required. They also observed that there was no paste separation or dewetting on cooling. This temperature-sensitive delayed wetting implies that a surface reaction which promotes wetting takes place between the sodium and the UN powder. The exact nature of the reaction is not clear. It may be the removal of some interfering substance from the surface by sodium or the formation of some compound that in turn is wetted by molten sodium.

CORROSION BY NaK

Corrosion problems in the SNAP-8 power system were the subject of a sizable program at Oak Ridge, the results of which are now available in a summary report.[19] The SNAP-8 system utilizes a compact NaK-cooled BeO-reflected reactor fueled with (uranium–zirconium) hydride. The proposed primary-circuit materials for the various components are:

Material	Application
Chromized Hastelloy N	Fuel cladding
Hastelloy C	Lower grid plate
Type 347 S.S. (later type 316)	BeO cladding
Type 316 S.S.	Reactor vessel and piping
Croloy 9 M and type 316 S.S.	NaK-to-mercury boiler

The circuit operates with surface temperatures between 1100 and 1425°F (593 and 774°C) and has a design life of 10,000 hr.

Some of the more important conclusions reached, on the basis of 11 loop experiments and assorted auxiliary studies, are:

1. The most pronounced deleterious corrosion effect expected in the SNAP-8 circuit is decarburization of the Croloy 9M, with consequent loss of strength.
2. Mass-transfer deposits tend to build up in the electromagnetic-pump cell and in the cold leg. If oxygen is kept low (< 30 ppm, achievable by cold trapping), the deposits are mostly nickel, chromium, and manganese; otherwise, they are mostly iron and chromium.
3. Hastelloy N is attacked intergranularly (estimated 1½ mils maximum in 10,000 hr at 1300°F), the rate being more sensitive to temperature than to oxygen; the opposite is true for the iron-base materials.
4. Hydrogen that escapes from the hydride fuel by diffusion or through a leak in the Hastelloy N cladding has no deleterious effect on corrosion by NaK. It can be cold trapped to minimize its diffusion into the mercury circuit. Its solubility in NaK depends on the square root of hydrogen pressure and varies only slightly with temperature. Its activity in NaK can be diminished greatly by adding a few at.% lithium to the NaK.

Boron carbide samples from two different vendors were exposed in type 316 stainless-steel capsules to 1000°F NaK-78 for times to 10,000 hr and temperatures to 1000°F, to see what would happen to the B_4C if the control-element cladding failed in a NaK-cooled reactor.[20] The finer-grained material, whose stoichiometry showed a slight carbon deficiency, was much more resistant than the other, which was coarse grained and had a slight carbon excess. It was concluded from this study that 1000°F NaK penetration into stainless-steel-clad B_4C control drums could cause some fragmentation of the B_4C as a result of a reaction between potassium and free carbon. The stainless-steel capsule walls showed evidence of carbon and boron pickup to depths as great as 9 mils but no other compositional changes.

CORROSION AND EROSION BY POTASSIUM

In studies of the effect of oxygen content and heat-treatment on the compatibility of niobium–1 wt.% zirconium in potassium containing 1500 ppm dissolved oxygen at 815°C (1500°F), Oak Ridge workers[21] found that niobium–1 wt.% zirconium specimens containing 2100 ppm oxygen gained weight, whereas those containing 4100 to 4700 ppm oxygen lost weight during 100-hr exposures. These weight gains and losses represented takeups and releases of oxygen, respectively, depending on whether the niobium–1 wt.% zirconium started out with fewer or greater than 2 atoms of oxygen for each atom of zirconium. A pretest heat-treatment at 1200°C (2192°F) given some specimens did not affect the oxygen exchange.

After the test all specimens were partially covered by a dark, tightly adherent corrosion product less than 1 mil thick, identified tentatively by electron diffraction as NbO_2. The liquid-immersed capsule surfaces increased significantly in oxygen content in the first 10-mil layer. Takeup of oxygen by the capsule walls and tab specimens reduced the oxygen content of the potassium to below 50 ppm.

An important consideration in the selection of a material for the blades of a potassium vapor turbine is the ability of the material to resist erosion by impinging liquid droplets in regions where the vapor quality is low. On the basis of erosion tests with 1400°F (760°C) liquid potassium, workers at AiResearch Mfg. Co.[22] found that the molybdenum-base alloys molybdenum–0.5 wt.% titanium, TZM (molybdenum–0.5 wt.% titanium–0.08 wt.% zirconium), and TZC (molybdenum–1.25 wt.% titanium–0.15 wt.% zirconium–0.15 wt.% carbon) suffered the least attack. Stellite 6B and René 41 were almost as good, but the niobium- and tantalum-base alloys tested were significantly worse. The latter include X-315 (niobium–15 wt.% tungsten–3 wt.% zirconium–0.1 wt.% carbon), F-48 (niobium–15 wt.% tungsten–5 wt.% molybdenum–1 wt.% zirconium), SCb-61 (niobium–10 wt.% tantalum–2 wt.% molybdenum–1 wt.% zirconium), T-111 (tantalum–8 wt.% tungsten–2 wt.% hafnium), and D-11 (niobium–1 wt.% zirconium).

CORROSION BY MERCURY

A mercury corrosion study was carried out by Nejedlik and Vargo[23] with the objectives of (1) correlating the corrosion resistance of metals with such factors as solubility, crystal structure, atomic size, melting point, and valence and (2) determining the effects of alloying elements on mercury corrosion in iron-, cobalt-, and nickel-base alloys. Corrosion was measured by weight changes per unit area of tab specimens in the 900°F (482°C) condensing zones of bent-glass refluxing capsules for times up to 120 days. Conclusions are based on results of tests on 28 unalloyed metals, 34 iron-base alloys, 15 cobalt-base alloys, and 11 nickel-base alloys.

Table IV-1 shows the corrosion results for elements, along with associated properties. Metals with the best resistance to attack by mercury are transition metals with (1) a high melting point, (2) a body-centered cubic lattice, (3) a maximum most stable valence of 4 to 6, and (4) an atomic diameter less than 3 A. Note that all face-centered cubic metals tested have poor resistance to mercury corrosion.

When the 30-day weight losses are plotted against atomic number of the solute metal, a significant periodicity shows up, with pronounced minimum-loss points in each period, corresponding to the elements carbon, silicon, vanadium, iron, cobalt, niobium, molybdenum, tantalum, and tungsten. Since solubility shows a similar periodicity, it appears that solubility and corrosion resistance are governed by the external or electronic structure of the atoms.

The atomic-size factors (ratio of the radius of the solvent mercury atom to the radius of the solute atom) listed in Table IV-1 indicate that metals with size

Table IV-1 MERCURY CORROSION RESISTANCE OF SOME ELEMENTS AND THEIR ASSOCIATED PROPERTIES[23]

Corrosion rating	Element	Melting point °F	Melting point °C	Crystal structure	Valence	Atomic diameter D_M, A	Atomic-size factor, D_{Hg}/D_M	Weight loss, mg/in.²
Excellent	Nb	4380	2416	BCC	3, *5**	2.94	1.06	0
	Mo	4760	2627	BCC	3, 5, *6*	2.80	1.11	0
	Ta	5425	2996	BCC	*5*	2.94	1.05	0
	W†	6170	3410	BCC	*6*	2.82	1.11	0
	C†	6700‡	3705	Hex	2, *4*	1.54	2.01	0
Good	V	3150	1732	BCC	2, 4, *5*	2.71	1.15	0.9
	Fe†	2802	1539	BCC	2, *3*	2.52	1.23	1.1
	Co†	2723	1495	HCP	2, *3*	2.50	1.24	4.5
	Si	2605	1430	Diamond cubic	*4*	2.34	1.33	0.75
Fair	Be†	2340	1282	HCP	*2*	2.25	1.38	11
	Ti†	3300	1826	HCP	3, *4*	2.93	1.06	75
	Cr†	3430	1888	BCC	2, 3, 6	2.57	1.21	64
	Zr†	3200	1760	HCP	*4*	3.19	0.97	223
Poor	Ni	2651	1455	FCC	2, 3	2.49	1.35	Nonresistant
	Na	208	97	BCC	*1*	3.72	0.86	Nonresistant
	Mg	1202	650	HCP	*2*	3.20	0.97	Nonresistant
	Al	1220	660	FCC	*3*	2.82	1.10	Nonresistant
	K	145	63	BCC	*1*	4.62	0.67	Nonresistant
	Ca†	1560	849	FCC	*2*	3.94	0.78	Nonresistant
	Mn†	2273	1245	Cubic (complex)	7, 6, 3, 4, *2*	2.5	1.24	Nonresistant
	Cu	1981	1083	FCC	1, *2*	2.56	1.21	Nonresistant
	Zn	787	420	HCP	*2*	2.66	1.16	Nonresistant
	Ge	1760	960	Diamond cubic	*4*	2.79	1.11	Nonresistant
	Ag	1761	961	FCC	*1*	2.88	1.18	Nonresistant
	In	314	156	FCT	*3*	3.24	0.96	Nonresistant
	Sn†	449	232	BCT	2, *4*	3.16	0.98	Nonresistant
	Au	1945	1063	FCC	*1*, 3	2.88	1.18	Nonresistant
	Pt	3224	1773	FCC	2, *4*	2.77	1.12	Nonresistant

*Most stable valence is in italic type.
†Other crystal structures are known or probable.
‡Carbon volatizes without melting at ordinary pressures.

factors below 1.0 have poor corrosion resistance, although a size factor greater than 1.0 does not ensure good resistance to mercury. The resistance of an alloy was influenced markedly by alloying additions. The effects were sensitive to (1) corrosion resistance of each alloying element, (2) quantity of each element present in the alloy, and (3) nature of the alloying action, such as formation of new phases, solid solutions, intermetallics, or other complex interactions.

CORROSION BY OTHER NONALKALI LIQUID METALS

Preliminary results from static, isothermal exposures of molybdenum capsules, half filled with low-oxygen (<10 ppm) liquid metal and sealed under 10^{-4} torr pressure, gave the following indications:[24]

1. Cadmium produced no detectable attack of the molybdenum after 300 hr at 1292°F (700°C).
2. Lead reacted slightly with the molybdenum below the liquid level after 300 hr at 1472°F (800°C), but there was no sign of interaction in the vapor zone.
3. Tin reacted slightly with the molybdenum in both the liquid and vapor zones after 300 hr at 1472°F (800°C).
4. Zinc diffused completely through the molybdenum wall, leaving the capsule empty at both 1292 and 1472°F (700 and 800°C).

At Ames Laboratory[25] the Sessile-drop method was used to measure the wetting of types 310, 410, 430, and 502 stainless steel, and of 4¾ chromium–½ molybdenum steel, by lead–bismuth eutectic. Using the formation of a 90° contact angle as the criterion for wetting, type 310 was wet at 515°C (960°F), type 410 at 540°C (1004°F), type 502 at 580°C (1076°F), and type 430 at 640°C (1184°F). Below 560°C (1040°F), type 502 steel exhibited the highest contact angles, indicating the least tendency to be wet by molten lead–bismuth. At higher temperatures type 430 was the least wettable. Surface tension values, calculated from drop profiles, ranged from 405 dynes/cm at 460°C (860°F) to 365 dynes/cm at 572°C (1060°F). Although wetting is believed to play a role in both corrosion and heat transfer, it is usually only a secondary consideration in the selection of a container material for most liquid-metal applications.

CORROSION BY REPROCESSING SOLUTIONS

At Argonne[26] corrosion tests at temperatures up to 1000°C (1832°F) were conducted to determine the suitability of tantalum, molybdenum, tungsten, and some alloys of these metals as containers for zinc and zinc-rich fuel reprocessing solutions containing magnesium and uranium, in both the absence and presence of molten chloride salts. Tungsten, although showing the best corrosion resistance, suffered slight intergranular attack at 1000°C. The alloy molybenum–30 wt. % tungsten was deemed useful for some applications, although molybdenum was leached out at 800°C (1472°F). Unalloyed tantalum and molybdenum were severely attacked, and tantalum–10 wt. % tungsten failed by stress-induced liquid-metal embrittlement.

In a similar study[27] corrosion of 1020 carbon steel, types 405 and 304 stainless steel, and tantalum by liquid cadmium–magnesium–zinc was investigated at 500, 750, and 850°C (932, 1382, and 1562°F). Carbon steel and type 405 stainless showed excellent resistance to the cadmium–magnesium binary, but their

resistance decreased with increasing additions of zinc. Type 304 stainless was severely corroded because nickel was leached out. Tantalum exhibited good corrosion resistance up to 850°C to all solutions but those containing greater than 95 wt. % zinc. (E. M. Simons)

Metal–Water Reactions

Argonne[7] has recently reported on experiments, designed to determine the rate and stoichiometry of the reaction of stainless steel with steam, performed at 1400°C (2552°F) in a high-pressure-furnace apparatus. This reaction had been studied previously by an induction-heating method over the temperature range from 1100 to 1300°C (2012 to 2372°F). However, samples induction heated to 1400°C underwent rapid swelling and foaming, and, as a sample disintegrated, all control of temperature was lost because of changes in inductive coupling between the induction coil and the sample.

The high-pressure furnace, which was designed to operate at a maximum pressure of 1000 psi and at temperatures up to 1700°C (3092°F), allows heating of a sample by a molybdenum heater and is unaffected by sample disintegration. Water is introduced into the lower part of the furnance by a positive-displacement pump and is converted to steam. At the start of an experiment, the sample is elevated from a moderate-temperature section, where reaction with steam is negligible, into the high-temperature section. Some unreacted steam and the hydrogen produced by the metal–steam reaction are continuously removed from the upper part of the steam zone (high-temperature section) through an outlet valve. The extent and the rate of metal–steam reaction are determined by continuously monitoring the amount of hydrogen collected. On completion of the experiment, the sample is lowered to its initial position.

The current isothermal experiments were performed at 1400°C at various steam pressures. The samples were type 304 stainless steel (16.8 wt.% chromium, 8.3 wt. % nickel, 1.7 wt. % manganese, and 73.2 wt. % iron) disks, $^3/_4$ in. in diameter and $^1/_4$ in. long, and had a nominal weight of 13 g. Steam flow rate through the furnace was 5 ml of water/min, which is equivalent to a linear flow rate of steam past the sample of approximately 2 ft/sec. At the steam flow rate employed, sufficient steam passed through the furnace each minute to oxidize the sample to completion.

The results of two experiments at 1-atm pressure are plotted in Fig. IV-2, which also includes a typical rate curve obtained by the induction-heating method. The principal difference between the rate curves obtained by the two methods is a result of the shorter heat-up time associated with the induction-heating method.

The effect of pressure on the stainless steel–steam reaction at 1400°C was examined. The results of typical experiments performed at 1, 2, and 12 atm are compared in Fig. IV-3, where it can be seen that the reaction rate is independent of steam pressure.

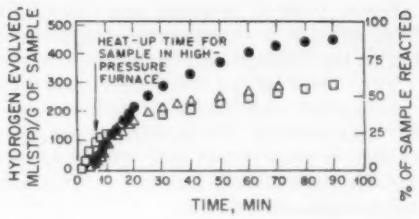

Fig. IV-2 Rate of reaction between type 304 stainless steel and steam at 1400°C (2552°F) and 1-atm pressure.[7] (Sample size: $^3/_4$ in. in diameter by $^1/_4$ in. thick.) ● and △, high-pressure furnace; □, induction heated.

The results expressed in Figs. IV-2 and IV-3 indicate that approximately one-third of a sample had reacted in about 10 min. The nature of the reaction (swelling and foaming) prevents a simple interpretation of the reaction-rate law expressed in terms of original sample surface area. It seems clear that the reaction rate will be a function of sample size and shape and that the overall rate of consumption of metal may be higher with thinner sample sections.

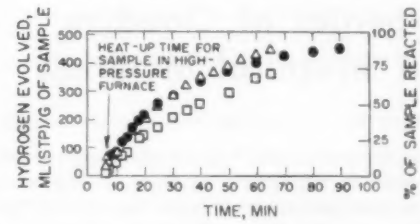

Fig. IV-3 Rate of reaction between type 304 stainless steel and steam at 1400°C (2552°F) and various pressures.[7] (Sample size: $^3/_4$ in. in diameter by $^1/_4$ in. thick.) ●, 1 atm; □, 2 atm; △, 12 atm.

The stoichiometry of the stainless steel–steam reaction was determined by a series of four experiments in which small samples of type 304 stainless steel were completely reacted with steam at 1500°C (2732°F). The results of the experiments are given in Table IV-2.

Table IV-2 DETERMINATION OF THE TOTAL HYDROGEN GENERATED BY THE REACTION OF TYPE 304 STAINLESS STEEL WITH STEAM AT 1500°C (2732°F) AND 1-ATM PRESSURE[7]

(Steam Flow Rate, 10 ml of Water/min)

Sample weight, g	Approximate time of completion of reaction, min	Total exposure time, min	Hydrogen generated, liters (STP)/g of S.S.
4.83609	60	100	0.522
3.87858	45	90	0.516
1.14582	12	26	0.510
2.34223	16	25	0.492
		Average	0.510

The average yield of hydrogen was 0.51 ± 0.01 liter (STP)/g, which is somewhat greater than values calculated on the assumptions that the reaction products are Cr_2O_3 and FeO and that nickel does not react. Such calculations yield a value for hydrogen generation of 0.40 liter (STP)/g. If it is assumed that the nickel forms NiO, a value of 0.44 liter (STP)/g is obtained. The experimental value of 0.51 liter (STP)/g indicates that higher oxides are formed.

X-ray diffraction studies of the oxidation products of the four experiments showed that the major phase was of the Fe_3O_4 or spinel type. Other likely spinels, $FeCr_2O_4$, $NiFe_2O_4$, and $NiCr_2O_4$, could not be distinguished from Fe_3O_4 by X-ray analysis. Calculation of the hydrogen yield on the basis of complete conversion to spinel compounds of the type M_3O_4 results in a value of 0.54 liter (STP)/g, which is only slightly greater than the observed value. It was therefore concluded that the oxidation by steam of type 304 stainless steel leads primarily to the formation of spinel type oxides in which the nickel and chromium atoms substitute freely into the Fe_3O_4 lattice.

(A. W. Lemmon, Jr.)

Selected Mechanical Properties of Cladding and Structural Materials

Aluminum

Results from a study[28] of the effect of a vacuum environment on the fatigue behavior of 1100 aluminum show a substantial increase in fracture life at all stress levels in vacuum, compared with results in air. This increase is attributed to a decrease in the crack-propagation rate in the absence of oxygen or water vapor. A transition pressure of 10^{-2} to 10^{-3} torr was observed, below which crack retardation was marked. The existence of such a critical pressure was attributed to the effects of molecular adsorption rates on crack growth. The crack growth rate was found to be dependent on the cyclic stress frequency, as well as on pressure level in accordance with the adsorption mechanism.

Nickel-Base Alloys

Creep studies of Hastelloy X were performed by investigators at Battelle–Northwest.[29] They found that data obtained at 1950 and 2100°F (1066 and 1149°C) compared favorably with data reported by other authors at lower temperatures. Table IV-3 shows minimum creep rates, rupture life, and elongation for a variety of stress levels. Rupture life is much shorter and minimum creep rate is higher than would be predicted from extrapolation of higher stress data. This is believed to be due to grain growth and its influence on intergranular crack propagation.

Table IV-3 CREEP-RUPTURE DATA[29] OF HASTELLOY X

Temp., °F	Stress, psi	Minimum creep rate, hr^{-1}	Elongation, %	Time to rupture, hr
2100	5000	4.8×10^{-1}	24.7	0.4
	4000	3.0×10^{-1}	23.5	0.6
	3000	1.1×10^{-1}	23.4	2.0
	2500	3.1×10^{-2}	19.8	4.3
	1300	7.7×10^{-3}	23.0	21.0
	900	1.4×10^{-3}	10.8	65.0
	500	7.2×10^{-4}	14.0	114.5
	300	2.0×10^{-4}	14.2	340.0
1950	8000	3.0×10^{-1}	27.0	0.7
	6000	1.5×10^{-1}	32.9	3.9
	4000	3.2×10^{-2}	26.5	7.3
	2500	4.8×10^{-3}	19.0	36.0
	1500	1.3×10^{-3}	24.1	250.0

Various nickel alloys were tested by General Electric Company[30] at room temperature, 1100, and 1300°F (593 and 704°C) after heating for 5000 hr in the 1000 to 1300°F (538 to 593°C) temperature range, with the following results:

Incoloy 825 exhibited increases in strength at all temperatures, with a maximum increase of approximately 80% after exposure at 1000 to 1200°F. Under all conditions, total elongation values remained above 15%.

Inconel 718 showed substantial increases, up to 100%, in strength at all test temperatures, particularly after exposure at 1000 to 1200°F. Prolonged exposure at 1300°F resulted in overaging and loss of strength at all tensile temperatures. Elongation values dropped as low as 6%.

Hastelloy X showed a 50% increase in strength at each tensile temperature after exposure at 1300°F, with relatively minor reductions in elongation.

Hastelloy F exhibited significant increases in strength (about 200%) after prolonged exposure at 1200 and 1300°F. The corresponding elongation values were reduced to approximately 5%.

All exposure conditions produced increases in strength of *Inconel 625* at each tensile temperature. Exposure at 1200°F resulted in the largest strength increases, 100 to 200%, while the corresponding elongation values were reduced to 10%.

Prolonged exposure of *René 62*, particularly at 1200 and 1300°F, produced increases of 300 to 400% in strength both at room and elevated tensile temperatures. The corresponding elongation values dropped to essentially zero.

Increases in strength of 200 and 300% were measured for *Incoloy 801* at all tensile temperatures after extended exposure. Elongation values were reduced, but remained above 15%.

The tensile properties of *Incoloy 800* were relatively stable, with the largest strength increases, 50 to 60%, measured after exposure at 1000 and 1100°F. Elongation values were very stable and remained above 20%.

Steels

The British have issued a Steels Data Manual[31] that covers the properties of a large number of steels. They review the following topics in some detail: mechanical properties, physical properties, effects of stress re-

lief on pressure-vessel steels, chemical properties, and the effects of irradiation.

Studies on the fatigue-limit behavior of iron and mild steel were conducted at Wright-Patterson Air Force Base.[32] The investigators made a critical review of the research in recent years on the fatigue-limit behavior of iron and mild steel and conducted experiments on zone-refined iron to demonstrate the importance of interstitial-dislocation reactions to the nature of fatigue limit. They attempted to clarify the controversy over whether the fatigue limit in ferritic materials results from a characteristic peculiar to the iron (bcc) lattice, or from strong initial dislocation locking and dynamic strain aging. It was shown that each of the existing theories has some merit and that each of the mechanisms thus far proposed is necessary, but individually insufficient, to explain fully the fatigue-limit behavior.

Recent work in England[33] involving tests to failure on 5-ft-diameter 14-ft-long cylindrical steel pressure vessels containing 6- to 24-in.-long slits confirmed that for constant-load conditions (such as those existing in a pneumatic test) crack arrest does not occur; whereas under conditions nearer to the constant-strain case (such as those in a hydraulic test), the extent of crack propagation is controlled by fracture toughness and total energy available. Since energy availability controls fracture appearance through plastic zone size, strain rate, and crack speed, cleavage and shear fractures may exist side by side at the same temperature. It was therefore suggested that interpretation of service and test failures of steel structures should be based on an analysis of factors such as load history, stress level, flaw size, and Charpy value, rather than on the appearance of the fracture. The safety implications of these effects in relation to proof testing, annealing out of radiation damage, and material monitoring are discussed.

The response of alloy steels to dynamic strain aging in both quenched-and-tempered and ausformed conditions was investigated at Lawrence Radiation Laboratory.[34] Strength, ductility, and toughness were measured as functions of straining and tempering temperatures. Structural observations were made on the strained and unstrained steels. By appropriate choice of strain and tempering temperatures, the strength of quenched and tempered steels was increased by about 40,000 psi, i.e., to the base strength of the ausformed steels. The strength of the ausformed steels was increased by about the same amount, suggesting that the strengthening effects are additive. In the ausformed steels, yield strengths of 270,000 psi were achieved by dynamic strain aging with a reliability ratio (K_c/σ_{ys}) of 1. Since the slope of K_c/σ_{ys} vs. σ_{ys} is small, it is suggested that this process may be used to attain yield strengths of 300,000 psi with exceptional toughness.

A parabolic relation was found by Belgian workers[35] between the total deformation per cycle of alternate biaxial bending and the number of cycles to failure for ASTM A-302B, Ducol W30, and Soudotenax 56 steels. The fatigue life of the steels was shortened by a series of alternate trapezoidal stresses, the extent dependent upon the test temperature and the steel type. Fatigue cracks appeared in the middle of the samples at about 50% of the total life. The change in the transition temperature with amount of plastic fatigue tended to reach a maximum at 20% of the fatigue life and then decrease.

Charpy-V-notch impact bending tests on fatigue samples damaged under tensile stress and compression were continued on three types of steel (ZD, ZS, and ZA).[36] Fatigue processing consisted in a number of comparatively small cycles of alternate plastic deformations at ambient temperature. The behavior of the steels under study was rather different according to the importance of the damage to which they were subjected. However, it was possible to trace a general tendency in which impact energies corresponding to crystalline ruptures increase in relation to the number of cycles of the damage applied. Finally, Charpy V transition temperatures tend to increase in a significant manner; however, this increase does not seem to be related to the initial values of the transition temperature of the materials under study. Additional side-bend embrittlement tests after fatigue under alternate biaxial bending at ambient temperature and at 300°C were also carried out. These tests confirmed the general impression that an embrittlement of the steel occurs already with the first cycles of plastic fatigue.

Refractory Metals and Alloys

Notched fatigue tests were conducted by Thompson Ramo Wooldrige Inc.[37] on TZM alloy (molybdenum – 0.5 wt. % titanium – 0.08 wt. % zirconium) in the stress-relieved condition at an ambient temperature of 982°C (1800°F) and on TZC alloy (molybdenum – 1.2 wt. % titanium – 0.25 wt. % zirconium – 0.15 wt. % carbon) after annealing at 1700°C (3092°F) at an ambient temperature of 1093°C (2000°F). No well-defined endurance limit was observed in either alloy, and fracture occurred in TZC at peak stresses as low as 9030 psi in 143 hr (9.75×10^3 cycles).

A summary of creep data[38] obtained to date on tungsten, tungsten – 25 wt. % rhenium, Sylvania A, molybdenum-base alloys TZC and TZM, niobium-base alloys Nb 132M and As-30, and the tantalum alloy T-222 is presented. Considering the high-strength refractory alloys on a strength-to-weight basis, the TZC material was found to have creep resistance that was significantly superior to the other alloys. The data obtained on T-222 indicate that it has creep resistance that is substantially inferior to that of the molybdenum-base alloys. Preliminary results indicated that no consistent variation in chemical composition had occurred in any of the materials as a result of the creep-test exposure.

The effects of recrystallization on the strengthening effects of work hardening of refractory metals were

studied by Probst.[39] Hafnium, titanium, and zirconium additions to molybdenum proved to be effective in raising its recrystallization temperature. Addition of 0.1 wt. % zirconium to arc-melted molybdenum increased the recrystallization temperature to 2800°F (1538°C) from 2150°F (1177°C) for unalloyed molybdenum. The strength of tungsten at 3500°F (1927°C) was increased by adding small amounts of alloying elements in solid solution. Hafnium was an effective strengthener. The technique of dispersion strengthening is discussed for thoria-dispersed (TD) nickel. The stronger nickel at 2200°F (1204°C) could withstand about 4500 psi for 1000 hr. Unalloyed nickel would have to be restricted to a temperature no higher than about 1200°F (649°C). The TD nickel displayed a strength of 4100 psi at 2500°F (1371°C), only 150°F (270°C) below its melting point. Thermal shock may be a problem if heating or cooling is rapid.

The tensile and creep properties of arc-melted and electron-beam-melted tungsten over the temperature range from 2250 to 4140°F (1232 to 2280°C) were studied at Lewis Research Center of the National Aeronautics and Space Administration.[40] The tensile and creep strengths varied with grain size, the finer grained materials being stronger. The activation energy for transient creep at 2250 to 3500°F (1232 to 1927°C) was 95,000 cal/gram mole and that for steady-state creep at 3300 to 4000°F (1815 to 2205°C) was 141,000 cal/gram mole. At 2875 to 3300°F (1580 to 1815°C), the apparent activation energy for steady-state creep decreased with decreasing temperature. It is suggested that cross slip is rate controlling during transient creep, and dislocation climb is rate controlling during steady-state creep above 3300°F (1815°C).

Studies were made in Brussels[41] on the mechanical properties (particularly under conditions of tensile testing) of molybdenum, niobium, and titanium, which were rolled in vacuum and in air. The results indicate that the strength and ductility characteristics of hot-rolled niobium and titanium depend substantially on the atmospheric conditions during rolling. When rolled in a vacuum of approximately 10^{-5} mm Hg, niobium and titanium had lower tensile strengths and yield points and higher relative elongations and reductions of area when rolled under the usual conditions in air. Such differences were not found between the tensile properties of molybdenum specimens rolled in vacuum and in air.

Experiments on the removal of interstitial impurities from niobium by heating in high vacuum to more than 2400°C (4352°F) and the effects of this treatment on the mechanical properties are described by Taylor and Christian.[42] The actual impurity levels achieved are not known, but it was clear from the measured physical and mechanical properties that considerable improvements were attained. The resistivity ratio $\rho_{300°K}/\rho_{4.2°K}$ was about 200:1 and about 4000:1 in an as-grown and a treated crystal, respectively. In the as-grown crystals, the resolved shear stress at the yield point was about 4000 g/mm² at room temperature, whereas crystals annealed in about 1×10^{-8} torr had a resolved shear stress of 850 to 900 g/mm². All mechanical tests were made in compression at a strain rate of 6×10^{-4}/sec. Two crystals annealed in a vacuum of 5×10^{-8} torr gave yield stresses of 950 and 1300 g/mm² when the final temperature was the melting point and 2240°C (4064°F), respectively.

The change in the mechanical properties of cold-swaged niobium reduced 90% in cross section was investigated by Russian workers[43] on isochronal annealing before and after electron-beam zone melting. They found that zone-melted niobium had greater ductility, greater uniform elongation, and increased work hardening but had lower strength. Furthermore, zone-melted swaged niobium showed a yield point in the temperature range from 20 to 700°C (68 to 1292°F). For both kinds of niobium, increased strength was found between 400 and 600°C (752 and 1112°F) and was attributed to the influence of carbon in the samples.

Zirconium

The elevated-temperature creep characteristics of polycrystalline alpha and beta zirconium were studied[44] in vacuum under constant tensile stress. Equipment was designed so that testing could be conducted in vacua of less than 10^{-6} mm Hg up to 1500°C (2732°F). The creep of alpha-zirconium was studied from 660 to 845°C (1220 to 1553°F), with the stresses ranging from 870 to 5400 psi. The steady-state creep rate, $\dot{\epsilon}_s$, was observed to be related to the applied stress, σ, and temperature, T, by the equation $\dot{\epsilon}_s = C\sigma^{\frac{1}{2}}D \exp(-\eta/\sigma RT)$, where $D = D_0 \exp(-Q/RT)$ is the coefficient of self-diffusion, C is a constant, and $\eta = (2.54 \times 10^7$ psi-cal) is another constant. The experimental value of Q is about 50,000 cal/mole. The usual creep behavior of alpha zirconium is considered in terms of a recent model for steady-state creep. The creep of beta zirconium was studied from 975 to 1425°F (1787 to 2597°F), with the stresses ranging from 100 to 300 psi. The measured creep characteristics of beta zirconium agree very well with those found by other investigators.

The anisotropy of mechanical properties observed in alpha-zirconium alloys can be related to the preferred orientation of the materials reported by Oak Ridge.[45] The influence of preferred orientation on anisotropy of yield strengths, plastic flow, creep, fracture, strain rate and temperature sensitivities, and the stability of such textures to further deformation is discussed in terms of the deformation systems observed in single crystals. It was concluded that other deformation systems are forced to operate because of the restraints of neighboring grains in polycrystalline materials. (J. A. DeMastry)

Selected Metallurgical Aspects of Cladding and Structural Materials

Light Metals

The isochronal recovery of work hardening in aluminum–Al_2O_3, SAP type alloys was investigated.[46] It was found that, for a given degree of work hardening, recrystallization temperature was increased rapidly with increasing oxide content.

A British patent has been issued for a heat-treatment that improves the creep resistance of a magnesium alloy containing 0.05 to 1 wt.% zirconium.[47] The creep rate at 400°C (752°F) is decreased from 8×10^{-4} to 2×10^{-7} hr^{-1} under a load of 200 psi following the heat-treatment. The heat-treatment consists in heating the alloy at 550 to 640°C (1022 to 1184°F) for 100 hr in CO_2, followed by furnace cooling.

Defense Metals Information Center has issued a complete summary report on the titanium–8 wt.% aluminum–1 wt.% molybdenum–1 wt.% vanadium alloy.[48] Included in the report are physical metallurgy, mechanical properties, weldability, formability, and corrosion resistance. The alloy is a combination of alpha and beta titanium and thereby combines the best properties of each.

Zirconium and Zirconium Alloys

A relation[49] between the thermal expansion and index of preferred orientation was established for Zircaloy-4. From this relation the physical properties of single-crystal Zircaloy-4 can be predicted if physical properties of polycrystalline Zircaloy-4 are known. These relations also hold for predicting properties for polycrystalline Zircaloy-4 if the single-crystal properties are known

Workers[50] at Bettis Atomic Power Laboratory found that hydride-platelet precipitation in alpha zirconium occurs on various pyramidal planes inclined to the basal plane of the hexagonal close-packed cell at angles between 10 and 50° and also between 75 and 90°. In Zircaloy-4 the hydride platelets are aligned parallel to pyramidal planes positioned from 5 to 25° to the basal plane.

The resistance to stress rupture of zirconium was found by the Canadians[51] to be increased by the addition of 1 wt.% Y_2O_3, which causes dispersion strengthening. Typical test results are shown in Table IV-4.

Homogenization of structure and mechanical properties in welded Zircaloy-2 tubes can be achieved by optimum cold work and heat-treatment, according to the British.[52] For longitudinal welds a cold reduction in wall thickness of 45 to 55% is recommended, whereas a 35 to 40% reduction is best for circumferential welds. At the intersection of circumferential and longitudinal welds, the optimum reduction is 43 to 47%. A 1-hr anneal at 820 to 860°C (1508 to 1580°F) should follow the cold work.

Rensselaer Polytechnic Institute[53] has devoted considerable attention to the alloying effect of rare-earth metals on zirconium. Among the things investigated are solid solubilities, surface tensions, phase diagrams, phase transformations, recrystallization, and fracture mechanisms.

The heat-treatment response of zirconium–niobium alloys was examined in Great Britain[54,55] and in Russia.[56] The British investigated zirconium containing 1.2 to 4.9 wt.% niobium and 300 to 2500 ppm oxygen.[54] In the transformation studies the alloys were quenched from 700 to 1000°C (1292 to 1832°F) followed by aging at 500°C (932°F). It was shown that oxygen content affects the properties as a solid-solution hardener and that its effect is not sensitive to quenching and aging treatments. If the martensitic phase is to be obtained on quenching, it is necessary to have a niobium content of 2.5 wt.%, and the quenching temperature should exceed 850°C (1562°F), with the cooling rate exceeding 80°C/sec (144°F/sec). The above heat-treatment results in the alpha martensitic structure rather than the beta plus omega structure, which is less desirable because of lower elevated-temperature strength. The Soviet investigators[56] quenched zirconium that contained up to 17.5 wt.% niobium from 800°C (1472°F). This resulted in a metastable beta phase, indicating that the cooling rates were not sufficiently fast. When the metastable beta phase was aged at 400°C (752°F), a niobium-rich beta phase and a niobium-depleted omega phase were formed. The stability of the metastable beta phase increased with increased niobium content. It has been shown that the temperature for martensite formation in zirconium–niobium alloys is decreased by increased cooling rates and increased niobium content.[55]

Hardness measurements revealed that age-hardening occurred at 500°C (932°F) in zirconium–2.5 wt.% niobium that was quenched from 875°C (1607°F) and then cold worked to 10 to 20% reductions.[51] The peak hardness occurred after 11 and 9 hr of aging for the 10%- and 20%-reduced material, respectively. Specimens that were reduced 30, 40, and 50% did not exhibit a peak in hardness but showed a continuous decrease in hardness as a function of time. An explanation for this might be that the peaks

Table IV-4 STRESS-RUPTURE DATA AT 500°C (932°F) OF ZIRCONIUM SINTERS CONTAINING 1 VOL.% MICRONIZED YTTRIUM OXIDE[51]

Specimen	Stress, psi	Rupture time, hr	Reduction of area, %	Elongation, %	Minimum creep rate, hr^{-1}
1% Y_2O_3	8000	439.1	65.9	62.7	2.2×10^{-4}
1% Y_2O_3	8000	329.1	74.0	70.6	4.6×10^{-4}
Plain Zr	8000	75.0	53.0	37.3	2.0×10^{-3}
Plain Zr	8000	79.3	56.1	42.0	3.6×10^{-3}

in hardness occurred before the first hardness measurement was made after 4 hr of aging.

Iron and Nickel Alloys

It has been demonstrated that stainless steels[57] containing 0.25 wt.% carbon can be obtained which have room-temperature yield strengths above 200,000 psi and an elongation of 28%. These properties are obtained by deforming the steel in the austenitic condition and following this with a heat-treatment of alternate heating to elevated temperature and cooling to progressively decreasing cryogenic temperatures. A stainless steel containing 0.47 wt.% carbon exhibited a room-temperature yield strength of 300,000 psi and an elongation of 12%. High silicon and molybdenum contents were necessary for the best results.

In research at Risley, aging of 20 wt.% chromium–25 wt.% nickel–niobium stainless steels up to 2000 hr at 600 to 800°C (1112 to 1472°F) did not result in sensitization.[58] The degree of sensitization was determined by measuring the amount of intergranular corrosion by the Strauss test. The maximum amount of sigma-phase formation occurs at 700°C (1292°F), and the new phase appears as isolated particles at grain boundaries. Other precipitates include NbC and M_6C particles that also show a preference for grain boundaries. The amount of these precipitates increases with increasing carbon content.

Multilayer tanks[59] made of type 301 stainless steel behaved better than single-layer tanks of the same thickness, when burst tested at −320 to −423°F (78 to 21°K). Both types of tanks contained sharp notches as flaws. In the burst tests the multilayer tanks exhibited 15 to 20% higher burst strength than the single-layer tanks. During failures the outer layer failed before total failure of the tank occurred. The stainless steel, which had been 70% cold reduced, failed at a lower burst strength than the material which had been cold reduced 60%.

The properties of carbonyl-deposited nickel [$Ni(CO)_4 \rightarrow Ni + 4CO$] were compared with those of electrodeposited nickel.[60] The hardness and ductility of both types of nickel were generally the same. The carbonyl process has the following advantages: (1) higher purity, (2) better control over uniformity, (3) 10 to 15 times faster rate of application, and (4) ability to plate on nonconductors. The limitations of the carbonyl process were (1) difficulty of maintaining an optimum temperature at the plating surface and (2) requirement for a postdeposition heat-treatment to produce a satisfactory bond with some materials.

Refractory Metals

The thermal conductivity, specific heat, and linear thermal expansion of 15 refractory materials were measured by Hedge, Kostenko, and Lang[61] from room temperature to the melting point of the material. Among the materials investigated were six niobium, three tantalum, and two molybdenum alloys.

The strain aging of commercially pure niobium was studied in Great Britain by using both yield-point return and internal-friction measurements.[62] The yield-point return is dependent on aging time to the two-thirds power ($t^{2/3}$). Also, oxygen diffuses to dislocations during early stages of strain aging, but it subsequently returns to solid solutions after more extensive aging. It is believed that the oxygen atoms are then replaced by carbon atoms at the dislocations.

French workers found that, if niobium is heated in the presence of nitrogen at 1625°C (2957°F), nitrogen is concentrated in the body-centered cubic structure.[63] This concentration continues until a transformation of the lattice into the hexagonal close-packed structure is caused by crystallographic shear. The precipitates are in the range of 1000 to 20,000 A in diameter. The solubility of nitrogen in niobium–1 wt.% zirconium[64,65] was determined as a function of temperature and nitrogen partial pressure and is given in Figs. IV-4 and IV-5. The partial molar-free energy expression for the dissolution of nitrogen in the normal solutions is given by $\Delta F^\circ = -51{,}500 + 20.74\,T$ (°K) cal/mole.

The sticking probability (S = atoms that stick to surface/atoms that strike surface) of nitrogen on ultraclean niobium surfaces was studied as a function of temperature (RT to 1800°C) and pressure (6×10^{-9} to 6×10^{-5} torr).[66] At room temperature, S is about

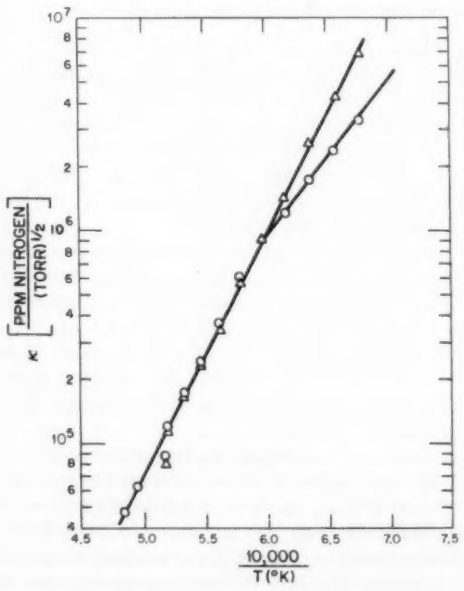

Fig. IV-4 Temperature dependence of the equilibrium constant for solutions of nitrogen in niobium–1 wt.% zirconium.[64] ○, N_2 concentration <100 ppm; △, N_2 concentration >100 ppm.

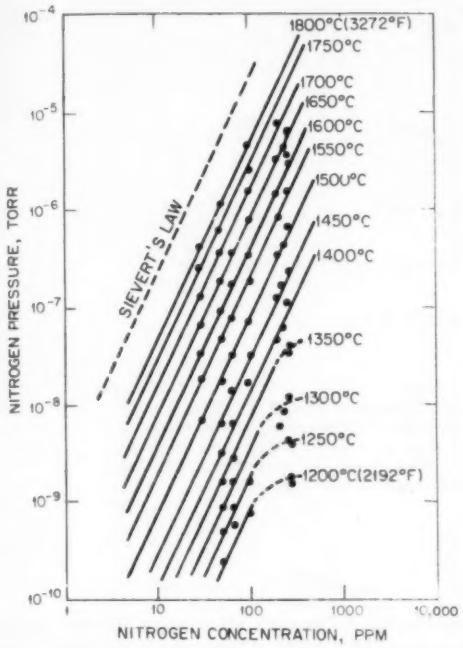

Fig. IV-5 Isothermal equilibrium for solutions of nitrogen in niobium–1 wt.% zirconium.[64]

0.5 and reaches a saturation value. At temperatures above 600°C (1112°F), the sticking factor is about 0.1 and is independent of pressure and further temperature increases. At higher temperatures where diffusion of nitrogen in niobium becomes significant, no saturation is reached on the surface because the nitrogen atoms diffuse into niobium as quickly as they hit the surface.

at 1400°C (2552°F) increased from 72 to 96 R_B by a 10 wt.% addition of molybdenum. Additions of titanium reduced both the hot hardness and high-temperature strength of niobium. The 1000°C (1832°F) strength of niobium was increased 2 to 2.5 times by solid-solution strengthening through 7 to 10 wt.% molybdenum additions.

The addition[68] of minor amounts of yttrium (about 5 ppm) increased the recrystallization temperature of tantalum from 1050°C (1922°F) to about 1500 to 1750°C (2732 to 3182°F). Since the solubility of yttrium in tantalum is very low (>1 ppm) at 1585°C (2885°F), the excess yttrium segregates to the grain boundaries and dislocations. Consequently the yttrium atoms suppress grain growth by requiring a considerable amount of energy to be dragged along by the migrating grain boundary.

The solubility of tantalum in various rare-earth metals was determined at Ames[24] to be given by the expression at.% (tantalum solubility) = $CT + D$, where C and D are the constants given in Table IV-5, and T is the temperature, °K.

An attempt was made to produce high-temperature high-strength whisker-reinforced alloys directly from a melt.[69] Tensile tests showed that whisker reinforcement was successfully achieved in the tantalum–20 vol.% Ta_2C system. A room-temperature fracture strength in excess of 150,000 psi was achieved when specimens were tested in the direction of aligned Ta_2C phase. The fracture mechanism was cleavage of Ta_2C whiskers followed by plastic flow of matrix. Preliminary elevated-temperature tests indicated a rapid decrease in fracture strength with increasing temperature. It was concluded from the decreasing number of fractured carbide whiskers with increasing test temperature, and from the absence of whisker pullout, that the whisker ratio and the shear strength

Table IV-5 SOLUBILITY OF TANTALUM IN RARE-EARTH METALS[24]

Rare earth	1000 C, (°K)$^{-1}$	D	Temperature range °C	Temperature range °F	Tantalum solubility at upper temperature, at.% tantalum
Yttrium	1.819	−2.965	1640–2075	2984–3767	1.30
Lanthanum	0.020	−0.005	1350–1950	2462–3542	0.039
Cerium	0.275	−0.435	1430–1990	2606–3614	0.187
Praseodymium	0.183	−0.277	1640–2060	2984–3740	0.150
Neodymium	0.201	−0.322	1550–2070	2822–3758	0.149
Samarium	0.134	−0.199	1670–2080	3038–3776	0.116
Europium	0.111	−0.190	1670–1875	3038–3407	0.048
Ytterbium	0.071	−0.121	1540–1760	2804–3200	0.023

In a Russian study of the effect of 2 to 10 wt.% titanium and 5 to 10 wt.% molybdenum on high-temperature properties of niobium,[67] additions of titanium were found to decrease the recrystallization temperature of niobium about 50°C (90°F), whereas molybdenum additions increased the recrystallization temperature about 100°C (180°F). The hot hardness of niobium at 900°C (1652°F) was increased from 88 to 106 Rockwell B (R_B) and that of the matrix are the limiting factors for effective load transfer.

General Electric Company[70] has shown that the weldability of molybdenum is considerably improved by minimizing the carbon content. The thermal conductivity[71] of recrystallized molybdenum decreased linearly from 0.871 watt/(cm)(°C) at 915°C to 0.727 watt/(cm)(°C) at 1900°C. The vapor pressure of molybdenum from 1200 to 3000°K (2160 to 5400°R)

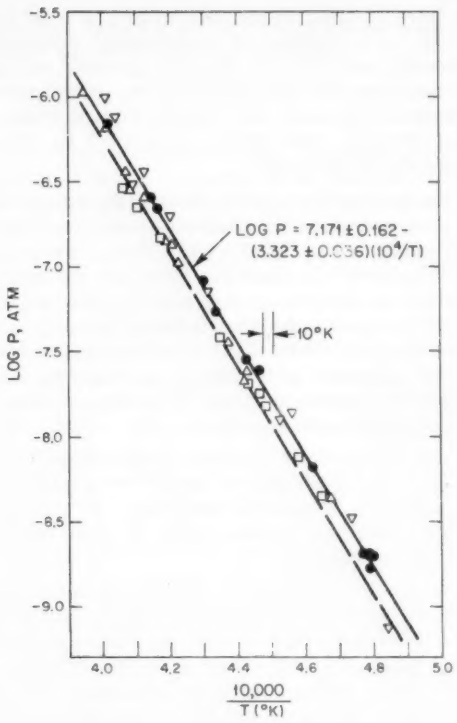

Fig. IV-6 Vapor pressure of molybdenum.[72] *●, Los Alamos;*[72] *□, Edwards, Johnston, and Blackburn; Δ, Vozella, Miller, and DeCrescente; ∇, Jones, Langmuir, and MacKay; – –, Zwikker (no data points reported).*

at a background pressure of 5×10^{-9} torr was measured by Los Alamos Scientific Laboratory[72] with the results shown in Fig. IV-6, along with the data of others for comparison.

The strengthening effect of interstitials on the tensile properties of tunsten was studied by Schnitzel at Westinghouse Electric Corporation.[73] Carburization followed by a high-temperature quench produced a significant strengthening contribution. Even greater strengthening was obtained at these temperatures if the specimens were deformed mechanically after carburizing and quenching. Cavities of the size range 20 to 400 A were found in tungsten wire that was fabricated by sintering.[74] These observations were made by Ryan in Australia, using a field ion microscope. The vapor pressure of tungsten was found by workers at the University of Cincinnati[75] to obey the relation $\log P\,(\text{atm}) = 7.933 - 45{,}087/T$ in the temperature range of 2574 to 3183°K.

Age-hardening studies were made by General Electric[70] on three differently heat-treated tungsten–30 wt.% rhenium alloys:

1. Hot rolled and treated for 1 hr at 3000°C (5432°F), followed cold work at 1450°C (2642°F); stress-relief treatments interspaced between cold reductions.
2. Hot rolled and treated for 62 hr at 1650°C (3002°F) in a H_2–H_2O atmosphere. The atmosphere is believed to reduce carbon content and promote small grain size. The alloy was cold worked and stress relieved as in item 1.
3. Hot rolled and treated 64 hr at 1400°C (2552°F) in hydrogen.

Specimens from each alloy were solution treated for 1 hr at 1800, 2000, 2200, and 2400°C (3272, 3632, 3992, and 4352°F) in vacuum. The specimens were then aged for 2, 10, and 100 hr at 1000, 1200, 1400, 1600, and 1800°C (1832, 2192, 2552, 2912, and 3272°F). Hardness values taken after each treatment are shown in Figs. IV-7 and IV-8 (page 187).

The significant result was that treating the specimens at 3000°C or solution annealing at about 2200°C resulted in suppression of the sigma phase and consequently lower hardness values. Maximum age hardening occurred in specimens that were treated at 1650 and 1400°C before cold working and then aged at 1400°C or above.

The thermal conductivity and linear thermal expansion of vanadium–titanium alloys were determined,[76] as shown in Table IV-6 and Fig. IV-9 (page 188). The most creep-resistant vanadium–titanium–chromium alloys appear to be vanadium–15 wt. % titanium–7.5 wt.% chromium and vanadium–5 wt.% titanium–15 wt.% chromium. From Fig. IV-10 (page 188) it appears that the lower the titanium-to-chromium ratio is in this ternary system, the lower the creep rate.[76] This is explained by the increased bulk modulus of vanadium alloys that have lower titanium-to-chromium ratios, as illustrated in Fig. IV-11 (page 188).

Predictions of multicomponent phase diagrams for the 30 metals of the three transition series: potassium through nickel, rubidium through palladium, and cesium through platinum are presented in a University of California publication.[77] The Engel correlation between electronic configuration and crystal structure is used, together with the regular solution theory of solubilities to predict the structures of various phases of a diagram and their ranges of composition.

(M. Kangilaski)

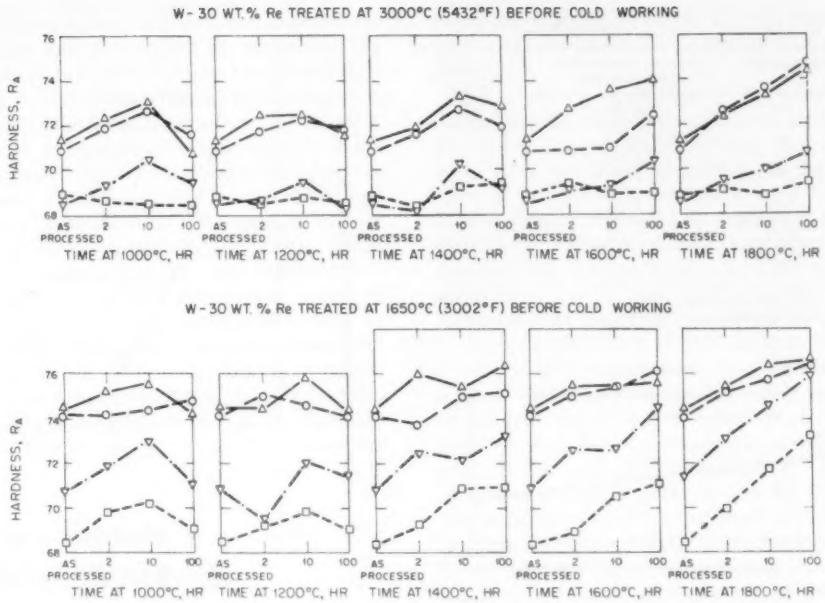
W - 30 WT.% Re TREATED AT 3000°C (5432°F) BEFORE COLD WORKING
HARDNESS, R_A
AS PROCESSED
TIME AT 1000°C, HR
TIME AT 1200°C, HR
TIME AT 1400°C, HR
TIME AT 1600°C, HR
TIME AT 1800°C, HR
W - 30 WT. % Re TREATED AT 1650°C (3002°F) BEFORE COLD WORKING

Fig. IV-7 Influence of solution anneal and aging temperature on age hardening of tungsten–30 wt.% rhenium alloy.[70] Solution annealed: ○, 1800°C (3272°F); △, 2000°C (3672°F); ▽, 2200°C (3992°F); □, 2400°C (4352°F).

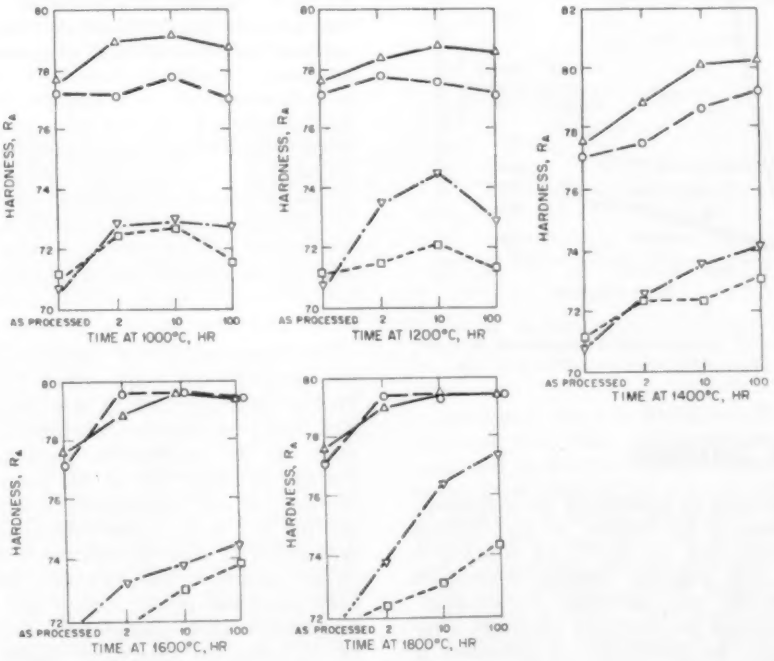

Fig. IV-8 Influence of solution anneal and aging temperature on age hardening of tungsten–30 wt.% rhenium alloy treated 64 hr at 1400°C (2552°F) in hydrogen after cold working.[70] Solution annealed: △, 1800°C (3272°F); ○, 2000°C (3632°F); ▽, 2200°C (3992°F); □, 2400°C (4352°F).

Table IV-6 THERMAL CONDUCTIVITY OF VANADIUM–20 WT.% TITANIUM[76]

Temperature, °C	Thermal conductivity,* watt/(cm)(°C)
100	0.153
200	0.192
300	0.220
400	0.241
500	0.257
600	0.271
700	0.283
800	0.296
900	0.306
1000	0.317
1100	0.33†

*Probable accuracy, ±10%.
†Extrapolated.

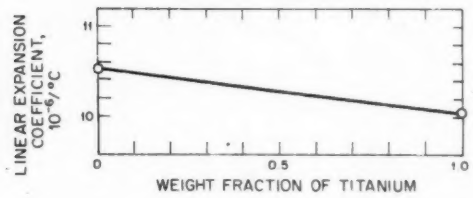

Fig. IV-9 Average[76] linear thermal expansion coefficient vs. weight fraction of titanium in vanadium from 25 to 960°C (77 to 1760°F).

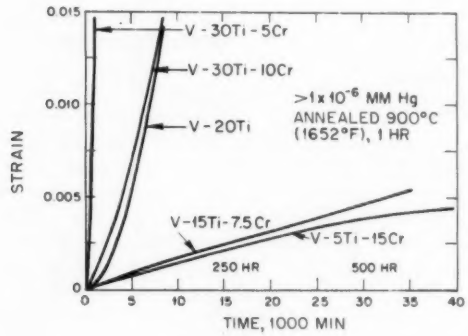

Fig. IV-10 Creep[76] of annealed vanadium–titanium–chromium alloy sheet specimens tested at 15 kg/mm² stress and 650°C (1202°F).

Diffusion Studies

Plutonium diffusion in magnesium and magnesium alloys was studied by the British[78] at temperatures of 420 to 500°C (788 to 932°F) for times up to three months. The reported diffusion coefficients varied considerably with plutonium concentration. The author discussed the ability of aluminum additions to decrease the penetration of plutonium in magnesium alloys by compound formations.

At Argonne[79] the diffusion of uranium in liquid cadmium, zinc, bismuth, and aluminum was measured by capillary-bath techniques as a function of temperature. The diffusivities of uranium in these solvents over the indicated temperature ranges were given as

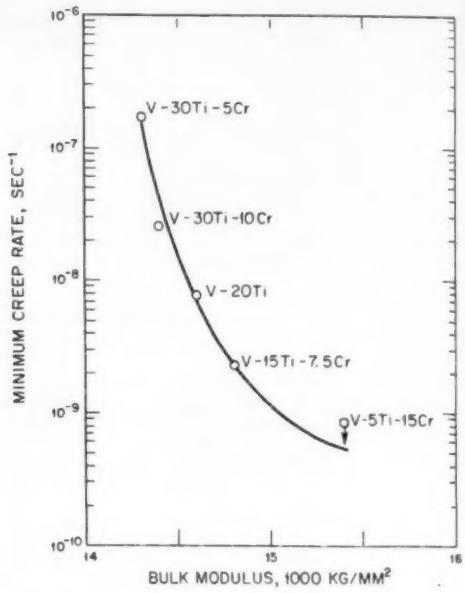

Fig. IV-11 Log minimum strain rate vs. arithmetic mean bulk modulus for vanadium–titanium–chromium alloys annealed at 900°C (1652°F) for 1 hr and tested at 15 kg/mm² stress at 650°C (1202°F) in <1 × 10⁻⁶ mm Hg vacuum.[76]

Solvent	D, 10^{-6} cm²/sec	Temperature range °C	Temperature range °F
Cadmium	1.3–2.3	490–650	914–1202
Bismuth	2.3–5.1	490–725	914–1337
Cadmium	1.3–2.3	450–650	842–1202
Aluminum	0.5–4.5	700–850	1292–1562

The interdiffusion of niobium–vanadium alloys was studied[80] at temperatures between 1400 and 1750°C (2552 and 3182°F). Examination of the diffusion zones by electron-microprobe analyzer indicated that the interdiffusion coefficient decreases by a factor of about 3½ in the range of 0 to 75 at.% niobium for all temperatures studied. Between 75 and 100 at.% niobium, the coefficient drops sharply by a factor of about 15 relative to the coefficient at higher vanadium concentrations. Kirkendall shifts were measured in all couples and were larger in the niobium/alloy couples than could be accounted for by maximum theoretical shifts in the couples. A large nonequilibrium vacancy flux, possibly caused by dislocation movement in the diffusion zone, was suggested as an explanation for the anomalous effect.

The diffusion of carbon into tantalum carbide and niobium carbide was determined by measuring the growth of carbide layers at various temperatures.[81] The values of diffusivity determined by layer growth measurements in the tantalum–carbon system were about five times any previously determined by standard techniques. Values of activation energy for carbon diffusion in TaC and Ta_2C were 86,000 and 89,000 cal/mole, respectively. The diffusion results for carbon in the niobium–carbon system were given by the equation $D = 1.2 \exp(-79{,}000/RT)$ cm^2/sec. The parameters for diffusion of carbon in Cb_2C could not be determined. Above 200°C (3632°F) the diffusivity of carbon in Nb_2C appeared to decrease with temperature, as determined by layer-growth observations and calculations. The authors indicate that the probable source of error is in the niobium–carbon phase diagram. (A. N. Ashurst)

Radiation Effects in Nonfuel Materials

Stainless Steel

The ductility of austenitic stainless steel after irradiation was shown to be dependent on the irradiation temperature, the service temperature, the grain size, the heat-treatment, and the insoluble second-phase distribution. Martin, Weir, and coworkers at Oak Ridge[82,83] have studied the radiation-induced change in the ductility of a number of stainless steels. Type 304 stainless steel was investigated up to 600°C. In general, the ductility of stainless steel, solution annealed prior to irradiation, was better than that of steel cold worked prior to irradiation. An exception to this generality was noted under the conditions of irradiation followed by straining at 200°C (392°F). Here, low ductility was observed for irradiated stainless steel that was solution annealed prior to irradiation. Cold working, followed by carbide precipitation at an intermediate temperature, improved the ductility of irradiated stainless steel tested at 200°C (392°F). Also studied were the effects of very small concentrations of boron on the irradiation embrittlement of type 304 stainless steel irradiated to a higher exposure, about 1.0×10^{21} neutrons/cm^2 (>1 Mev), in a thermal-neutron test reactor. Only small variations were found in the ductilities after irradiation of all electron-beam-melted heats, although there was an order of magnitude difference between the highest and lowest concentrations of boron. The concentrations of helium expected from the ^{10}B reaction were calculated for each of the alloys. However, the lack of variation in ductility of the electron-beam-melted heats is more easily explained when one considers the helium from all sources, since the difference in total concentration is less than a factor of 2. It was concluded that removing the ^{10}B from the alloy is not the ultimate solution for improving the ductility of irradiated alloys.

The effect of irradiation on thin-walled type 304 stainless-steel-clad fuel rods was investigated by the Westinghouse Atomic Power Division.[84] These rods were irradiated as part of the Saxton reactor core to a fast-flux exposure of about 1.1×10^{21} neutrons/cm^2 (>1 Mev). Postirradiation examinations showed no evidence of failure or crack formation, although the cladding was subjected to plastic deformation.

Workers at Argonne[17] are using tube-burst tests to evaluate the effect of fast-neutron irradiation on EBR-II 304 stainless-steel fuel cladding. Fuel and sodium were removed and the tubes tested in burst at several temperatures from 20 to 550°C (68 to 1022°F). The fast-flux exposure is calculated to be about 1.1 to 1.5×10^{22} neutrons/cm^2. A comparison of the tangential rupture stress for irradiated and unirradiated tubes as a function of test temperature is given in Fig. IV-12. Elongation measurements based on tube-diameter increases are inconclusive owing to fragmentation and tearing in the rupture area.

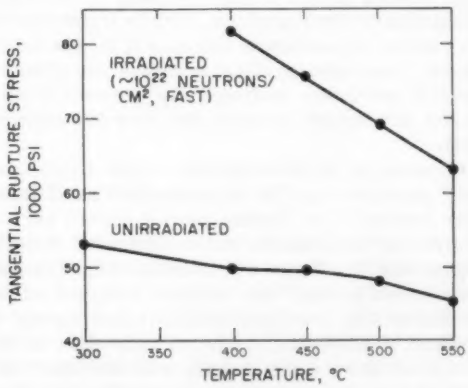

Fig. IV-12 Rupture stress vs. test temperature for EBR-II type 304 stainless-steel cladding tubes.[17]

AISI types 304, 316, 316-L, and 17-4 PH stainless reflector pins have been used by Los Alamos[85] personnel in the Los Alamos Molten Plutonium Reactor Experiment (LAMPRE) for about two years at temperatures near 500°C (932°F). The pins received a total dose of 8×10^{20} to 2.2×10^{21} neutrons/cm^2. Calculations indicate that 40% of the total neutrons had energies greater than 0.9 Mev, and 90% were above 0.1 Mev. The tensile and creep properties are being measured in cooperation with Oak Ridge to determine the magnitude of elevated-temperature embrittlement due to fast-neutron (n,α) reactions. Preliminary data show that the ductilities of irradiated 304, 316, and 316-L steels decrease

markedly at test temperatures greater than 600°C (1112°F). Insignificant changes were noted for test temperatures below 600°C. It was reported that this confirms that atomic-displacement damage is annealed out during irradiation at 500 to 550°C (932 to 1022°F), and the effect of helium (alpha particles) is apparent only above 600°C. The ductility of 17-4 PH steel, however, shows very little change at test temperatures over 600°C. It is postulated that the intragranular precipitates act as sinks for helium and prevent migration to the grain boundaries where it can cause embrittlement. Little change in yield strength was noted between irradiated materials and controls up to test temperatures of 900°C (1652°F).

Workers at Vallecitos Atomic Laboratory[86] studied the effect of neutron irradiation on annealed and cold-worked type 304 stainless steel at several temperatures. Specimens were irradiated to 1.25×10^{20} neutrons/cm^2 (>1 Mev) at 43°C (109°F). They found an increase in yield and ultimate strength after irradiation in both the annealed and cold-worked material at 20°C, with a lesser degree of increase noted in the cold-worked material. Irradiated and cold-worked specimens failed in a ductile manner with total elongations as low as 0.5% at 315°C (600°F). Although cold working produced large amounts of austenite-to-martensite transformation, neutron irradiation did not produce a measurable increase in the martensite content. Transmission electron microscopy of the irradiated specimens confirmed the presence of martensite and epsilon phase in the type 304 stainless steel.

Personnel of the Westinghouse Atomic Power Division[87] examined type 348 stainless-steel fuel cladding after removal from Yankee reactor cores I and II to confirm its acceptability and to determine its irradiation stability. Visual and metallographic examinations revealed that the surface condition of the irradiated fuel rods was excellent and showed no evidence of corrosion, cracks, or other defects. The microstructure of the cladding was essentially unchanged as a result of neutron irradiation in Yankee. Although the cladding showed marked increases in hardness and strength, the remaining ductility was demonstrated to be adequate.

To evaluate the loss of ductility, Bettis[88] workers made fatigue and burst tests on type 347 stainless-steel tubes that had been irradiated in the Engineering Test Reactor. The tests associated with this study used representative conditions of pressure cycling and geometry to determine the bursting pressure and fatigue life of both unirradiated control specimens and sections of an irradiated in-pile tube. Results show that irradiation increased the tensile strength and the low-cycle fatigue life of these stainless-steel tubes subjected to pressure cycling.

A cooperative program carried out between General Electric Company, Cincinnati, and General Electric Company, Vallecitos, on the radiation-induced property changes of an iron–chromium–aluminum–yttrium alloy showed that irradiation at 700°C (1292°F) to 3.4×10^{20} neutrons/cm^2 ($E \geq 1$ Mev) and subsequent testing at 600 and 700°C (1112 and 1292°F) produced a decrease in strength but no adverse effect on ductility.[70] Control specimens were given a thermal treatment at 700°C in a 50 vol.% argon–50 vol.% helium atmosphere for a time equal to the irradiation time.

An investigation made at Harwell[89] concerned fission-fragment damage in several austenitic steels, a 20 wt.% chromium–20 wt.% nickel–0.44 wt.% niobium, an 18 wt.% chromium–37 wt.% nickel, and an 18 wt.% chromium–12 wt.% nickel alloy. Lattice-parameter measurements were made, and electron microscopy was used to study the effects of fission-fragment bombardment at about 60°C (140°F). It was found that the number of small lattice defects present is greater when irradiation dose rates are high for the 20 chromium alloy, whereas a somewhat lower dose rate produced the same effect in the two 18 chromium alloys.

Studies made at Battelle Memorial Institute[90] have shown that ^{133}Xe release during postirradiation heating of recoil-impregnated iron–20 wt.% chromium alloy foils is dependent on time, temperature, and concentration. Gas release as a function of heating time does not follow the behavior predicted by classical diffusion. Experiments indicate that neither an anomalous surface concentration nor specimen oxidation is responsible for observed release behavior. The dependencies are most readily explained in terms of diffusional release accompanied by fission-gas clustering and bubble formation, although other mechanisms may influence the release behavior. Evidence of gas-bubble formation was obtained.

Low-Alloy Steels

Charpy impact data obtained by Bettis[91] personnel on A-302B pressure-vessel steel following reirradiation after a postirradiation anneal at 650°F (343°C) shows that, when taking into consideration the effect of all neutrons having energies >67 kev, annealed and reirradiated material accrued less damage than the material irradiated to the same total dose without an intermediate anneal. These same data are inconclusive if considered on the basis of measurements of only neutrons having energies larger than 1 Mev. The effect of neutron irradiation on the embrittlement of several pressure-vessel steels, namely, A-302B, A-350LF1 (Modified), and A-212B, is the object of continuing research at the Naval Research Laboratory.[92]

An investigation made at Harwell[93] was concerned with the effect of a hydrogen concentration of approximately 1.4 cm^3 (NTP) per 100 g of steel on the room- and elevated-temperature tensile properties, notch-strengthening and brittle-fracture characteristics, and delayed fracture tendencies of a 1 wt.% chromium–½ wt.% molybdenum steel in the unir-

radiated and irradiated (1.0×10^{19} to 1.4×10^{19} fission neutrons/cm^2) conditions. The hydrogen embrittles this steel at room temperature and, to a lesser degree, at elevated temperatures. The embrittling effect of hydrogen on irradiation of steel does not differ significantly from hydrogen's effect on unirradiated steel. Limited results suggest the ductile-to-brittle transition temperatures of the unirradiated and irradiated steel are raised by the presence of hydrogen. However, hydrogen has no significant effect on the notch strength, and the irradiated steel is not prone to hydrogen-induced delayed fracture.

Tensile tests made on a 12 wt.% nickel–5 wt.% chromium–3 wt.% molybdenum maraging steel after irradiation to about 3.1×10^{19} neutrons/cm^2 (>1 Mev) by Chalk River[51] researchers show that the increase in yield strength is only about $\frac{1}{6}$ that usually found in the low-strength ferritic steels after similar irradiation. Results are given in Table IV-7. This smaller increase is attributed to the higher yield point of unirradiated material.

Incoloy 800, an iron-base alloy containing approximately 30 wt.% nickel and 20 wt.% chromium, is being considered by the Atomic Power Equipment Department, General Electric,[96] as cladding material for use at elevated temperatures. Three irradiation environments were investigated: superheated steam at 400°C (752°F), inert-gas mixture at 704°C (1300°F), and pressurized water at 177°C (350°F). Neutron exposures of 5×10^{19}, 1.2×10^{20}, and 2×10^{21} neutrons/cm^2 (>1 Mev) were followed by testing at 25 and 593°C (77 and 1100°F). Irradiations at approximately 400°C (752°F) produced a decrease in the ductility at 593°C test temperature without an increase in yield strength, whereas the properties determined at 25°C were only slightly different from those of the controls. The fracture at 593°C was a brittle transgranular fracture. The high neutron exposure below 177°C produces an increase in yield strength and a decrease in ductility at both 25 and 593°C. These were attributed to point-defect hardening.

Table IV-7 ROOM-TEMPERATURE TENSILE PROPERTIES OF THE 12 WT.% NICKEL–5 WT.% CHROMIUM–3 WT.% MOLYBDENUM STEEL[52]

Orientation	Irradiation neutrons/cm^2 (>1 Mev)	Yield strength (0.2% offset), 1000 psi	Ultimate tensile strength, 1000 psi	Elongation in 1 in., %	Reduction of area, %	No. of samples
Rolling direction	0	185	188	9.1	65	3
	3.1×10^{19}	194	202	7.5	68	3
Transverse direction	0	185	188	8.5	62	3
	3.1×10^{19}	197	203	7.4	67	3

Other studies made at Saclay[94] show hardening and embrittlement of carbon steels by neutron irradiation. The effects of grain size, structure prior to work hardening, and irradiation temperature were determined. Recovery occurred in two stages with retardation at about 300°C.

Thin sheet specimens of chromium–manganese steel containing 0.4% carbon, 6% manganese, and 1% chromium were heated to 1050°C, cooled to 500°C, hot rolled at 550°C to a reduction of 80%, and quenched in water. After this treatment the steel had an austenitic–martensitic structure. The specimens were irradiated with 5-Mev electrons at doses of 6×10^{14} to 8×10^{14} electrons/cm^2 and were subjected to rupture tests 24 hr after irradiation.[95] The electron irradiation caused a decrease in plasticity with $\theta = 138$ kg/mm^2 for the irradiated samples. The yield point, $\theta_{0.2}$, was 80.7 kg/mm^2 for the controls as compared with 69.3 kg/mm^2 for the irradiated samples. However, the elongation at rupture was 3.5% for the controls as compared to 4.3% for the irradiated samples. These anomalous results were explained by the fact that the steel is in a metastable state after the thermal mechanical treatment. Irradiation promoted the transition from the metastable state to an equilibrium state. Irradiation had the effect of a low-temperature anneal in this case.

Nickel-Base Alloys

Studies were made at Oak Ridge[97] on the property changes in Hastelloy N induced by irradiation at 700°C (1292°F) to about 7×10^{20} neutrons/cm^2 (E >1 Mev) and 9×10^{20} neutrons/cm^2 (thermal). The strength and ductility were determined as a function of test temperatures for the range 20 to 900°C (68 to 1652°F). The effect of strain rates of 0.002 and 0.2 in./min was determined for test temperatures of 500, 600, 700, and 800°C. The ductility was reduced for deformation temperatures of 500°C and above. The loss of ductility was more significant at the lower strain rates, and the specimen exhibited an intergranular fracture. Postirradiation annealing of the irradiated materials did not improve the ductility. The investigators believe that these data suggest that helium generation from the (n,α) reaction is the cause of the low ductility.

Another investigation of the effect of irradiation on nickel-base alloys was made by General Electric, Cincinnati.[98] They studied the influence of postirradiation annealing on the stress-rupture properties at 1200 and 1500°F (649 and 816°C) of a niobium-modified 80 wt.% nickel–20 wt.% chromium alloy that was irradiated at pile-ambient temperature. Results at both test temperatures show a substantial

radiation-induced decrease in ductility, which is partially recovered by annealing. The rupture life at 1200°F is reduced by irradiation (but it is increased at 1500°F) at lower stresses. Annealing appears to nullify radiation effects on rupture life.

Zirconium Alloys

The workers at Culcheth[99] have studied the combined effects of irradiation and hydrogen on the impact properties of cold-worked Zircaloy-2 and a zirconium–2½ wt.% niobium alloy in the annealed, cold-worked, and heat-treated conditions. Materials containing nominally 120, 300, and 500 ppm hydrogen were irradiated in the Dounreay Materials Testing Reactor at 300°C (572°F) to 2.3×10^{20}, 4.7×10^{20}, and 5.3×10^{20} neutrons/cm^2 (fast). Impact tests were made after irradiation. It was found that irradiation and hydrogen lower the impact properties but that these effects are not arithmetically additive. Irradiation can increase the (3 ft-lb) transition temperature by as much as 200°C (360°F). The effect of irradiation is more marked on the material with the lower hydrogen content. Also, at low hydrogen levels, the impact properties of the Zircaloy-2 are superior to those of the zirconium–2½ wt.% niobium alloy. There was little difference noted in the impact properties as a result of increasing the dose from 2.3×10^{20} to 5.2×10^{20} neutrons/cm^2.

Other Materials

The effects of irradiation at −423°F (20°K) on a wide variety of materials was investigated by Aerojet-General Corp.[100] These materials, which include A-356, 6061, and 7075 aluminum alloys; 347, A-286, and 410 stainless steels; Hastelloy C, Inconel X-750, and Inconel 713C nickel-base alloys; and A-110 AT titanium alloy, were irradiated in liquid hydrogen for about 400 hr. This reviewer estimates that this is equivalent to approximately 5×10^{17} neutrons/cm^2 ($E > 0.5$ Mev). Tests were made at −423°F (the irradiation temperature) in liquid hydrogen immediately after irradiation without allowing the specimens to warm up. The following trends were observed from the results:

1. Cast and as-welded materials are affected more by neutron radiation at liquid-hydrogen temperatures than are wrought materials.
2. The tensile strength does not increase consistently for all materials.
3. A radiation-damage threshold level (dose to produce a change in properties in excess of the standard deviation) of 1×10^{17} neutrons/cm^2 was established for Inconel X-750, Hastelloy C, 7075-T6, A-286, Inconel 713C (cast), A-110-HT weldment, cast 347 stainless steel, A-356, and 6061.

Some 28 papers on the radiation-induced effects on properties of a number of materials are included in a 1965 ASTM publication.[101] This publication offers excellent coverage of relatively recent research including papers on the atomistic aspects of irradiation damage on metals, engineering properties and behavior of metals and alloys in nuclear environments, and design criteria, code, and safety considerations of irradiation damage to reactor structural and containment components.

Basic Studies of Radiation Effects

Helium atoms formed by the (n,α) reaction from ^{10}B are believed to contribute to the low ductility of a number of materials at elevated temperature. A study was made by members of the staff at University of Queensland, Australia,[102] on helium-gas precipitation in irradiated copper–boron alloys. The lattice parameter increased during irradiation at 100°C (212°F), decreased during annealing to a value below that for the unirradiated material, and finally increased with more annealing. After complete annealing the lattice parameter is equal to that of the unirradiated materials. The authors explain this behavior by suggesting that, during annealing, each helium atom captures two vacancies and enters substitutional solution before migrating to form gas bubbles. As the gas bubbles form, helium leaves solution and the number of helium-vacancy combinations is reduced.

The amount of gas formed by fast-neutron-flux reaction, helium from (n,α), and hydrogen from (n,p) were calculated by Atomics International[103] investigators for several fuel-cladding materials. It is assumed that the fuel-cladding materials had been exposed to a fast-neutron flux of 10^{16} neutrons/(cm^2)(sec) for a period of two years. The final results for the six fuel-cladding materials of interest appear below:

Alloy	Atoms of hydrogen/10^6 atoms alloy	Atoms of helium/10^6 atoms alloy
316 S.S.	8600	400
304 S.S.	6875	350
Nb	1130	70
V–10% Ti	770	140
V–20% Ti	920	175
Zircaloy-2	350	175

German[103] investigators have calculated the recoil spectrum of the primary knock-ons for reactor irradiation of aluminum, iron, copper, silver, and gold. The neutron flux density and energy distribution is that for the low-temperature irradiation facility at the Munich Technical University reactor (FRM). The contributions of elastic and inelastic scattering processes of fast neutrons were calculated separately. The anisotropy of elastic scattering was taken into account. Using these recoil spectra, the expected production rate of Frenkel defects was calculated, assuming the displacement model of Kinchin and Pease. These calculated production rates agree with the values deduced from electrical-

resistivity measurements only, if one uses a mean displacement energy of 50 ev for aluminum, 160 ev for copper, 190 ev for silver, and 130 ev for gold. A similar comparison of theory and experiment for deuteron irradiation gives quite different displacement energies, using the same displacement model. Therefore it was deduced that the Kinchin–Pease model cannot account for the right dependence of the number of stable Frenkel pairs on the energy of the primary knock-ons.

Researchers at Harwell[106] have made an attempt to determine experimentally the relation between density of defect clusters and critical shear stress of single crystals of neutron-irradiated copper. Single crystals and foils were irradiated to 2.5×10^{18} neutrons/cm^2 and examined after annealing for various times at 275, 306, and 336°C (527, 583, and 632°F). They found that a single linear relation existed between critical shear stress at 4.2°K and the square root of the density of clusters less than 50 A in diameter after anneals at all three temperatures. A linear relation was not found for larger clusters. They concluded that irradiation hardening is almost entirely the result of small vacancy clusters and that the average value of resistance per cluster is 1.25×10^{-4} dyne. (F. R. Shober)

Ceramic Technology

The September 1965 issue of the *Proceedings of the British Ceramic Society* is devoted to a review of "Fabrication Science."[106] Topics covered include "Preparation, Characterization, and Properties of Powders," "Forming Processes," "Sintering and Related Processes," and "Other Fabrication Routes." The introductory paper, by J. Williams of Harwell, to the section on powders is particularly useful. The author concludes that it is of importance to control the following powder properties:

1. Particle size
2. Particle-size distribution
3. Particle shape
4. The physical nature of the bounding surfaces
5. The chemical nature of the bounding surfaces

Although there has been reasonable improvement in the degree to which authors of technical reports indicate the characteristic size and shape of experimental materials, little attention has been given to the boundary characteristics.

Other papers in this collection which will be of particular value to workers in this field include the articles by J. White on sintering and that of Vasilos and Spriggs on hot pressing.

Morgan and Scala have obtained very high density in a variety of oxides by a variation on conventional hot pressing which they have designated "calcintering."[107] In this process a precursor, thermally decomposable compound (typically, a hydrate) is pressed at room temperature and heated under pressure in a permeable die to obtain densification. The authors, by this technique, have obtained translucent, near-theoretical density in MgO at 1000°C (1832°F). The process would seem to have advantages for producing limited quantities of simple shapes.

Carneglia[108] has made a detailed examination of recent strength–grain-size data for MgO, BeO, and Al_2O_3 ceramics. For large grain sizes the strength σ is inversely proportional to the square root of the mean grain diameter D (Knudson equation, $\sigma = A/D^{1/2}$). For small grain sizes an additive term was required (Petch equation, $\sigma = B + C/D^{1/2}$). In these relations A, B, and C are constants for a given material and processing technique.

It is inferred from this that three modes of fracture initiation may be significant: (1) true brittle behavior, (2) initiation by plastic yield, and (3) initiation by viscous slide at grain boundaries. Which of these occurs in a given case is thought to be dependent on the material, grain size, impurities, and temperature.

Feith, at General Electric, has measured the thermal conductivity of BeO, CaO-stabilized ZrO_2, Y_2O_3-stabilized ZrO_2 plus zirconium, and Y_2O_3 at higher temperatures than have previous workers, using a radial-heat-flow device.[109] The data are presented in Figs. IV-13 to IV-16, together with literature data selected by the author. (H. D. Sheets)

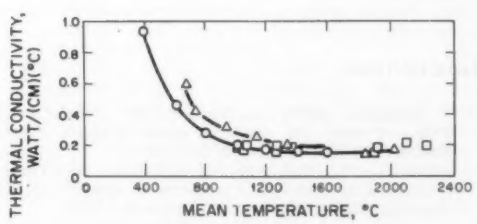

Fig. IV-13 Thermal conductivity[109] as a function of temperature for BeO. □, Feith (ρ = 100%); ○, Kingery (ρ = 100%); △, Taylor (ρ = 99%).

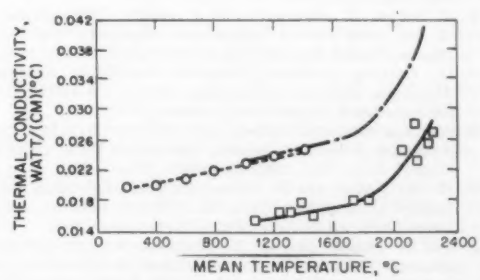

Fig. IV-14 Thermal conductivity[109] as a function of temperature for CeO-stabilized ZrO_2. □, Feith (ρ = 66.3%); —·—, this work (ρ = 100%); — — ○, Kingery (ρ = 100%).

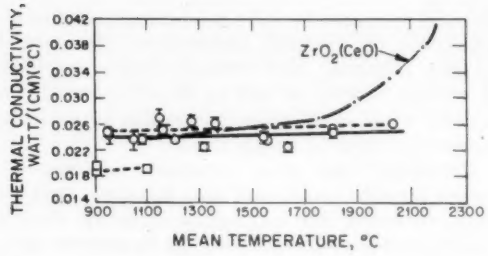

Fig. IV-15 Thermal conductivity as a function of temperature for Y_2O_3-stabilized ZrO_2 plus zirconium.[109] ○, *ρ = 97%;* ––, *ρ = 100%;* □, *Kingery* [$ZrO_2(Y_2O_3)$].

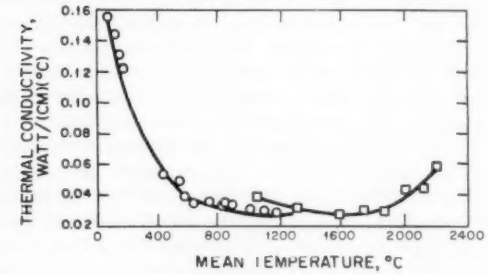

Fig. IV-16 Thermal conductivity[109] *as a function of temperature for Y_2O_3. Corrected to 100% density:* □, *Feith;* ○, *Kingery.*

References

1. T. Nakayama and T. Koizumi, The Structure of Oxide Films Formed on the Zirconium Surface, *Nippon Kinzoku Gakkaishi*, 29: 472-478 (1965).
2. B. Cox and C. Roy, The Use of Tritium as a Tracer in Studies of Hydrogen Uptake by Zirconium Alloys, Canadian Report AECL-2519, December 1965.
3. W. D. Burch (Comp.), Transuranium Quarterly Progress Report for Period Ending February 28, 1965, USAEC Report ORNL-3880, Oak Ridge National Laboratory, January 1966.
4. Centre d'Étude de l'Énergie Nucléaire, In-Pile Corrosion of Nuclear Materials. Final Report, March 1, 1962–March 31, 1964, USAEC–Euratom Report EURAEC-1522, 1965.
5. J. Board, G. Holyfield, and J. Dalley, The Oxidation of Superheat Materials in Steam: Austenitic Stainless Steels, British Report TRG-Report-1148, August 1965.
6. G. Östberg (Comp.), Progress Report on Reactor Materials and Fuel Elements, July 1–December 31, 1965, Swedish Report S-343, January 1966.
7. Argonne National Laboratory, Reactor Development Program Progress Report, November 1965, USAEC Report ANL-7122, Dec. 27, 1965.
8. G. R. Taylor and P. Cohen, Corrosion Product Behavior in Stainless-Steel-Clad Water Reactor Systems, *Nucl. Appl.*, 1(5): 446-452 (October 1965).
9. P. R. Swann and J. D. Embury, Microstructural Aspects of Stress-Corrosion Failure, in *High-Strength Materials*, pp. 327-362, John Wiley & Sons, Inc., New York, 1965.
10. Argonne National Laboratory, Chemical Engineering Division Semiannual Report, January–June 1965, USAEC Report ANL-7055, October 1965.
11. Materials Advisory Board, National Academy of Sciences–National Research Council, Coated Refractory Metal Technology, 1965, Oxidation-Resistant Coatings for Refractory Materials, Report MAB-210-M, November 1965.
12. R. Syre, Handbook on the Properties of Niobium, Molybdenum, Tantalum, Tungsten, and Some of Their Alloys, French Report AGARDograph-94, May 1965.
13. L. E. Link (Ed.), Reactor Technology, Selected Reviews—1965, USAEC Report TID-8541, January 1966.
14. H. W. Savage, Technology of Liquid Metals, USAEC Report ORNL-tr-854, translated from Italian Report RTI/ING(65)-1, April 1965.
15. S. K. Lee, An Investigation of Nickel-Base Brazing Alloys and Brazed Joints for Service in Liquid Sodium, USAEC Report NAA-SR-11326, Atomics International, Dec. 15, 1965.
16. R. C. Andrews, R. H. Hiltz, L. H. Kirschler, S. J. Rodgers, and F. Tepper, Effect of High-Temperature Sodium on Austenitic and Ferritic Steels, Topical Report No. 4, Results of Mechanical Properties Tests of 316 SS Specimens in 1200°F Sodium Contaminated with Carbon, USAEC Report MSAR-65-194, MSA Research Corp., December 1965.
17. Argonne National Laboratory, Reactor Development Program Progress Report, January 1966, USAEC Report ANL-7152, Feb. 24, 1966.
18. M. M. Rubright, The Corrosion of Croloy 2¼ Steel in the Products of a Sodium-Water Reaction; Systems of Sodium Hydroxide in Water and in Molten Sodium, USAEC Report BAW-1280-30, The Babcock & Wilcox Co., Nov. 15, 1965.
19. H. W. Savage, E. L. Compere, W. R. Huntley, B. Fleischer, R. E. MacPherson, and A. Taboada, SNAP-8 Corrosion Program Summary Report, USAEC Report ORNL-3898, Oak Ridge National Laboratory, December 1965.
20. C. J. Lymperes and H. Slotnick, The Compatibility of Compacted Boron Carbide in Stainless Steel—Alkali Metal Systems, USAEC Report TIM-822, Pratt & Whitney Aircraft, CANEL, July 27, 1965.
21. Oak Ridge National Laboratory Status and Progress Report, December 1965, USAEC Report ORNL-3911, Jan. 6, 1966.
22. E. A. Kovacevich, Erosion Properties of Selected Turbine Materials in Water and Potassium, Report AFAPL-TR-65-130, AiResearch Mfg. Co., January 1966.
23. J. F. Nejedlik and E. J. Vargo, Material Resistance to Mercury Corrosion, *Electrochem. Technol.*, 3: 250-258 (September–October 1965).
24. A. F. Voigt (Ed.), Reactor Materials Development Quarterly Report for Division of Reactor Development USAEC, October–December 1965, USAEC Report IS-RD-4, Ames Laboratory.
25. D. J. Cleary, Wetting Characteristics of Liquid Lead-Bismuth Eutectic on Stainless Steels, Thesis, USAEC Report IS-T-56, Ames Laboratory, November 1965.
26. P. A. Nelson, M. L. Kyle, G. A. Bennett, and L. Burris, Jr., Corrosion of Refractory Metals by Zinc-Magnesium-Uranium and Halide Salt Systems, *Electrochem. Technol.*, 3: 263-269 (September–October 1965).
27. M. L. Kyle, P. A. Nelson, and L. Burris, Jr., Corrosion of Steels and Tantalum by Molten Cadmium-Magnesium-Zinc Systems, *Electrochem. Technol.*, 3: 258-262 (September–October 1965).
28. M. J. Hordon and M. E. Reed, Study of the Mechanism of Atmospheric Interaction with the Fatigue of Metals, Report N66-11747 (NASA-CR-68036), National Research Corp., August 1965.
29. D. H. Nyman, High-Temperature Creep-Rupture Properties of Hastelloy X in Vacuum, USAEC Report BNWL-167, Battelle–Northwest, November 1965.
30. F. A. Comprelli, High-Temperature Tensile Properties of Selected Alloys After Prolonged Thermal Exposure, USAEC Report GEAP-4794, General Elec-

tric Company, Atomic Power Equipment Department, February 1965.
31. B. J. Seddon (Comp.), Steels Data Manual, Properties of Interest in Reactor Design, British Report TRG-Report-840, Apr. 9, 1965.
32. A. M. Adair and H. A. Lipsitt, On the Fatigue Limit Behavior of Iron and Mild Steel, Report ARL-65-255, Aerospace Research Laboratories, Office of Aerospace Research, December 1965.
33. W. H. Irvine, *The Significance of Recent Developments in Fracture Mechanics in Great Britain in Relation to the Safety of Reactor Pressure Vessels*, American Society for Testing and Materials, Special Technical Publication No. 380, pp. 429-437, 1965.
34. V. F. Zackay, W. W. Gerberich, R. Busch, and E. R. Parker, The Strength and Toughness of Dynamically Strain Aged Alloy Steels, USAEC Report UCRL-16363, University of California Lawrence Radiation Laboratory, October 1965.
35. Centre National de Recherches Metallurgiques, A Study on Embrittlement by Plastic Fatigue in Reactor Vessels, Quarterly Report No. 6, April 1–June 30, 1965, USAEC–Euratom Report EURAEC-1441, July 1965.
36. Centre National de Recherches Metallurgiques, A Study on Embrittlement by Plastic Fatigue in Reactor Vessel Steels, Special Report No. 3, December 15, 1963–December 31, 1964.
37. C. R. Honeycutt, and J. C. Sawyer, Determination of Elevated-Temperature Fatigue Data on Refractory Alloys in Ultra-High Vacuum, Quarterly Report No. 5, July 1–October 1, 1965, Report NASA-CR-54775, Thompson Ramo Wooldridge Inc., Oct. 15, 1965.
38. J. C. Sawyer and E. A. Steigerwald, Generation of Long Time Creep Data of Refractory Alloys at Elevated Temperatures, Ninth Quarterly Report, June 26–September 26, 1965, Report NASA-CR-54773, Thompson Ramo Wooldridge, Inc., Oct. 8, 1965.
39. H. B. Probst, The Behavior of Materials at High Temperatures, *Ind. Res.*, 7(12): 60-66 (November 1965).
40. W. D. Klopp, W. R. Witzke, and P. L. Raffo, Effects of Grain Size on Tensile and Creep Properties of Arc-Melted and Electron-Beam-Melted Tungsten at 2250-4140°F, *Trans. AIME*, 233: 1860-1866 (October 1965).
41. E. Votava, Effect of Purity on the Mechanical Properties of Niobium, *J. Less-Common Metals*, 9: 409-415 (December 1965).
42. G. Taylor and J. W. Christian, The Effect of High Vacuum Purification on the Mechanical Properties of Niobium Single Crystals, *Acta Met.*, 13: 1216-1218 (November 1965).
43. Ya. B. Gurevich and V. L. Orzhekhovskii, Effect of Hot Plastic Deformation on the Structure and Properties of Molybdenum, Niobium, and Titanium, Report JPRS-32317, translated from *Izv. Akad. Nauk SSSR, Metal.*, No. 4: 137-143 (July–August 1965).
44. A. J. Ardeli, Creep and Atomic Mobility in Polycrystalline Zirconium, Ph. D. Thesis, Stanford University, 1964.
45. M. L. Picklesimer, Deformation, Creep, and Fracture in Alpha-Zirconium Alloys, USAEC Report ORNL-P-1753, Oak Ridge National Laboratory, 1965.
46. D. Nobili and R. De Maria, Isochronal Recovery of Work Hardening in Aluminum-Alumina Alloys, *J. Nucl. Mater.*, 17: 5-19 (August–September 1965).
47. P. Greenfield, Improvements Relating to Heat Treatment Processes for Magnesium Alloys, British Patent No. 1,007,139, Oct. 13, 1965.
48. R. A. Wood, The Ti-8Al-1Mo-1V Alloy, DMIC Report S-10, Battelle Memorial Institute, Defense Metals Information Center, Apr. 1, 1965.
49. J. J. Kearns, Thermal Expansion and Preferred Orientation in Zircaloy, USAEC Report WAPD-TM-472, Westinghouse Electric Corporation, Bettis Atomic Laboratory, November 1965.
50. W. J. Babyak, Hydride Habit in Zirconium and in Unstressed and Stressed Zircaloy-4, USAEC Report WAPD-T-1757(Rev.), Westinghouse Electric Corporation, Bettis Atomic Power Laboratory, June 1965.
51. Atomic Energy of Canada, Ltd., unpublished.
52. J. M. Davies and C. Steer, Homogenizing the Structures and Mechanical Properties of Welded Zircaloy-2 Tubes, British Report AERE-M-1561, September 1965.
53. W. R. Clough, Metallurgical Studies of Zirconium and Thorium and of the Alloying Behavior of Rare Earth—Transition Metal Systems, USAEC Report NYO-2159-1, Rensselaer Polytechnic Institute, Nov. 1, 1965.
54. J. Winton and R. A. Murgatroyd, The Effect of Variations in Composition and Heat Treatment on the Properties of Zirconium-Niobium Alloys, British Report TRG-Report-1049, July 30, 1965.
55. D. Stewart, B. A. Hatt, and J. A. Roberts, High Speed Thermal Analysis of Zr-Nb Alloys, *Brit. J. Appl. Phys.*, 16: 1081-1088 (August 1965).
56. N. F. Lashko, On the Metastable Polymorphism of Alloys Based on Elements of the Fourth Group (in Russian), *Metalloved Titana*, pp. 74-79, Nauka, Moscow, 1964.
57. K. V. Ravi, The Microstructure and Properties of Martensite Formed from Cyclically Transformed Austenite, Thesis, USAEC Report UCRL-16121, University of California, Lawrence Radiation Laboratory, August 1965.
58. R. Sumerling, J. H. Pearce, S. Freeman, and E. Dobing, U. K. Atomic Energy Authority, unpublished information, 1965.
59. W. S. Pierce, Strength Comparison of Flawed Single-Layer and Multilayer AISI 301 Stainless-Steel Pressure Vessels at Cryogenic Temperatures, Report N65-34501 (NASA-TN-D-2949), October 1965.
60. R. G. Kogan, Evaluation of Carbonyl Nickel, USAEC Report BDX-613-77, Bendix Corp., September 1965.
61. J. C. Hedge, C. Kostenko, and J. I. Lang, Thermal Properties of Fifteen Refractory Metals, AIAA Fifth Annual Structures and Materials Conference, AIAA Publication CP-8, 1964.
62. Z. C. Szkopiak and A. P. Miodownik, The Mechanism of Strain-Aging in Commercially Pure Niobium, *J. Nucl. Mater.*, 17: 20-29 (August–September 1965).
63. H. Bibring, B. Jouffrey, and F. Girard, Examination by Electron Microscope of Niobium Contaminated at High Temperature by Interstitial Elements, USAEC Report ANL-Trans-218, translated from paper presented to Journees d'Atomne de la Societe Francaise de Metallurgie, October 1964.
64. H. Inouye, Equilibrium Solid Solutions of Nitrogen in Nb-1 Wt.% Zr Between 1200–1800°C, USAEC Report ORNL-TM-1355, Oak Ridge National Laboratory, February 1966.
65. H. Inouye, Equilibrium Solid Solutions of Nitrogen in Nb-1 Wt.% Zr Between 1200 and 1800°C, USAEC Report ORNL-P-1677, Oak Ridge National Laboratory, 1965.
66. R. A. Pasternak and R. Gibson, Interaction of Niobium with Active Gases at Very Low Pressures, *Acta. Met.*, 13: 1031-1038 (October 1965).
67. I. E. Kontorovich, L. Ya. Savkina, and G. V. Estulin, Effect of Titanium and Molybdenum on the Recrystallization Temperature and Strengthening of Columbium Alloys (in Russian), *Issled Stalie i Splavov*, pp. 147-149, Nauka, Moscow, 1964.
68. L. D. Kirkbride, The Effect of Yttrium on the Recrystallization and Grain Growth of Tantalum, *J. Less-Common Metals*, 9: 393-408 (December 1965).
69. F. D. Lemkey, B. J. Bayles, and M. J. Salkind, Research Investigation of Phase-Reinforced High Temperature Alloys Produced Directly From the Melt, Final Report, Report AMRA-CR-64-05/4, United Aircraft Corp., July 31, 1965.
70. General Electric Company, Nuclear Materials & Propulsion Operation, High Temperature Materials Pro-

gram Progress Report No. 55, Part A, USAEC Report GEMP-55A, Jan. 21, 1966.
71. A. D. Feith, Measurements of the Thermal Conductivity and Electrical Resistivity of Molybdenum, USAEC Report GE-TM-65-10-1, General Electric Company, Nuclear Materials & Propulsion Operation, 1965.
72. R. J. Fries, An Ultra-High Vacuum Thermobalance for Langmiur Vaporization Studies; Vapor Pressure of Molybdenum, USAEC Report LA-3423, Los Alamos Scientific Laboratory, November 1965.
73. R. H. Schnitzel, Strengthening of Tungsten at Intermediate Test Temperatures from 300 to 1600°C, *Am. Soc. Metals, Trans. Quart.*, 58: 687-690 (1965).
74. H. F. Ryan, Cavities in Tungsten, *J. Less-Common Metals*, 9: 307-308 (1965).
75. R. Szwarc, E. R. Plante, and J. J. Diamond, Vapor Pressure and Heat of Sublimation of Tungsten, *J. Res. Nat. Bur. Std., A*, 69: 417-421 (September–October 1965).
76. Argonne National Laboratory, Reactor Development Program Progress Report, December 1965, USAEC Report ANL-7132, Jan. 25, 1966.
77. L. Brewer, Prediction of High-Temperature Metallic Phase Diagrams, *High Strength Materials*, pp. 12-103, New York, 1965.
78. D. J. Hodkin and P. G. Mardon, The Diffusion of Plutonium in Magnesium and Magnesium Alloys, *J. Nucl. Mater.*, 16: 271-289 (July 1965).
79. J. C. Hesson, H. E. Hootman, and L. Burris, Jr., Diffusivity of Uranium in Various Liquid Metal Solutions, *Electrochem. Technol.*, 3: 240-244 (September–October 1965).
80. R. C. Geiss, C. S. Hartley, and J. E. Steedly, Jr., Interdiffusion in Niobium-Vanadium Alloys, *J. Less-Common Metals*, 9: 309-320 (1965).
81. R. Resnick, R. Steinitz, and L. Seigle, Determination of Diffusivity of Carbon in Tantalum and Columbium Carbides by Layer Growth Measurements, *Trans. AIME*, 233: 1915-1918 (October 1965).
82. W. R. Martin and J. R. Weir, Influence of Preirradiation Heat Treatment on the Postirradiation Ductility of Stainless Steel, *Nucl. Appl.*, 1(5): 478-483 (October 1965).
83. W. R. Martin, J. R. Weir, R. E. McDonnald, and J. C. Franklin, Irradiation Embrittlement of Low-Boron Type 304 Stainless Steel, *Nature*, 208: 73-74 (Oct. 2, 1965).
84. D. R. McClintock, F. Paxon, and H. M. Ferrari, Performance of Thin-Walled Stainless Steel Clad Fuel Rods, *Nucl. Appl.*, 1(5): 425-431 (October 1965).
85. Los Alamos Scientific Laboratory, Quarterly Status Report on Advanced Reactor Technology (ART) for Period Ending January 31, 1966, USAEC Report LA-3482, February 1966
86. J. S. Armijo, J. R. Low, and U. E. Wolff, Radiation Effects on Mechanical Properties and Microstructure of Type 304 Stainless Steel, *Nucl. Appl.*, 1(5): 462-477 (October 1965).
87. W. R. Smalley, Evaluation of Highly Irradiated Yankee Fuel Cladding, *Nucl. Appl.*, 1(5): 319-424 (October 1965).
88. L. A. Waldman and M. Doumas, Fatigue and Burst Tests on Irradiated In-Pile Stainless Steel Pressure Tubes, *Nucl. Appl.*, 1(5): 439-445 (October 1965).
89. B. E. Smith, An X-Ray Study of Fission Fragment Damage in Steels, *J. Nucl. Mater.*, 17: 167-171 (October 1965).
90. A. A. Bauer, D. L. Morrison, F. R. Winslow, J. Bugl, and T. S. Elleman, Postirradiation Heating Fission Gas Release from Iron-20 Wt. % Chromium Alloy, *J. Nucl. Mater.*, 13(1): 75-86 (1964).
91. D. J. Seman and E. J. Pasierb, Considerations on the Annealing of Irradiated Pressure-Vessel Steel, *Trans. Am. Nucl. Soc.*, 8(2): 416-417 (November 1965).
92. L. E. Steele, J. R. Hawthorne, and H. E. Watson, Irradiation Effects on Reactor Structural Materials, Quarterly Progress Report, February 1–April 30, 1965, Report AD-617319, Naval Research Laboratory, May 15, 1965.
93. G. H. Broomfield, Hydrogen Effects in an Irradiated 1 Percent Cr, ½ Percent Mo PWR Pressure Vessel Steel, *J. Nucl. Mater.*, 16: 249-259 (July 1965).
94. J. Lemaire and E. Cibois, Influence of Irradiation by Fast Neutrons on the Mechanical Properties of Some Carbon or Low-Alloy Steels, *Rev. Met. (Paris)*, 62: 785-790 (September 1965).
95. L. N. Bystrov, L. I. Ivanov, and O. A. Bannykh, The Effect of Electron Irradiation on the Mechanical Properties of Steel Subjected to a Thermal Mechanical Treatment, *Fiz. Metal. i Metalloved.*, 19: 791-792 (May 1965).
96. H. J. Busboom, F. A. Comprelli, and C. N. Spalaris, Radiation Damage in Incoloy-800, *Trans. Am. Nucl. Soc.*, 8(2): 418 (November 1965).
97. W. R. Martin and J. R. Weir, Effect of Elevated Temperature Irradiation on Hastelloy N, *Nucl. Appl.*, 1(2): 160-167 (April 1965).
98. R. C. Robertshaw, Neutron-Irradiation Effects on a Nb-Modified 80 Ni-20 Cr Alloy, *Nucleonics*, 23(1): 60 (November 1965).
99. D. S. Wood, J. Winton, and D. Watkins, The Effect of Irradiation on the Impact Properties of Some Zirconium Alloys, British Report TRG-Report-1962, Aug. 18, 1965.
100. W. Weleff, C. E. Dixon, and C. W. Funk, Radiation Effects on Materials at Liquid Hydrogen Temperature, *Trans. Am. Nucl. Soc.*, 8(2): 419-420 (November 1965).
101. *Proceedings of Symposium on Flow and Fracture of Metals and Alloys in Nuclear Environment*, American Society for Testing and Materials, Special Technical Publication No. 380, 1965.
102. B. Russell and I. J. Hastings, A Preliminary Investigation of Helium-Gas Precipitation in Irradiated Copper-Boron Alloys, *J. Nucl. Mater.*, 17: 30-36 (August–September 1965).
103. H. Alter, The Production of Hydrogen and Helium in Reactor Fuel-Cladding Materials, USAEC Report NAA-SR-Memo-10626, Atomics International, Nov. 16, 1964.
104. W. Koehler and W. Schilling, Displacement Probabilities of Lattice Atoms in Various Metals by Reactor Radiation, *Nukleonik*, 7: 389-399 (August 1965).
105. M. J. Makin, F. J. Minter, and S. A. Manthrope, The Correlation Between the Critical Shear Stress of Neutron-Irradiated Copper Crystals and the Density of Defect Structures, *Phil. Mag.*, 13: 729 (1966).
106. Proceedings of the British Ceramic Society — Fabrication Science, No. 3, British Ceramic Society, Stake-on-Trent, October 1965.
107. P. E. D. Morgan and E. Scala, The Formation of Fully Dense Oxides by Pressure Calcintering of Hydroxides, Report No. 346, Materials Science Center, Cornell University, Aug. 30, 1965.
108. S. C. Carneglia, Petch Relation in Single-Phase Oxide Ceramics, *J. Am. Ceram. Soc.*, 48: 80-83 (November 1965).
109. A. D. Feith, Thermal Conductivity of Several Ceramic Materials to 2500°C, USAEC Report GE-TM-64-10-4, General Electric Company, Nuclear Materials and Propulsion Operation, 1964.

Section V

Reactor Materials

Special Fabrication Techniques

Melting, Casting, and Fabrication

Methods employed at Atomics International in the melting and casting of the carbides of uranium are described in some detail in a 1965 report.[1] Large-scale arc-melting furnaces are finding extensive use. A specially designed tilt-casting skull-melting furnace has been constructed. This furnace is equipped with a vacuum system and a 12,000-amp 40-volt d-c power supply; an automatic arc-voltage control rapidly retracts the graphite electrode when the power is shut off. Melting in this furnace is generally conducted with sintered UC feed stock, although unreacted UO_2–graphite pellets can be used. The use of unreacted material often results, however, in greater carbon pickup, less composition control, and considerably more spatter. The size of the batch normally employed in melting varies with enrichment, as required by criticality considerations.

As an alternative to the tilt casting of UC melts, centrifugal casting has been studied by Atomics International. The arc melting of the reacted pellets is done in a graphite crucible that can be rotated around its vertical axis. Several molds are located in radial holes in the upper part of the crucible. The crucible is surrounded by a magnetic coil that prevents arc deflections. The furnace can be evacuated and filled with argon. Melting is achieved by an electric arc, originated from an upper graphite electrode that is connected to the negative side of a 380-kva rectifier. From the crucible the current is conducted through the axis and a sliding contact to the positive side of the power supply. The skull is built up by melting a total amount of 10 to 12 kg of UC and allowing it to solidify at the walls of the crucible. When all the walls are sufficiently covered with UC, the crucible is ready for use. For the casting of rods, 3 to 5 kg of pellets is put into the crucible. The furnace is evacuated and then filled with argon to a pressure of 300 mm Hg. Melting is carried out in about 5 min, and the current is increased slowly to 4000 amp. For casting, rotation speeds up to 700 rpm are used. As a result of the rotation, the liquid UC moves upward at the wall of the crucible, enters the molds, and is then forced into them by a force several times that of gravity. After the molds are filled, the arc is cut off, while the rotation is continued (for about 30 sec) until all UC has solidified. After cooling to room temperature, the cast rods are removed from the molds and the charge for the next cycle is put into the crucible.

In tilt casting, shrinkage cavities, centerline pipes, and internal cracks are occasionally found in the cast rods, especially when the diameter exceeds 1 in. To obtain sound casting without voids, it is important that freezing of the rods proceeds from the bottom to the top. One way to achieve this is to pour slowly; this creates a moving hot top. By proper speed of pouring (i.e., filling the molds within 6 sec, while the UC in the crucible is still heated by the arc), the shrinkage voids can be completely eliminated. The effects of the quenching rate on the physical quality of the cast rods have been studied by Atomics International by controlling the mold temperature. Temperatures in the range of 1000 to 1300°C (1832 to 2372°F) appear as optimal for casting rods of diameters in the order of $\frac{1}{2}$ in. At higher temperatures, high carbon pickup on the periphery and sticking of the UC to the mold occur; whereas at lower temperatures the solidification period is accelerated and the rod structure, as well as the reproducibility of the casting, is affected adversely.

Other melting methods for the preparation of uranium–carbon alloys which do not require the use of graphite electrodes, thus eliminating a major factor in composition-control problems, are under investigation. The French[2] have successfully applied electron-beam melting in a system design for the continuous casting of UC. Granulated carbide is fed from a hopper into a smaller water-cooled hollow cylinder. A 20-kw electron beam is then focused on the carbide. The carbide melts rapidly and runs down into a mold. At the base of the mold is a plunger that is withdrawn at the same rate as the carbide pours in. The product of this technique is similar in density and in grain size to arc-cast material.

The melting of sintered UC melt stock by hollow-cathode-discharge melting (HCD) is currently under consideration at Atomics International. HCD melting, though similar to electron-beam melting, differs specifically by operating at a furnace pressure in the range of 20 to 200 μ. The electron-beam melting

furnace operates under high vacuum, in the 10^{-5} torr range. Melting of UC at the higher pressure of the HCD process is expected to reduce the uranium-volatilization losses and composition-control problems previously encountered in electron-beam melting of UC. Plasma-arc melting is also a technique considered to have good potential as a melting process for UC that must meet a relatively narrow carbon-content specification. The potential advantages of plasma-arc melting are: (1) absence of a carbon-contamination source and (2) operation in an inert atmosphere at pressures up to atmospheric.

Argonne National Laboratory[3] recently developed techniques for the consolidation and fabrication of high-quality small-diameter (<5 mm) thin-wall (<0.55 mm) tubing of vanadium–20 wt.% titanium. Such tubing is being considered for nuclear-fuel cladding. In the developed process vanadium chips and titanium sponge are initially mixed and are compacted in the form of rods. The rods are then electron-beam melted. Next, the electron-beam-melted ingot is remelted by arc melting, and the arc-cast ingot is broken down by extrusion. Tube blanks are produced by a secondary extrusion operation. The tube blanks are cold finished by swaging and drawing. Intermediate anneals are used as required.

Fundamental research at Harvard University on the solidification of metals is discussed in a recent report.[4] Emphasis was placed on atomic processes that occur at the interface between a crystalline solid and liquid and on the influence of crystallography, heat flow, and diffusion on the morphology of the growing crystals. (S. G. Nelson)

Rolling, Swaging, and Coextrusion

Investigators in Canada[5] have developed an extrusion technique for bonding aluminum to Zircaloy-2 without the formation of a diffusion zone. The aluminum can be bonded to the Zircaloy without difficulty, even when a thin layer of oxide is present on the surface of the Zircaloy. As noted by metallographic examination of the bond area, no detectable diffusion takes place during the bonding process. The bond layer can be stretched as much as 8% without affecting the bond. Heating of the bond zone at 260°C (500°F) for 1000 hr and water quenching from this temperature produces no noticeable change in bond strength. Welding close to the bond layer does not appear to affect the aluminum–Zircaloy bond.

Tests made on niobium–type 316 stainless-steel duplex tubing at Atomics International[6] indicate that the quality of the bond in coextruded and explosively bonded tubing is adequate for boiler-tube applications, particularly in SNAP mercury Rankine-cycle boilers. Ultrasonic testing techniques were used to determine unbonded regions of the metal tubing (see subsection on Nondestructive Testing). The strength of the dissimilar-metal bond in the as-received tubing was adequate for severe forming operations. Diffusion studies, coupled with thermal cycling and mechanical deformation tests, indicate that 0.2 to 0.3 mil of interdiffusion can be tolerated in the duplex tubing. This thickness corresponds to an in-service life of 45,000 to 100,000 hr at 1250°F (677°C).

At Savannah River Laboratory[7] coextruded Zircaloy-clad uranium-core tubular elements were investigated as potential fuels for a heavy-water-moderated and -cooled power reactor. Approximately 200 experimental ceramic tubular elements, 10 ft long, were fabricated. Tubes with cores of unalloyed uranium, uranium alloys with 2 wt.% zirconium and with iron, silicon, aluminum, and molybdenum (approximately 0.2% total) were produced. Utilizing the techniques developed for uranium fuel tubes, a number of Th–^{235}U metal fuel tubes were coextruded to pilot the manufacture of Th–^{233}U breeder reactor fuel. (R. J. Diersing)

Plating

Electroplating

In Russia,[8] during a study of rhenium plating on molybdenum, heat-treating of 2-μ rhenium coatings at 100°C (1832°F) for 15 min to improve the quality resulted in the following effects:

1. Diffusion of molybdenum and rhenium improved the bond, and a second layer of rhenium could be plated adherently.
2. Hydrogen was outgassed from the rhenium, and gross cracking of a second 2-μ-thick rhenium layer was avoided.

A rhenium–chromium alloy electrodeposit with a thickness of 10 μ was deposited adherently on copper with no cracking. Poor bonds were obtained on molybdenum, chromium, and tungsten, however. Large grains were observed in the alloy deposit on copper, but much smaller grains were seen in the alloy deposited on molybdenum. Thus the base metal profoundly affected the structure of the rhenium–chromium alloy plate.

Electrolysis of ethanol solutions of uranium or lanthanum nitrates (or ethanol solutions of the chlorides of other metals) yielded deposits on platinum cathodes by a process described as a combination of electroreduction and electroprecipitation.[9] Electroreduction was dominant for protactinium solutions and electroprecipitation for thorium. A stepwise process including reduction of U^{4+} followed by precipitation of $U(OH)_4$ was postulated for U^{6+}. (This is analogous to the well-known process for precipitating hydrated chromic oxide on cathode surfaces during electrolysis of solutions containing Cr^{6+}.) Procedures were developed at Oak Ridge National Laboratory for depositing thorium, protactinium, and other elements

with a high yield (up to 99% for some metals) during 1 hr of electrolysis and for depositing uranium during 2 hr of electrolysis. The development meets the need for reproducing uniformly thin radioactive sources for alpha and beta spectrophotometry and for disintegration-rate determinations of emitters.

(W. H. Safranek)

Nonelectrolytic Chemical Plating

Developments in nonelectrolytic chemical plating during the past quarter again centered largely on protective coatings. An unusual note was the relative large number of techniques that were studied for depositing tungsten. Some work was still being done in the rather well-plowed areas of vapor deposition of molybdenum disilicide and of tantalum metal.

Studies of the deposition of refractory metals and alloys by hydrogen reduction of mixtures of WF_6 and ReF_6 have continued[10] at Oak Ridge. Deposits of tungsten–rhenium alloys obtained with a moving hot zone are uniform in composition and thickness except for circumferential ridges that vary in height, width, and spacing. The cause of these ridges is not known. Alloys were also deposited on the outer surface of a "hot finger" mandrel located in a relatively large mixing chamber. A sample deposit, obtained at 600°C (1112°F) at a total pressure of 10 torrs, had a rhenium content of 25.2 (+1.2, −1.9)% over an 8-in. length.

Molybdenum was deposited[10] by hydrogen reduction of MoF_6 at 600, 700, and 800°C (1112, 1292, and 1472°F). At 800°C, smooth deposits were obtained, whereas, at lower temperatures, whiskers were deposited and MoF_3 was formed in amounts that increased with decreasing deposition temperatures.

The vapor deposition of tantalum by hydrogen reduction of $TaCl_5$ was studied[11] briefly by Polyakov and Zamesova, but very little new information was reported. The effect of substrate temperature on the rate of deposition and coating quality was investigated. The deposits contained tantalum hydrides in addition to tantalum, and high-quality coatings could be obtained only at temperatures above 1000°C (1832°F).

A series of protective coatings has been developed for niobium and niobium alloys to prevent air oxidation when heated. Baranow and Lever[12] dip the niobium in a molten solution of aluminum and tin, with or without additions of chromium and titanium, for a period of 1 to 30 min at a temperature of 1040 to 1260°C (1904 to 2300°F). The coated niobium may then be given a diffusion treatment in an inert atmosphere at 1040°C for 1 hr. Priceman and Sama[13] enrich the surface of the niobium or niobium alloy with titanium by titanizing and then deposit a protective aluminum coating thereon by pack calorizing. The coating is claimed to be protective in air at 590 to 1260°C (1094 to 2300°F). Grubessich and Sama[14] dip the niobium or niobium alloy into a molten bath containing 85 wt.% tin, 10 wt.% aluminum, and the balance selected from zinc, iron, chromium, and tin.

Pratt & Whitney Aircraft has developed[15] the slurry-coating technique for applying protective coatings to the refractory metals and alloys. The slurry is applied by spraying to the properly cleaned and etched substrate. Two of the best coatings have been designated PWK-1 and PWK-35 and are applied as two-layer coatings. The compositions are given in Table V-1. The optimum total thickness for these coatings falls in the range of 3 to 5 mils. On niobium–1 wt.% zirconium alloy and four niobium–titantium alloys, the PWK-35 coating had a mean lifetime (for a number of specimens) of 10,000 hr in 650°C (1202°F) air. In 871°C (1600°F) air, the mean lifetimes ranged from 1500 hr for the coated niobium–1 wt.% zirconium alloy to 3500 hr for the coated niobium–titanium alloys. Promising results have been obtained with these coatings applied to complex engineering structures and tested in impure helium for periods ranging up to 5000 hr at temperatures ranging up to 1093°C (2000°F).

Table V-1 COMPOSITION (WT.%) OF PRATT & WHITNEY AIRCRAFT SLURRY COATINGS[15]

	PWK-1 coating		PWK-35 coating	
	First layer	Second layer	First layer	Second layer
Tin	76.0	50.0	70.0	45.0
Aluminum	15.0	50.0	13.0	16.0
Zinc	5.0		2.0	
Chromium	2.0		4.0	30.0
Titanium			9.0	9.0
LiF (flux)	2.0		2.0	

Chu has studied[16] the vapor-phase siliconizing of molybdenum and tantalum at temperatures between 900 and 1450°C (1652 and 2642°F). The rate of siliconizing generally follows a parabolic law. The activation energy for the siliconizing process on molybdenum was estimated at 21.6 kcal/mole. A detailed evaluation of siliconized molybdenum and tantalum was made by metallography, microhardness determinations, and X-ray diffraction and electron-microprobe analysis.

Yajima, Satow, and Hirai have studied[17] the mechanism of pyrolytic graphite formation by pyrolysis of commercial propane gas. The formation rate obeyed a linear law and was almost independent of gas flow rate. Three types of microstructure were distinguished in the deposits: the fine regenerative structure, the string structure, and the coarse structure, for which the activation energies of formation were approximately 3, 10, and 60 kcal/mole, respectively.

An improved, modified process for applying coatings by vacuum evaporation, called "ion plating," has been developed[18,19] by Sandia Corp. In this process the sample or substrate and its holder are made the

cathode, and the evaporation source is made the anode, of a high-voltage d-c circuit. Part of the evaporated metal is ionized in the resultant d-c glow discharge and accelerated toward the cathode (substrate). Some sputtering of the substrate occurs, but the rate of evaporation is made high enough, relative to the ion current, that a net deposition of material occurs. The process is normally carried out in argon gas at a pressure of 10 to 100 μ and with an ion current of 0.25 to 1.0 ma/cm^2. On uranium the best coatings obtained were of chromium and aluminum, of which aluminum was the easier to apply and was self-healing in an oxidizing atmosphere. Aluminum coatings less than 5×10^{-4} in. thick provided good protection for uranium exposed to condensing-water-vapor atmosphere at 95°C (203°F) for periods up to 96 hr. Certain reactor parts are protected from corrosion more effectively by an ion-plated aluminum coating than by electroplated nickel. Examination of the aluminum coating stripped from several of the coated parts showed[19] the probable existence of an aluminum–uranium intermetallic interfacial layer formed during the deposition process. Coatings applied by conventional vacuum evaporation techniques are totally inadequate for corrosion protection of uranium, owing to the presence of pinholes. The ion-plated coatings apparently are porous but do not have the pinholes, probably because of the smearing-out action of the sputtering that takes place during deposition.

Theison has patented[20] a process for applying niobium coatings to UC_2 articles by vacuum evaporation. The articles are given a final cleaning by glow discharge before being plated, and the niobium is heated for evaporation by electron bombardment.

(C. F. Powell)

Pressure Bonding

Fabrication of isotropic high-density graphite by gas-pressure bonding was summarized by workers at Battelle Memorial Institute.[21] Graphites ranging from the relatively low-purity natural grades to a high-purity, highly refined spectrographic grade were evaluated in this investigation. All materials were first hydropressed at 100,000 psi, inserted in tantalum containers, outgassed, and then pressure bonded at temperatures ranging from 1650 to 2700°C (3000 to 4890°F) and pressures ranging from 440 to 2040 atm (6600 to 30,600 psi). Bonding times of 1 and 2 hr were employed in these tests. Removal of the containers by pickling in HF did not produce any deleterious effects in the graphite. Densities up to 2.24 g/cm^3 (99% of theoretical) were obtained with high-purity graphites. Generally, with graphites characterized by platelike particles, severe orientation was noted in the bonded structures. The use of artificial graphites, however, resulted in essentially isotropic materials. It was apparent that loading characteristics of the powders were the major factors influencing isotropy in the pressure-bonded graphites. Strength determinations on these materials yielded values that were not significantly different from those for commercial materials. The uniform directional strength in the isotropic pressure-bonded graphites was noteworthy. (S. W. Porembka)

Nondestructive Testing

Ultrasonic Techniques

An ultrasonic system for observing the formation of fatigue cracks in center-notched sheet specimens of unalloyed aluminum, aluminum alloys, mild steel, and a nickel-base alloy was developed at Lewis Research Center.[22] A through-transmission technique was used to measure relatively long cracks; however, the reflection technique was more sensitive to small cracks and was used to detect cracks as small as 0.0005 in. in each alloy while the fatigue test was in progress. A significant result of this investigation appears to be the detection of cracks within approximately 1 to 3% of the total specimen life for all the materials over the range of stresses considered. Results were more reproducible on cracks longer than 0.010 in. when the through-transmission technique was used.

A pulse-echo technique, now being used by several organizations[5,23] to inspect small-diameter tubing, is designed to transmit focused ultrasonic energy through the wall of the tubing which is filled with liquid, and to take advantage of the curvature of the opposite inner surface to focus the reflected energy on the inner surface of the incident wall. Thus the beam is concentrated, resulting in a high sensitivity to defects. If no defect exists, the reflected energy is a maximum. If a defect is present, the amount of energy returning to the transducer is reduced according to the extent of the defect.

Atomic Power Development Associates, Inc.,[24] have presented concepts for general-purpose ultrasonic scanning systems for use in liquid sodium. Table V-2 contains acoustic properties of liquid sodium obtained as a result of their studies. Figure V-1 is the absorption coefficient of, and Fig. V-2 the intensity attenuation in, liquid sodium at various temperatures and frequencies. These data are essential to the final design of systems for locating foreign objects in a sodium bath. The authors discuss various imaging methods, including electronic–acoustic image converters for such use, but they give no indication of having used these techniques. (D. Ensminger)

NDT Techniques Other Than Ultrasonic

Changes in thermal properties of fuel pins as a result of burnup are being detected by investigators at Argonne[25,26] using the thermal-pulse method of

measuring thermal diffusivity and conductivity. In tests at room temperature, no change in the thermal properties of a fuel pin with a burnup of 0.32 at.% was noted, but there was a substantial change in both the thermal diffusivity and the thermal conductivity for these pins with burnups of 1.8 and 3.0 at.%. One specimen whose central area was marked by a large amount of "porosity" underwent about a 50% loss in thermal diffusivity and conductivity. The investigators expect to make these measurements in both the axial and radial directions at many points along the fuel pin to detect any anisotropy in the thermal properties, as well as any variation of these properties in the axial and radial directions along the length of the fuel pin.

The phase-sensitive eddy-current instrument being developed by investigators at Oak Ridge[27] for detection of flaws, thickness, and measurement of electrical conductivity in metal objects is being improved. The equipment now operates at 12 different frequencies from 1 to 5000 kc. The total harmonic distortion is less than 0.5% on most ranges for an output of 1.5 watts. The reduced distortion allows a greater range of compensation for liftoff. The d-c drift has been reduced to represent a 5% conductivity change for a one-week period and 0.3% for 1 hr.

(A. F. Leatherman)

Table V-2 VELOCITY OF SOUND AND CHARACTERISTIC ACOUSTIC IMPEDANCE OF LIQUID SODIUM[24]

Temperature, °C	Velocity of sound, 10^5 cm/sec	Characteristic acoustic impedance, 10^6 g/(cm²)(sec)
97.83	2.526	0.2342
100	2.525	0.2339
105	2.522	0.2334
110	2.520	0.2329
115	2.517	0.2323
120	2.514	0.2318
125	2.512	0.2313
130	2.509	0.2308
135	2.507	0.2303
140	2.504	0.2297
145	2.501	0.2292
150	2.499	0.2287
155	2.496	0.2281
160	2.493	0.2276
165	2.491	0.2271
170	2.488	0.2266
175	2.486	0.2261
180	2.483	0.2255
185	2.480	0.2250
190	2.478	0.2245
195	2.475	0.2240
200	2.472	0.2234
205	2.470	0.2229
210	2.467	0.2224
215	2.465	0.2219
220	2.462	0.2214
225	2.459	0.2208
230	2.457	0.2203
235	2.454	0.2198
240	2.451	0.2192
245	2.449	0.2188
250	2.446	0.2182
255	2.444	0.2178
260	2.441	0.2172
265	2.438	0.2167
270	2.436	0.2162
275	2.433	0.2157
280	2.431	0.2152
285	2.428	0.2146
290	2.425	0.2141
295	2.423	0.2136
300	2.420	0.2131
305	2.417	0.2126
310	2.415	0.2121

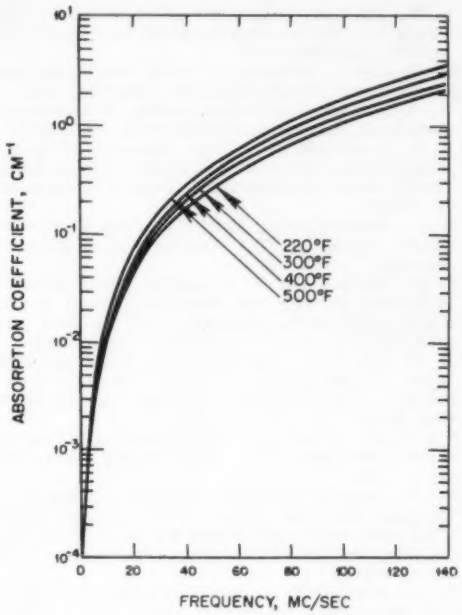

Fig. V-1 Absorption coefficient of liquid sodium.[24]

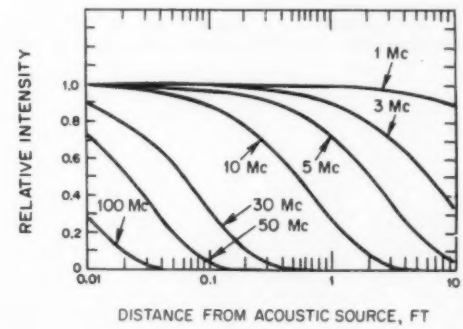

Fig. V-2 Intensity attenuation in liquid sodium.[24]

References

1. O. O. Gamba, The Nature and Properties of the Carbides of Uranium, USAEC Report NAA-SR-10929, Atomics International, Aug. 31, 1965.
2. A. Accary, Preparation and Fabrication of Uranium-Carbon Alloys, *J. Nucl. Mater.*, 8(3): 281-306 (May 1963).
3. W. R. Burt, Jr., W. C. Kramer, F. J. Karasek, and

R. M. Mayfield, Fabrication of 20 Wt.% Ti-V Alloy Tubing for Nuclear-Fuel Cladding, *Nucl. Appl.*, 1(6): 589-596 (December 1965).
4. B. Chalmers, Interaction of Solid Metal and Liquid Alloys, USAEC Report TID-22271, September 1965.
5. R. D. Watson, Diffusionless Bonding of Aluminum to Zircaloy-2, Canadian Report CRE-1139, April 1965.
6. P. B. Ferry and J. P. Page, Metallurgical Study of Niobium/Type 316 Stainless Steel Duplex Tubing, USAEC Report NAA-SR-11191, Atomics International, Jan. 5, 1966.
7. S. R. Nemeth (Comp.), Metal Fuel Tube Manufacture, USAEC Report DP-976, Savannah River Laboratory, July 1965.
8. I. M. Kvobova and V. I. Layner, The Electrolytic Deposition of Thick and Reguline Rhenium Layers, Report JPRS-32773, translated from *Izv. Akad. Nauk SSSR, Metally*, No. 4: 137-143 (July–August 1965).
9. S. M. Kim, J. E. Noakes, L. K. Akers, and W. W. Miller, Electrodeposition of Actinides and Lanthanides, USAEC Report ORINS-48, Oak Ridge Institute of Nuclear Studies, Inc., Dec. 15, 1965.
10. Oak Ridge National Laboratory Status and Progress Report, December 1965, USAEC Report ORNL-3911, Jan. 6, 1966.
11. Ya. M. Polyakov and G. Z. Zamesova, Deposition of Tantalum from the Vapor Phase, USAEC Report UCRL-Trans-1211 (L), translated by T. Watt from *Izv. Vysskikh Uchebn. Zavedenii, Tsvetn. Met.*, No. 4: 130-134 (1964).
12. S. Baranow and R. C. Lever, Coating for Niobium, U. S. Patent No. 3, 216, 851, to USAEC, Nov. 9, 1965.
13. S. Priceman and L. Sama, Protective Coatings for Niobium and Its Alloys, U. S. Patent No. 3,219,474, to USAEC, Nov. 23, 1965.
14. J. Grubessich and L. Sama, Oxidation Resistant Coatings for Nb and Nb Alloys, U. S. Patent No. 3,219,477, to USAEC, Nov. 23, 1965.
15. L. A. Friedrich, E. C. Hirakis, and N. S. Bornstein, Modified Tin–Aluminum Slurry Coatings for Multi-Thousand-Hour Applications, USAEC Report TIM-945, Pratt & Whitney Aircraft, CANEL, October 1965.
16. G. P. K. Chu, Mechanism of Siliconizing of Molybdenum and Tantalum by Vapor Deposition, Ph. D. Thesis, University of Missouri, 1964.
17. S. Yajima, T. Satow, and T. Hirai, Mechanism of the Pyrolytic Graphite Formation, *J. Nucl. Mater.*, 17: 116 (October 1965).
18. R. D. Bland, J. E. McDonald, and D. M. Mattox, Ion-Plated Coatings for the Corrosion Protection of Uranium, USAEC Report SC-DR-65-519, Sandia Corp., October 1965.
19. D. M. Mattox and R. D. Bland, Ion Plating of SPRF Reactor Parts, USAEC Report SC-DR-65-530, Sandia Corp., November 1965.
20. R. Theison, Improvements in or Relating to Niobium-Coated Uranium Carbide Articles, British Patent No. 1,005,102, Sept. 22, 1965.
21. D. C. Carmichael, P. D. Ownby, and E. S. Hodge, Hot Isostatic Compaction of Graphite, USAEC Report BMI-1746, Battelle Memorial Institute, Oct. 5, 1965.
22. S. J. Klima, D. J. Lesco, and J. C. Freche, Ultrasonic Technique for Detection and Measurement of Fatigue Cracks, Report N65-32647 (NASA-TN-D-3007), National Aeronautics and Space Administration, Lewis Research Center, September 1965.
23. Oak Ridge National Laboratory, unpublished, Feb. 4, 1966.
24. S.-P. Ying and C. C. Scott, Concepts for General-Purpose Under-Sodium Scanning Systems, USAEC Report APDA-179, Atomic Power Development Associates, Inc., Nov. 8, 1965.
25. Argonne National Laboratory, Reactor Development Program Progress Report, January 1966, USAEC Report ANL-7152, Feb. 24, 1966.
26. Argonne National Laboratory, Reactor Development Program Progress Report, February 1966, USAEC Report ANL-7176, Mar. 23, 1966.
27. Oak Ridge National Laboratory, unpublished, Apr. 6, 1966.

LEGAL NOTICE

This journal was prepared under the sponsorship of the U. S. Atomic Energy Commission. Neither the United States, nor the Commission, nor any person acting on behalf of the Commission:

A. Makes any warranty or representation, expressed or implied, with respect to the accuracy, completeness, or usefulness of the information contained in this journal, or that the use of any information, apparatus, method, or process disclosed in this journal may not infringe privately owned rights; or

B. Assumes any liabilities with respect to the use of, or for damages resulting from the use of any information, apparatus, method, or process disclosed in this journal.

As used in the above, "person acting on behalf of the Commission" includes any employee or contractor of the Commission, or employee of such contractor, to the extent that such employee or contractor of the Commission, or employee of such contractor prepares, disseminates, or provides access to, any information pursuant to his employment or contract with the Commission, or his employment with such contractor.